3D inviscid methods for lifting surfaces

Revision

Lifting line — 1

For a **flat, unswept** wing of known geometry we can simply discretise Prandtl's lifting line method for the circulation distribution Γ(*y*), starting with the (linear) statement for each spanwise location y_0:

$$\frac{2\Gamma(y_0)}{a_0 V_\infty c(y_0)} + \frac{1}{4\pi V_\infty}\int_{-b/2}^{b/2}\frac{\mathrm{d}\Gamma(y)}{\mathrm{d}y}\frac{\mathrm{d}y}{y_0 - y} = \alpha + \alpha_{\text{aero}}(y_0) = \alpha + \alpha_{\text{geom}}(y_0) - \alpha_{L'=0}(y_0)$$

Recall α_{aero} is the angle between the reference line and the zero lift line at each section.

Make change of variables and use the Fourier sine series expansion for Γ

$$\Gamma(\theta_0) = 2bV_\infty \sum_{n=1}^{N} A_n \sin n\theta_0 \qquad\qquad \alpha_i(\theta_0) = \sum_{n=1}^{N} nA_n \frac{\sin n\theta_0}{\sin\theta_0}$$

which gives

$$\frac{4b}{a_0 c(\theta_0)}\sum_{n=1}^{N} A_n \sin n\theta_0 + \sum_{n=1}^{N} nA_n \frac{\sin n\theta_0}{\sin\theta_0} = \alpha + \alpha_{\text{aero}}(\theta_0)$$

For any particular spanwise station θ_i, this is

$$\frac{4b}{a_0 c(\theta_i)}\left[A_1 \sin\theta_i + A_2 \sin 2\theta_i + A_3 \sin 3\theta_i + \cdots\right] + \left[A_1 \frac{\sin\theta_i}{\sin\theta_i} + 2A_2 \frac{\sin 2\theta_i}{\sin\theta_i} + 3A_3 \frac{\sin 3\theta_i}{\sin\theta_i} + \cdots\right] = \alpha + \alpha_{\text{aero}}(\theta_i)$$

In order to solve for all the coefficients A_n, we need to form *N* equations, i.e. use *N* stations.

Revision

Lifting line — 2

This provides a matrix equation, with each row of the matrix corresponding to a different spanwise location.

$$\begin{bmatrix} \left(\frac{4b}{a_0 c(\theta_1)}\sin\theta_1 + 1\right) & \left(\frac{4b}{a_0 c(\theta_1)}\sin 2\theta_1 + 2\frac{\sin 2\theta_1}{\sin\theta_1}\right) & \left(\frac{4b}{a_0 c(\theta_1)}\sin 3\theta_1 + 3\frac{\sin 3\theta_1}{\sin\theta_1}\right) & \cdots & \left(\frac{4b}{a_0 c(\theta_1)}\sin N\theta_1 + N\frac{\sin N\theta_1}{\sin\theta_1}\right) \\ \left(\frac{4b}{a_0 c(\theta_2)}\sin\theta_2 + 1\right) & \left(\frac{4b}{a_0 c(\theta_2)}\sin 2\theta_2 + 2\frac{\sin 2\theta_2}{\sin\theta_2}\right) & \left(\frac{4b}{a_0 c(\theta_2)}\sin 3\theta_2 + 3\frac{\sin 3\theta_2}{\sin\theta_2}\right) & \cdots & \left(\frac{4b}{a_0 c(\theta_2)}\sin N\theta_2 + N\frac{\sin N\theta_2}{\sin\theta_2}\right) \\ \cdots & \cdots & \cdots & \cdots & \cdots \\ \left(\frac{4b}{a_0 c(\theta_N)}\sin\theta_N + 1\right) & \left(\frac{4b}{a_0 c(\theta_N)}\sin 2\theta_2 + 2\frac{\sin 2\theta_2}{\sin\theta_N}\right) & \left(\frac{4b}{a_0 c(\theta_N)}\sin 3\theta_N + 3\frac{\sin 3\theta_N}{\sin\theta_N}\right) & \cdots & \left(\frac{4b}{a_0 c(\theta_N)}\sin N\theta_N + N\frac{\sin N\theta_N}{\sin\theta_N}\right) \end{bmatrix} \begin{pmatrix} A_1 \\ A_2 \\ A_3 \\ \cdots \\ A_N \end{pmatrix} = \begin{pmatrix} \alpha + \alpha_{\text{aero}}(\theta_1) \\ \alpha + \alpha_{\text{aero}}(\theta_2) \\ \alpha + \alpha_{\text{aero}}(\theta_3) \\ \cdots \\ \alpha + \alpha_{\text{aero}}(\theta_N) \end{pmatrix}$$

(If we know that the wing and the flow is symmetric -*y* ↔ +*y*, then all the even-numbered A_n=0, so their equations, also corresponding columns, can be dropped. Alternatively, the equations only need to be formed for half the wing.)

We now solve for the A_n and can compute overall lift, downwash at each chosen location (and the total induced drag).

Kuethe & Chow

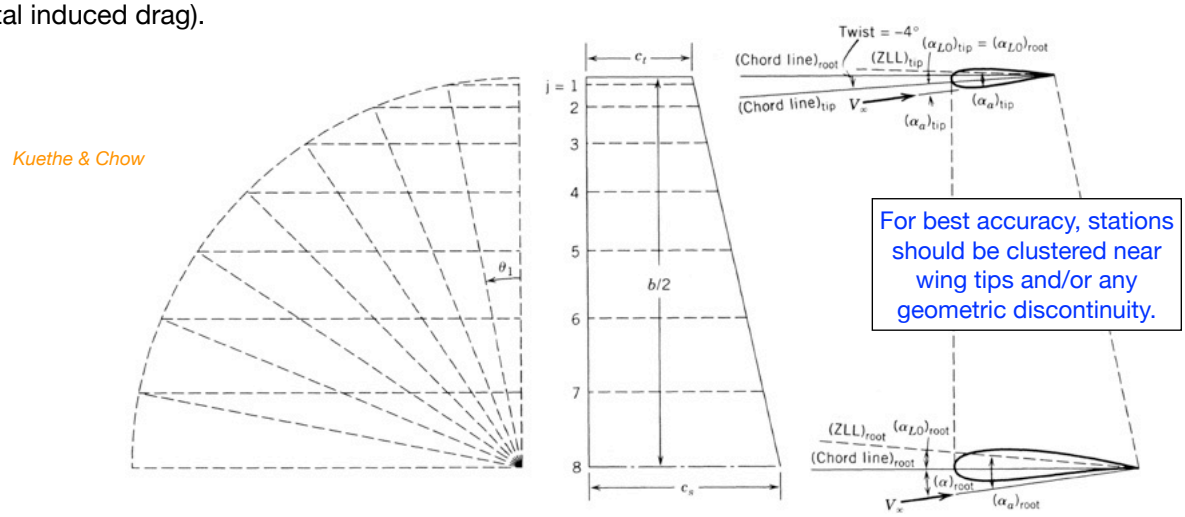

For best accuracy, stations should be clustered near wing tips and/or any geometric discontinuity.

Vortex lattice methods (Drela Chs 6, and 5)

Lifting surface theory

When it comes to estimating forces and moments on complete wings and aircraft, lifting surface theory is the 3D equivalent of (2D) thin airfoil theory. It replaces lifting surfaces with singularity sheets located at the mean camber surfaces, to compute inviscid lift and moments. Since induced drag is basically an inviscid effect, this can also be computed from lifting surface theory.

Viscous drag (including drag of non-lifting components) must be computed by other methods (typically based on BL integral equations, as in 2D).

We will come back to the topic of the Trefftz plane.

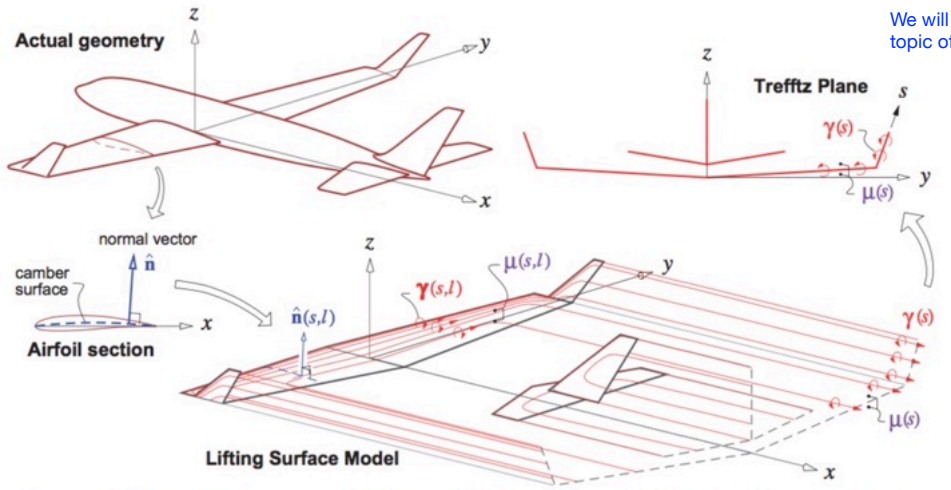

Drela

Figure 6.4: 3D configuration represented using a lifting-surface model. The model consists of vortex sheets with strength $\gamma(s,\ell)$ on the surfaces, and $\gamma(s)\,\hat{\mathbf{x}}$ on the trailing wakes and in the Trefftz plane.

In practice, the singularity sheets are very often further lumped into discrete vortices – the basis of Vortex Lattice (VL) methods, which are the mainstay of aircraft preliminary aerodynamic design. (E.g. OpenVSP.)

Vortex lattice method — 1

1. Classical lifting line theory does a good job when there is only one lifting surface to be analysed and it is planar + unswept. Also, owing to the use of global expansion functions (Fourier sine series), it's not so good if there are moderately extreme geometric planform discontinuities along the span.

2. More generally one uses discrete methods such as the vortex lattice method and the panel method. The basic formulation of these is linear.

3. We start with the simple horseshoe vortex lattice. Each spanwise subdivision Δy has a horseshoe vortex bound at the $c/4$ line. The horseshoe nominally extends downstream to ∞ and is closed to form a loop by the starting vortex — however this has washed so far downstream that we do not need to consider its influence.

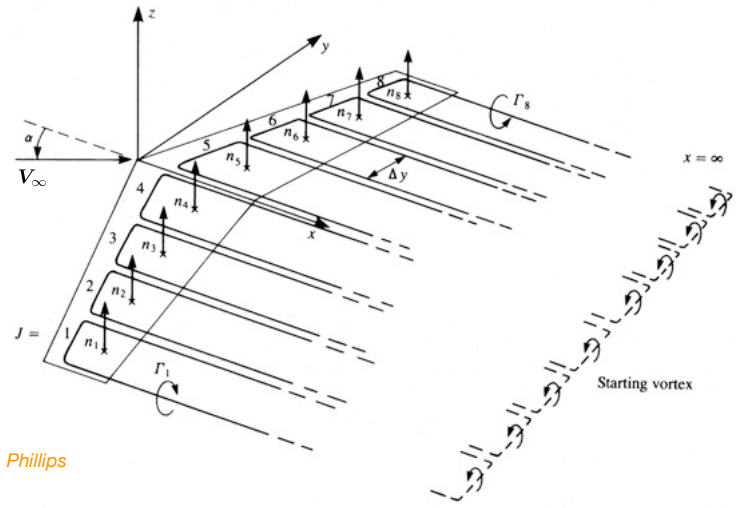

Phillips

4. Each lifting surface element also has a unit normal vector ***n*** associated with it, typically located at the $3c/4$ point on the mean camber line. The orientation of ***n*** accounts for wing non-planar geometry (dihedral, twist), airfoil geometry, and geometric angle of attack α.

5. The trailing vortex arms are assumed to be parallel with the free-stream. (This is an approximation, but is typically used.)

Vortex lattice method — 2

6. So far we have only shown one horseshoe vortex per spanwise strip. To increase accuracy, the chordwise direction is also subdivided into panels, each with its own horseshoe vortex and control points (with local values of ***n***) to form a Vortex Lattice. The problem formulation and solution methodology remain unchanged – there are just more unknowns.

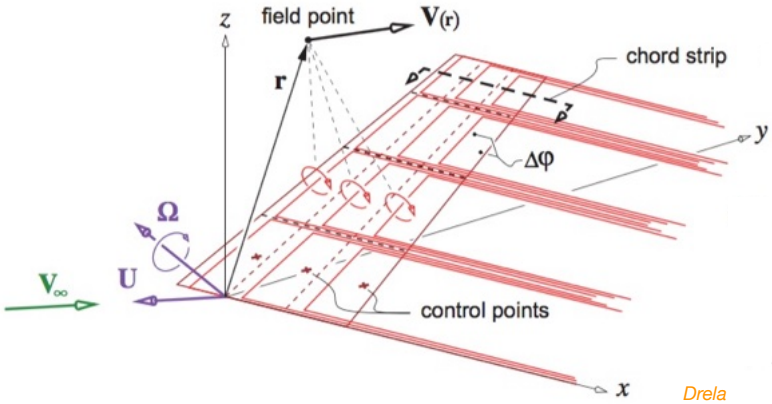

Drela

7. For generality we allow the aircraft to fly at angles of attack α, sideslip β, and have a rotation rate Ω about the CG.

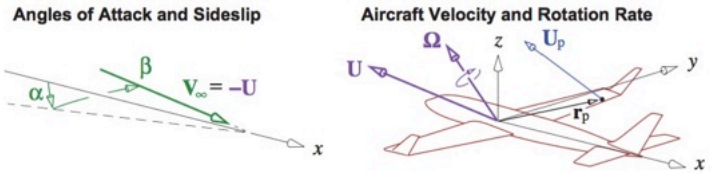

Figure 6.1: Aircraft velocity and rotation rate $\mathbf{U}, \boldsymbol{\Omega}$, and resulting velocity $\mathbf{U}_p$ of body point $\mathbf{r}_p$. Normalized velocity $\mathbf{U}/V_\infty$ is specified by the angles of attack and sideslip α, β. For computation, all vectors are specified via their components along the aircraft's xyz geometry axes.

The earth-frame velocity of any point $\boldsymbol{r}_p$ on the aircraft surface is

$$\mathbf{U}_p = \mathbf{U} + \boldsymbol{\Omega} \times \mathbf{r}_p$$

The aerodynamic "freestream" velocity $\mathbf{V}_\infty$ is directly opposite to $\mathbf{U}$, and is conventionally specified by the two aerodynamic flow angles α and β, applied in that order as shown in Figure 6.1.

$$\mathbf{U} = \begin{Bmatrix} U_x \\ U_y \\ U_z \end{Bmatrix} = -\mathbf{V}_\infty = V_\infty \begin{Bmatrix} -\cos\alpha\cos\beta \\ \sin\beta \\ -\sin\alpha\cos\beta \end{Bmatrix} \qquad (6.1)$$

$$V_\infty = \sqrt{U_x^2 + U_y^2 + U_z^2} \quad , \quad \alpha = \arctan\frac{-U_z}{-U_x} \quad , \quad \beta = \arctan\frac{U_y}{\sqrt{U_x^2 + U_z^2}} \qquad (6.2)$$

Vortex lattice method — 3

8. At any point the perturbation velocity owing to vortex sheet strengths is

$$\mathbf{V}_\gamma(\mathbf{r}) = \frac{1}{4\pi}\iint \boldsymbol{\gamma}(s,\ell) \times \frac{\mathbf{r}-\mathbf{r}'}{|\mathbf{r}-\mathbf{r}'|^3}\, ds\, d\ell$$

Drela

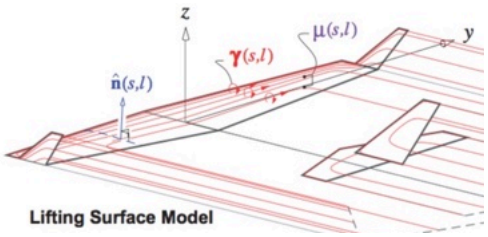

The total fluid velocity for an observer in the body reference frame is

$$\mathbf{V}(\mathbf{r}) = \mathbf{V}_\gamma - (\mathbf{U} + \boldsymbol{\Omega} \times \mathbf{r})$$

and the flow tangency boundary condition at each point ***r***(*s, l*) on the lifting surface is

$$\mathbf{V}(\mathbf{r}) \cdot \hat{\mathbf{n}} = \Big[\mathbf{V}_\gamma - (\mathbf{U} + \boldsymbol{\Omega} \times \mathbf{r})\Big] \cdot \hat{\mathbf{n}} = 0$$

9. Lumping the vortex sheets into horseshoe vortices with arms trailing downstream, we have

$$\mathbf{V}(\mathbf{r}) = \sum_{\text{h.v.'s}} \frac{\Gamma}{4\pi} \int \frac{d\boldsymbol{\ell}' \times (\mathbf{r}-\mathbf{r}')}{|\mathbf{r}-\mathbf{r}'|^3} - (\mathbf{U} + \boldsymbol{\Omega} \times \mathbf{r})$$

$$= \sum_{i=1}^{N} \Gamma_i \hat{\mathbf{V}}_i(\mathbf{r}) - (\mathbf{U} + \boldsymbol{\Omega} \times \mathbf{r})$$

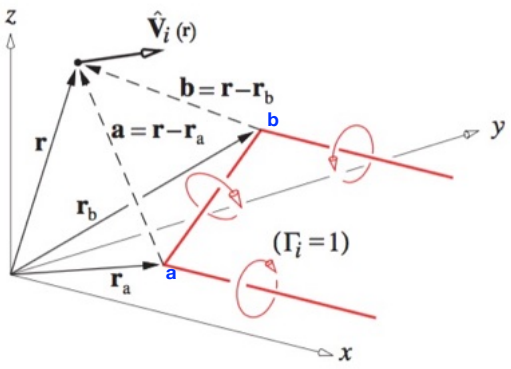

where for Γ_i of unit strength

$$\hat{\mathbf{V}}_i(\mathbf{r}) = \frac{1}{4\pi}\left\{ \frac{\mathbf{a}\times\mathbf{b}}{|\mathbf{a}||\mathbf{b}| + \mathbf{a}\cdot\mathbf{b}}\left(\frac{1}{|\mathbf{a}|} + \frac{1}{|\mathbf{b}|}\right) + \frac{\mathbf{a}\times\hat{\mathbf{x}}}{|\mathbf{a}| - \mathbf{a}\cdot\hat{\mathbf{x}}}\frac{1}{|\mathbf{a}|} - \frac{\mathbf{b}\times\hat{\mathbf{x}}}{|\mathbf{b}| - \mathbf{b}\cdot\hat{\mathbf{x}}}\frac{1}{|\mathbf{b}|} \right\}$$

From arm trailing from **a**. From arm trailing from **b**.

Vortex lattice method — 4

10. The flow tangency BC to be satisfied at each of *i* control points is *Drela*

$$\mathbf{V}(\mathbf{r}_i^c)\cdot\mathbf{n}_i \quad = \left(\sum_{j=1}^{N}\Gamma_j\,\hat{\mathbf{V}}_j(\mathbf{r}_i^c) \;-\; (\mathbf{U}+\boldsymbol{\Omega}\times\mathbf{r}_i^c)\right)\cdot\mathbf{n}_i \quad = 0$$

(We have here omitted Drela's inclusion of control surface deflections, for sake of simplicity.)

11. This amounts to a system of *i* equations to be satisfied, one for each control point (same as number of horseshoe vortices).

$$\left[\;A_{ij}\;\right]\left\{\bar{\Gamma}_j\right\} = \bar{U}_x\left\{\;\hat{\mathbf{x}}\cdot\mathbf{n}_{0_i}\;\right\} + \bar{U}_y\left\{\;\hat{\mathbf{y}}\cdot\mathbf{n}_{0_i}\;\right\} + \bar{U}_z\left\{\;\hat{\mathbf{z}}\cdot\mathbf{n}_{0_i}\;\right\}$$
$$+\;\bar{\Omega}_x\left\{\hat{\mathbf{x}}\times\mathbf{r}_i^c\cdot\mathbf{n}_{0_i}\right\} + \bar{\Omega}_y\left\{\hat{\mathbf{y}}\times\mathbf{r}_i^c\cdot\mathbf{n}_{0_i}\right\} + \bar{\Omega}_z\left\{\hat{\mathbf{z}}\times\mathbf{r}_i^c\cdot\mathbf{n}_{0_i}\right\}$$

$$\bar{\Gamma}_i \equiv \frac{\Gamma_i}{V_\infty} \quad , \quad \bar{\mathbf{U}} \equiv \frac{\mathbf{U}}{V_\infty} = \begin{Bmatrix}\bar{U}_x\\ \bar{U}_y\\ \bar{U}_z\end{Bmatrix} = \begin{Bmatrix}-\cos\alpha\cos\beta\\ \sin\beta\\ -\sin\alpha\cos\beta\end{Bmatrix} \quad , \quad \bar{\boldsymbol{\Omega}} \equiv \frac{\boldsymbol{\Omega}}{V_\infty} = \begin{Bmatrix}\bar{\Omega}_x\\ \bar{\Omega}_y\\ \bar{\Omega}_z\end{Bmatrix}$$

The system is solved for the set of horseshoe vortex strengths Γ_i.

Values of the Aerodynamic Influence Coefficient matrix ***A*** depend only on lifting surface geometry, through

$$A_{ij} \;\equiv\; \hat{\mathbf{V}}_{j(\mathbf{r}_i^c)}\cdot\mathbf{n}_{0_i}$$

AVL vortex lattice code

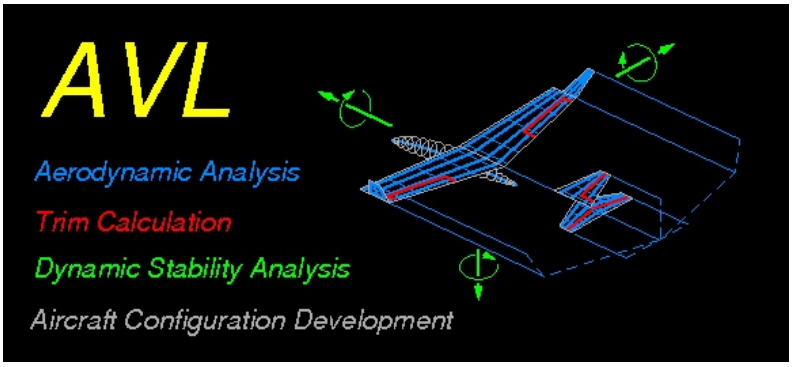

http://web.mit.edu/drela/Public/web/avl/

Background & capabilities

AVL uses the vortex lattice method (and optionally source/doublet lines) to carry out inviscid, subsonic aircraft configuration analysis.

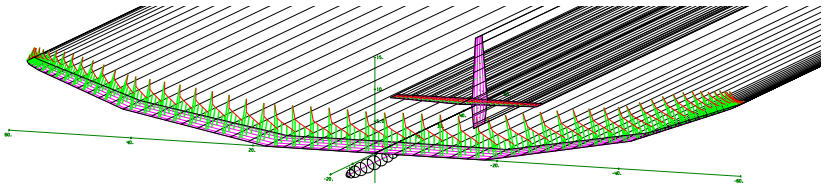

Load distribution & trailing vortices

Capabilites:

1. Aerodynamic components:
   - lifting surfaces
   - slender bodies
2. Configuration description:
   - keyword-driven geometry input file
   - defined airfoil sections with linear interpolation
   - section properties: NACA or from file
   - control deflections
   - scaling, translation, reflection of surfaces
3. Singularities
   - Horseshoe vortices (surfaces)
   - Source + doublet lines (bodies)
   - Finite vortex core-size option
4. Discretization spanwise/chordwise
   - uniform, sine, cosine, blend
5. Control deflections via normal-vector tilting
   - leading edge flaps
   - trailing edge flaps
6. General freestream description
   - α, β (AoA, sideslip) flow angles
   - *p, q, r* (roll, pitch, yaw) rates
   - subsonic Prandtl-Glauert compressibility
7. Aerodynamic outputs
   - direct forces and moments
   - Trefftz-plane analysis of lift and drag
   - derivatives of forces and moments
8. Trim calculation
   - operating variables: *α, β, p, q, r*, control deflections
   - constraints: direct and indirect (e.g. via specified C_L, moment equilibrium)
   - level/banked/looping flight
9. Optional mass definition file for trim and eigenmode analysis

Usage & examples — 1

AVL has greater capability than required just to define wing geometry, loading and drag.

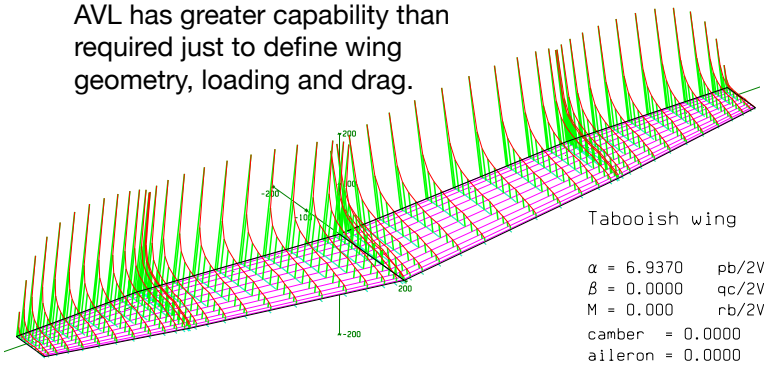

Two-panel wing geometry and C_p distribution for C_L=1.0.

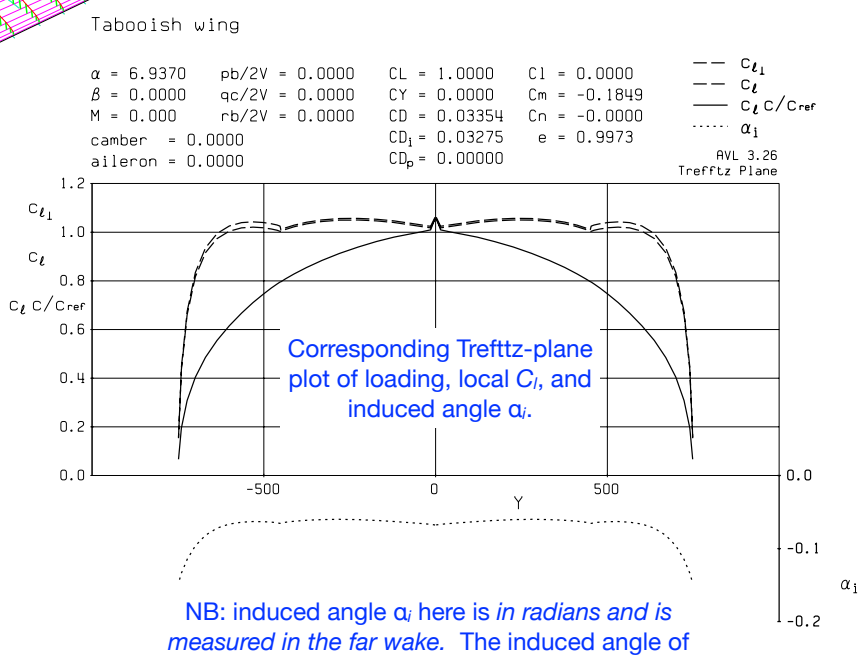

Corresponding Trefftz-plane plot of loading, local C_l, and induced angle α_i.

NB: induced angle α_i here is *in radians and is measured in the far wake.* The induced angle of attack at the lifting surface is half the far-wake value. All other angles in AVL are in degrees.

Usage & examples — 2

Example input file

```
Simple Wing, no controls
#Mach
 0.0
#IYsym    IZsym    Zsym
 0        0        0.0
#Sref     Cref     Bref
30.0      2.0      15.0
#Xref     Yref     Zref
0.50      0.0      0.0

#==========================================
SURFACE
Wing
#Nchordwise  Cspace    Nspanwise    Sspace
8            1.0        12          1.0
YDUPLICATE
0.0
ANGLE
2.0

#------------------------------------------------------
SECTION
#Xle     Yle     Zle      Chord    Ainc   Nspanwise  Sspace
0.       0.      0.       2.2      0.0    0          0

AFILE
sd7037.dat

#------------------------------------------------------
SECTION
#Xle     Yle     Zle      Chord    Ainc   Nspanwise  Sspace
0.4      7.5     0.75     1.8      0.0    0          0

AFILE
sd7037.dat
```

Corresponding geometry + load distribution for C_L=0.7

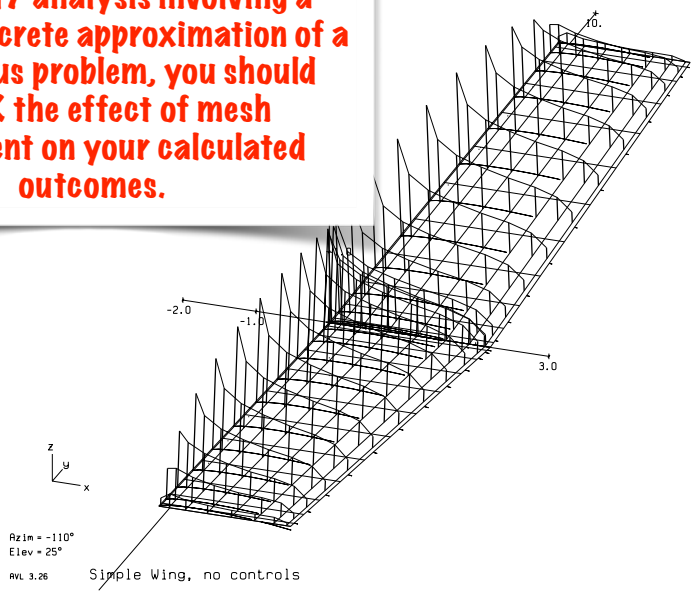

NB: in ANY analysis involving a meshed/discrete approximation of a continuous problem, you should CHECK the effect of mesh refinement on your calculated outcomes.

Alternatives to AVL

There are other VL codes available in the public domain, the main ones being:

1. OpenVSP - convenient interface to aircraft geometry definition

2. XFLR5 - combines VL (3D inviscid) with XFOIL (2D viscous drag)

3. Tornado - matlab

In one way or another, it is possible to do much the same inviscid calculations (including dynamic estimation of linearised stability modes) with each code above.

Overall, AVL has some nice abilities that the others lack, especially when it comes to dealing with control surface deflections and their constraints for trimmed flight and manoeuvres. Also it is straightforward to get load distributions output to text files for further analysis.

However, AVL development has stopped, and other codes, e.g. OpenVSP, are catching up. As of 2018, OpenVSP can reportedly do high-AoA vortex lift calculations that AVL cannot. OpenVSP can also include models for propeller or rotor discs.

3D Panel method — 1

The vortex lattice method as presented above assumes the lifting surfaces are thin. More generally we can break this restriction, using a 3D version of 2D panel methods. The method is still inviscid and is based on making the attached flows tangential at all the collocation points.

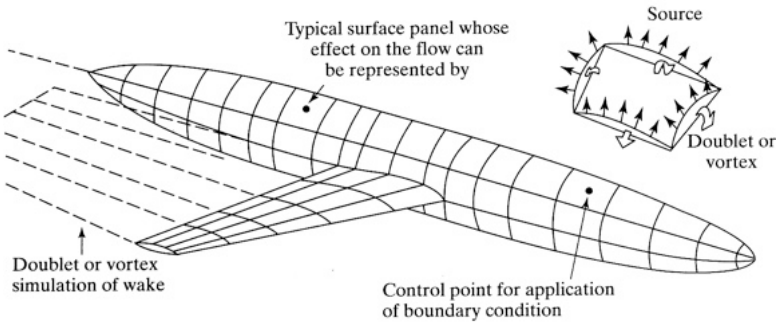

It is typical to use panels with both distributed source and normal-doublet strengths, rather than using 3D vorticity sheets. As we outlined earlier, the basic reason is that even in 3D the normal-doublet strength is a scalar (as is source strength), whereas the vorticity is a vector.

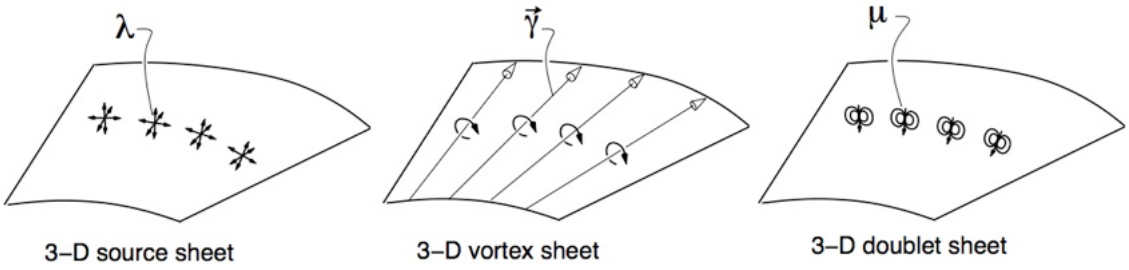

3D Panel method — 2

Generally the lifting components will be discretised using doublet distributions and non-lifting components with source distributions.

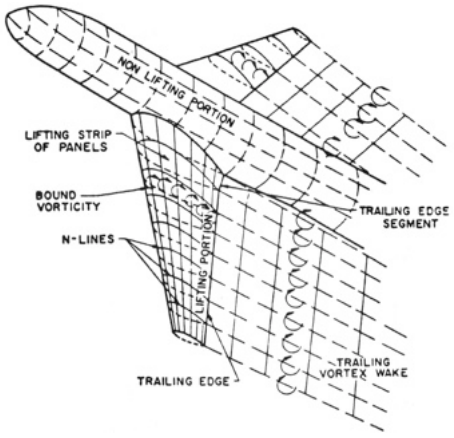

Indicative capability circa 1980

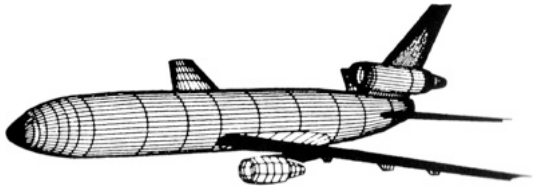

1000-panel transport aircraft model

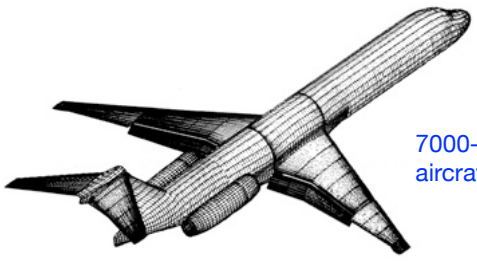

7000-panel transport aircraft model

More complete/recent methods allow for non-linear solutions that do not assume trailing vortices stay aligned with far-field flow.

Note vortex rollup:

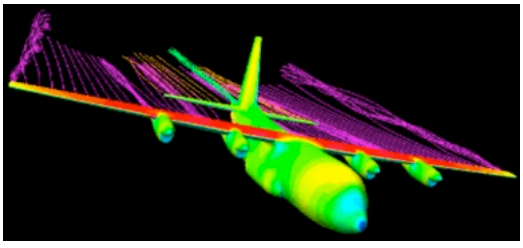

3D Panel method — 3

Panel methods are mature technology and like regular CFD codes, full-blown implementations were typically licenced/restricted (VSAERO, PANAIR, PMARC). Here are a few example results.

PANAIR is now publicly available through PDAS.

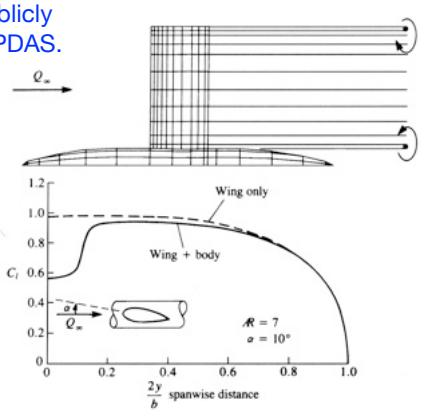

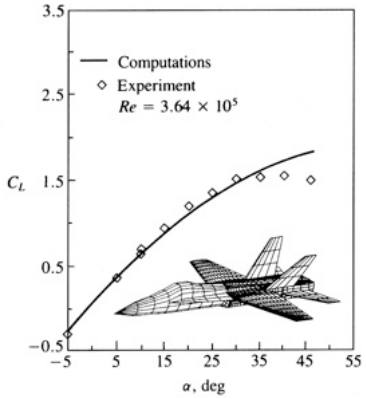

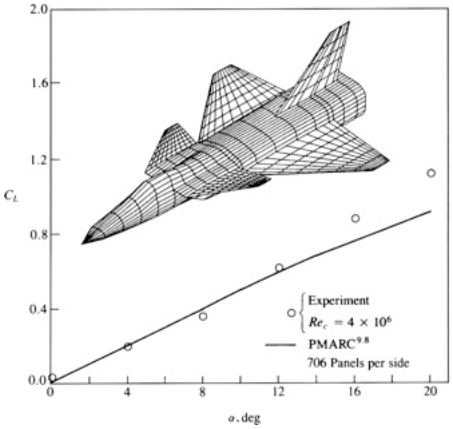

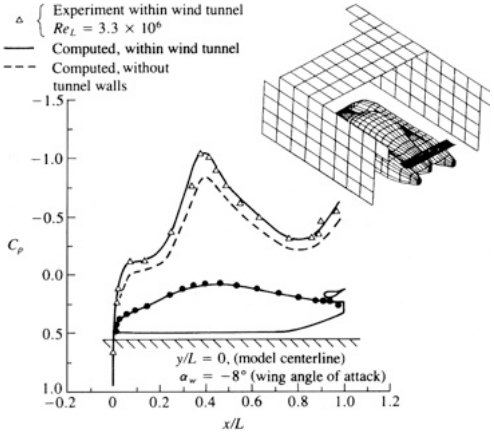

Modern capabilities

With modern computational tools, we can study either compressible inviscid transonic flows (Euler solvers + VII) or transonic subsonic viscous high-lift flows (Navier-Stokes+turbulence model, i.e. RANS). These tools are essential for modern design optimisation, but remain too slow for initial studies.

Application /Tools	Cruise	Take-off / Landing	Engine Integration	Rear End /Tails	Complete Aircraft
2D Euler/BL Coupled Tools	XLS, VICWA, ISES	HILI, MSES			
2D Navier-Stokes Codes		TAU			
3D Panel / Quasi-3D Codes		VSAERO, Q3D	VSAERO	VSAERO	VSAERO
3D Euler Codes (BL-modificaion)			MGAERO, FLOWer	MGAERO, FLOWer	MGAERO, FLOWer
3D Navier-Stokes Codes	FLOWer	TAU	TAU	FLOWer	TAU

Drela is reportedly (since 2013) developing a 3D code with BL models incorporated, IBL3.

Indicative capability circa 2000

Aerodynamic force analysis (Drela Chs 5 and 6)

Near-field vs far-field methods

Near-field force analysis is based on integrating pressure and viscous tractions (or their components in the *x*, *y* and *z* directions) over the surface of the aircraft to give $\boldsymbol{F} = D\boldsymbol{x} + Y\boldsymbol{y} + L\boldsymbol{z}$. This is typically the approach used in grid-based CFD methods.

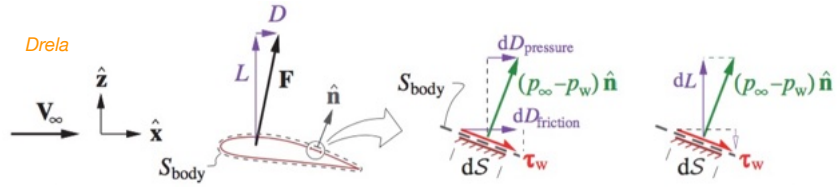

Figure 5.1: Surface pressure and viscous stress forces resolved into drag and lift components. Third dimension y and sideforce Y are not shown. The viscous stress contribution to lift and sideforce is typically negligible.

$$\begin{aligned} \mathbf{F} &= \mathbf{F}_{\text{pressure}} + \mathbf{F}_{\text{friction}} \\ \mathbf{F}_{\text{pressure}} &\equiv \oiint -p_w\,\hat{\mathbf{n}}\,d\mathcal{S} = \oiint (p_\infty - p_w)\,\hat{\mathbf{n}}\,d\mathcal{S} \\ \mathbf{F}_{\text{friction}} &\equiv \oiint \boldsymbol{\tau}_w\,d\mathcal{S} \quad , \qquad \boldsymbol{\tau}_w \equiv \bar{\bar{\tau}}_w \cdot \hat{\mathbf{n}} \end{aligned}$$

These surface integrals are taken over the body of the aircraft (or other immersed object).

$$\begin{aligned} D &= \mathbf{F}\cdot\hat{\mathbf{x}} = D_{\text{pressure}} + D_{\text{friction}} \\ D_{\text{pressure}} &\equiv \oiint (p_\infty - p_w)\,\hat{\mathbf{n}}\cdot\hat{\mathbf{x}}\,d\mathcal{S} \\ D_{\text{friction}} &\equiv \oiint \boldsymbol{\tau}_w\cdot\hat{\mathbf{x}}\,d\mathcal{S} \end{aligned}$$

$$\begin{aligned} Y &= \mathbf{F}\cdot\hat{\mathbf{y}} \simeq \oiint (p_\infty - p_w)\,\hat{\mathbf{n}}\cdot\hat{\mathbf{y}}\,d\mathcal{S} \\ L &= \mathbf{F}\cdot\hat{\mathbf{z}} \simeq \oiint (p_\infty - p_w)\,\hat{\mathbf{n}}\cdot\hat{\mathbf{z}}\,d\mathcal{S} \end{aligned}$$

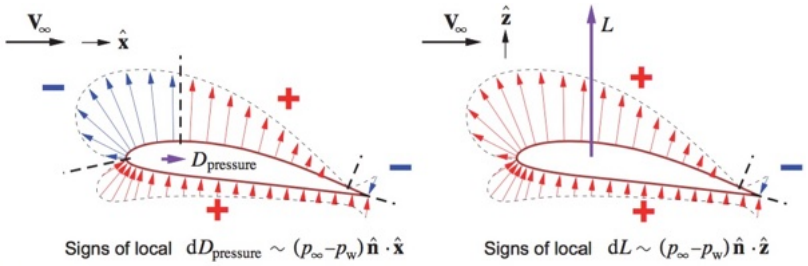

Figure 5.2: Streamwise components of the surface pressure forces on a streamlined shape almost entirely cancel, with the small net residual being the pressure drag. There is no such cancellation of the transverse components which form the much larger lift.

Unfortunately these near-field methods are quite unreliable/inaccurate for the pressure contribution to drag on streamlined bodies, since the projected tractions almost cancel in the +ve and –ve *x* directions.

This difficulty leads instead to a heavy reliance on far-field methods for aerodynamic force estimates.

Far-field (control volume) analysis

Starting from the integral momentum equation (integral form of Navier–Stokes)

$$\iiint \frac{\partial \rho \mathbf{V}}{\partial t}\,\mathrm{d}\mathcal{V} + \oiint \rho(\mathbf{V}\cdot\hat{\mathbf{n}})\,\mathbf{V}\,\mathrm{d}\mathcal{S} = \iiint \rho \mathbf{f}\,\mathrm{d}\mathcal{V} + \oiint -p\hat{\mathbf{n}}\,\mathrm{d}\mathcal{S} + \oiint \bar{\bar{\tau}}\cdot\hat{\mathbf{n}}\,\mathrm{d}\mathcal{S}$$

Assuming the flow is steady (time-average) and gravity force ***f*** is subsumed in hydrostatic pressure, this is

$$\oiint \left[\, \rho(\mathbf{V}\cdot\hat{\mathbf{n}})\mathbf{V} + p\hat{\mathbf{n}} - \bar{\bar{\tau}}\cdot\hat{\mathbf{n}} \,\right] \mathrm{d}\mathcal{S} = \mathbf{0}$$

Usually we assume that the body and CV are fixed in space, and flow goes through it.

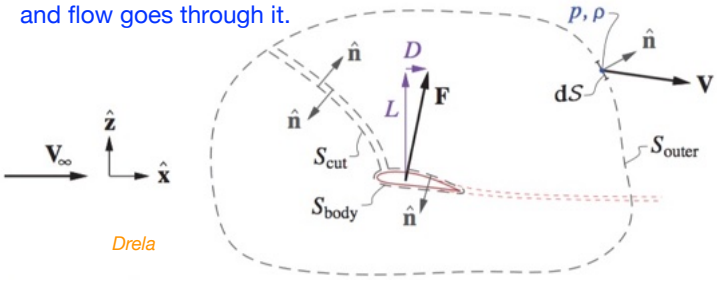

Drela

Taking a simply-connected control volume which excludes the body, and breaking up the integrals:

$$\oiint [\ ]\,\mathrm{d}\mathcal{S} = \oiint_{\text{body}} [\ ]\,\mathrm{d}\mathcal{S} + \oiint_{\text{outer}} [\ ]\,\mathrm{d}\mathcal{S} + \iint_{\text{cut}} [\ ]\,\mathrm{d}\mathcal{S} = 0$$

We can ignore the integral on the cut owing to cancellation:

$$\iint_{\text{cut}} [\ ]\,\mathrm{d}\mathcal{S} = 0$$

Since the velocity is zero on the surface of the body:

$$\oiint_{\text{body}} \left[\, \rho(\mathbf{V}\cdot\hat{\mathbf{n}})\mathbf{V} + p\hat{\mathbf{n}} - \bar{\bar{\tau}}\cdot\hat{\mathbf{n}} \,\right] \mathrm{d}\mathcal{S} = \oiint_{\text{body}} \left[\, p_w\hat{\mathbf{n}} - \boldsymbol{\tau}_w \,\right] \mathrm{d}\mathcal{S} = \mathbf{F}$$

where ***F*** is the force acting on the body (not on the fluid that immediately surrounds it):

Using the fact that $\oiint \hat{n}\,\mathrm{d}\mathcal{S} = 0$ and employing the continuity equation $\oiint_{\text{outer}} \rho(\mathbf{V}\cdot\hat{\mathbf{n}})\,\mathrm{d}\mathcal{S} = 0$, we end up with

$$\mathbf{F} = \oiint_{\text{outer}} \left[\, (p_\infty - p)\,\hat{\mathbf{n}} - \rho(\mathbf{V}\cdot\hat{\mathbf{n}})(\mathbf{V}-\mathbf{V}_\infty) \,\right] \mathrm{d}\mathcal{S}$$

Note: viscous stresses are taken to be zero on the outer boundary.

Far-field (control volume) analysis

$$\mathbf{F} = \oiint_{\text{outer}} \left[\, (p_\infty - p)\,\hat{\mathbf{n}} - \rho(\mathbf{V}\cdot\hat{\mathbf{n}})(\mathbf{V}-\mathbf{V}_\infty) \,\right] \mathrm{d}\mathcal{S}$$

To make further progress we assume that the trailing wake region is thin, that the trailing vortex arms are parallel to $\boldsymbol{V}_\infty$, which in turn is parallel to the *x* direction.

Drela

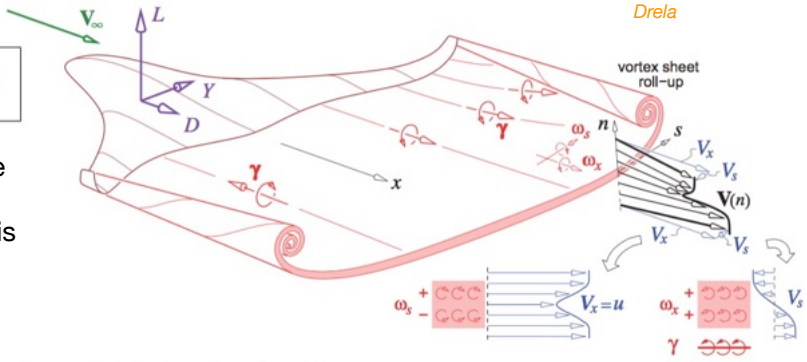

Figure 5.4: A body with lift, drag and sideforce, trailing a thin sheet of vorticity with components ω_x, ω_s. It will be assumed that the sheet trails straight back, and the equivalent lumped vortex sheet strength γ is in the streamwise direction. In effect this neglects the vortex sheet roll-up.

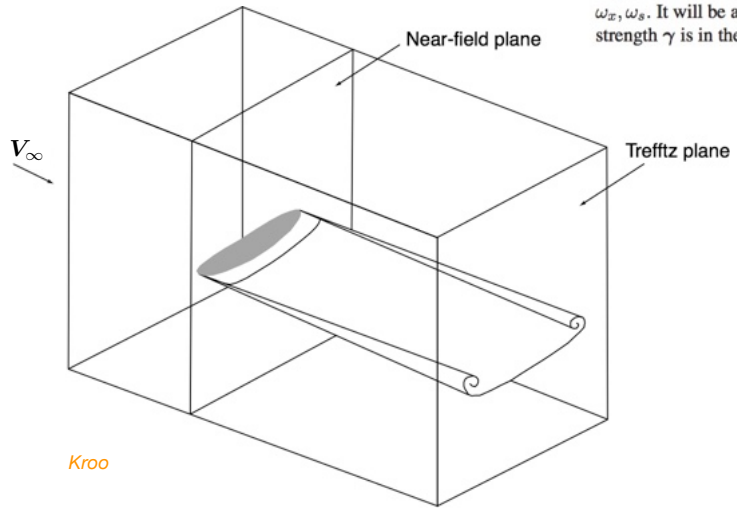

Kroo

The control volume is taken to be large enough that viscous stresses are zero on its boundaries, the faces align with *x, y, z* directions, and that on the far upstream face the pressure and velocity are uniform at p_∞, $\boldsymbol{V}_\infty$.

The far downstream plane is known as the Trefftz plane, where there may be significant perturbation velocity components *u, v, w* to the background $\boldsymbol{V}_\infty$. Likewise the pressure may differ from p_∞.

Far-field (control volume) analysis

Outside of the trailing wake (where vorticity and energy losses are confined), we can use Bernoulli's equation.

$$p_\infty + \tfrac{1}{2}\rho V_\infty^2 = p + \tfrac{1}{2}\rho(V_\infty \hat{\boldsymbol{x}} + \boldsymbol{v})^2 \qquad \text{or} \qquad p_\infty - p = \rho V_\infty u + \tfrac{1}{2}\rho(u^2 + v^2 + w^2)$$

The drag component of the momentum equation is $D = \iint_{TP} [\, p_\infty - p - \rho u(u - V_\infty) \,]\, dy\, dz$

So, outside of the trailing wake itself, we get the following inviscid contribution to drag (which is the induced drag)

$$D_i = \iint_{\mathrm{TP}} \tfrac{1}{2}\rho(v^2 + w^2 - u^2)\, \mathrm{d}\mathcal{S} \approx \iint_{\mathrm{TP}} \tfrac{1}{2}\rho(v^2 + w^2)\, \mathrm{d}\mathcal{S} \quad \text{if } u^2 \ll (v^2 + w^2)$$

and since the velocity components *v* and *w* are derivatives/components of a potential flow ϕ:

$$D_i \approx \iint_{\mathrm{TP}} \tfrac{1}{2}\rho \left[\left(\frac{\partial \varphi}{\partial y} \right)^2 + \left(\frac{\partial \varphi}{\partial z} \right)^2 \right] \mathrm{d}\mathcal{S}$$

Recall:

$$\boldsymbol{u} = \nabla \varphi = \left(\frac{\partial \varphi}{\partial x}, \frac{\partial \varphi}{\partial y}, \frac{\partial \varphi}{\partial z} \right)$$

is the velocity field associated with singularity distributions upstream.

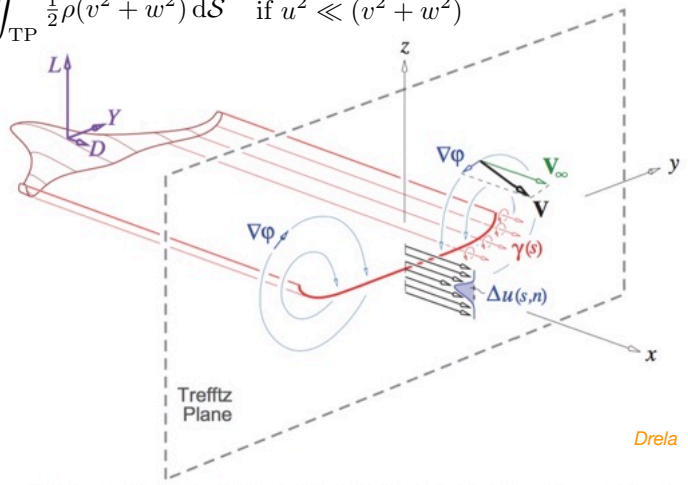

Figure 5.7: Flow in Trefftz plane behind a lifting 3D object, idealized from the actual flow shown in Figure 5.4. Trailing vortex sheet of strength $\gamma(s)$ generates crossflow perturbation velocity $\nabla\varphi$ which defines induced drag, and far-field lift and sideforce. Viscous axial velocity defect $\Delta u(s,n)$ within wake sheet defines profile drag.

Far-field (control volume) analysis

We note that we still have not dealt with the profile drag, whose effects are apparent on the Trefftz plane only within the thin wake region where Δ*u* is non-zero.

However, to get the profile drag contribution, we have only to integrate the momentum defect *P* along the wake coordinate *s*:

$$D_p = \int_0^{s_{\max}} P\, \mathrm{d}s = \rho V_\infty^2 \int_0^{s_{\max}} \theta(s)\, \mathrm{d}s$$

where θ is obtained from a BL-type analysis.

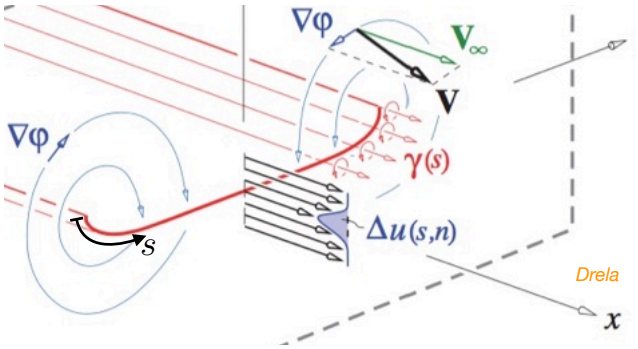

The total far-field drag is the sum

$$D = D_i + D_p = \iint_{\mathrm{TP}} \tfrac{1}{2}\rho \left[\left(\frac{\partial \varphi}{\partial y} \right)^2 + \left(\frac{\partial \varphi}{\partial z} \right)^2 \right] \mathrm{d}\mathcal{S} + \rho V_\infty^2 \int_0^{s_{\max}} \theta(s)\, \mathrm{d}s$$

Far-field (control volume) analysis

There is still a further manipulation to be made with the induced drag, however.

Using the vector-calculus identity

$$\nabla f \cdot \nabla f \;=\; \nabla \cdot (f\,\nabla f) \;-\; f\,\nabla^2 f$$

and the fact that if $f \equiv \varphi, \nabla^2 f \equiv \nabla^2 \varphi = 0$ in potential flow:

$$\begin{aligned} D_i &= \iint \frac{1}{2}\rho_\infty \nabla\varphi \cdot \nabla\varphi \, d\mathcal{S} && \text{(this is integrated all over Trefftz plane)} \\ &= \iint \frac{1}{2}\rho_\infty \nabla \cdot (\varphi \nabla\varphi) \, d\mathcal{S} \\ &= \oint \frac{1}{2}\rho_\infty \varphi \nabla\varphi \cdot \hat{\mathbf{n}} \, dl && \text{(this last using Gauss' (divergence) theorem)} \end{aligned}$$

Drela

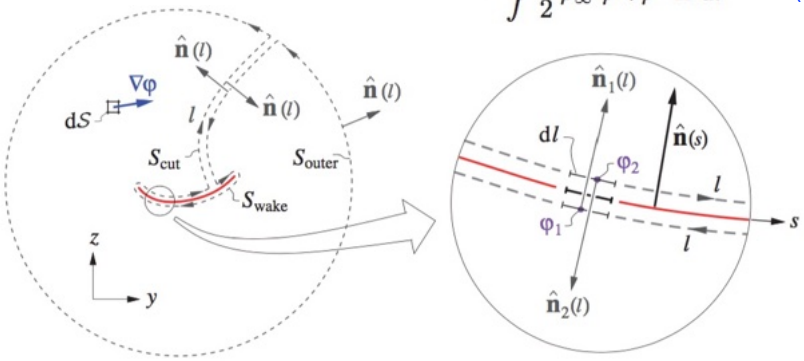

Figure 5.10: Induced drag line integral over l on entire contour perimeter is reduced to only a single integral over s on the vortex wake sheet.

The final integral has to have the potential continuous within its contour, so that has to exclude the wake region itself.

$$\begin{aligned} D_i &= \frac{1}{2}\rho_\infty \oint_{\text{wake}} \varphi \nabla\varphi \cdot \hat{\mathbf{n}} \, dl \\ &= \frac{1}{2}\rho_\infty \int [\,\varphi_1 \nabla\varphi_1 \cdot \hat{\mathbf{n}}_1 + \varphi_2 \nabla\varphi_2 \cdot \hat{\mathbf{n}}_2\,] \, ds \\ &= \frac{1}{2}\rho_\infty \int [\,\varphi_1 \nabla\varphi_1 \cdot \hat{\mathbf{n}} - \varphi_2 \nabla\varphi_2 \cdot \hat{\mathbf{n}}\,] \, ds \end{aligned}$$

$$D_i = -\frac{1}{2}\rho_\infty \int_0^{s_{\max}} \Delta\varphi \frac{\partial\varphi}{\partial n} \, ds$$

Far-field (control volume) analysis

$$D_i = -\frac{1}{2}\rho_\infty \int_0^{s_{\max}} \Delta\varphi \frac{\partial\varphi}{\partial n} \, ds$$

The further significance of this is that the potential jump ΔΦ is exactly the total circulation Γ bound back at the lifting surface, while

$\frac{\partial\phi}{\partial n} = v_n$ is the component of (*v, w*) which is normal to the sheet (and can be computed using singularity techniques).

$$D_i = -\frac{\rho}{2}\int_{\text{wake}} \Delta\varphi \frac{\partial\varphi}{\partial n} \, ds = -\frac{\rho}{2}\int_{\text{wake}} \Gamma v_n \, ds = \int_{\text{wing}} L' \frac{w}{V_\infty} \, dy = \int_{\text{wing}} \rho V_\infty \Gamma \frac{w}{V_\infty} \, dy = \rho \int_{\text{wing}} \Gamma \frac{w_{\text{Trefftz}}}{2} \, dy$$

downwash velocity at the wing *w* is defined positive downwards.

This set of relationships is simplified for an isolated and planar lifting surface.

So is this statement:

(If we know the lift force per unit span, $\rho V_\infty \Gamma$, we can find the induced drag force per unit span from the tilting of the lift vector through the downwash angle $\alpha_i = \tan^{-1}(w/V_\infty) \to w/V_\infty$.)

More fundamentally, induced drag is associated with irrecoverable losses to kinetic energy associated with creation of farfield flow components normal to the aircraft's flight path.

The key relationship here is $D_i = -\frac{\rho}{2}\int_{\text{wake}} \Gamma v_n \, ds$ which says that if we know the circulation distribution and the wake-normal induced velocity we can get the induced drag.

Furthermore, we can take the sum of contributions on the Trefftz plane (TP) of ALL the lifting surfaces, regardless of their axial (*x*) position. This is a really fundamental simplification, but we have to include the contributions of all the lifting surfaces to computing v_n along each wake trace on the TP.

Far-field (control volume) analysis

Thus far we have only considered the drag force (D) on objects inside the control volume and how that might be evaluated from information just on the Trefftz plane. Now we deal with the lift *L* and side force *Y*.

Recall:

$D = \boldsymbol{F}\cdot\hat{\boldsymbol{x}}$

$Y = \boldsymbol{F}\cdot\hat{\boldsymbol{y}}$

$L = \boldsymbol{F}\cdot\hat{\boldsymbol{z}}$

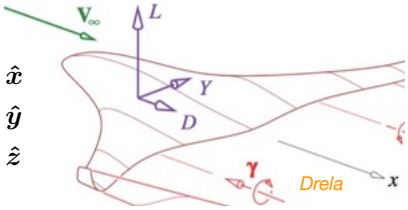

$$Y = \mathbf{F}\cdot\hat{\mathbf{y}} = \oiint_{\text{outer}} [(p_\infty - p)\,\hat{\mathbf{n}}\cdot\hat{\mathbf{y}} - \rho v\,(\mathbf{V}\cdot\hat{\mathbf{n}})]\;\mathrm{d}\mathcal{S}$$

$$L = \mathbf{F}\cdot\hat{\mathbf{z}} = \oiint_{\text{outer}} [(p_\infty - p)\,\hat{\mathbf{n}}\cdot\hat{\mathbf{z}} - \rho w\,(\mathbf{V}\cdot\hat{\mathbf{n}})]\;\mathrm{d}\mathcal{S}$$

After some manipulation (read Drela section 5.7) the surface integrals over the whole CV can be reduced to integrals confined just to the Trefftz plane, and then just along the trace of the wake on the Trefftz plane, which is where the trailing vorticity is concentrated:

$$Y = \rho_\infty V_\infty \iint_{TP} -z\,\omega_x\,\mathrm{d}n\,\mathrm{d}s = \rho_\infty V_\infty \int_0^{s_{\max}} -z\,\gamma\,\mathrm{d}s$$

$$L = \rho_\infty V_\infty \iint_{TP} y\,\omega_x\,\mathrm{d}n\,\mathrm{d}s = \rho_\infty V_\infty \int_0^{s_{\max}} y\,\gamma\,\mathrm{d}s$$

where $\gamma = \int_{n=-\infty}^{n=+\infty} \omega_x\,\mathrm{d}n$

However, since the trailing circulation strength is the spanwise/wake-trace (*s*) derivative of the circulation bound to the lifting surface, which is the same as the potential jump at the TE of the lifting surface involved,

$$Y = \rho_\infty V_\infty \int_0^{s_{\max}} z\,\frac{\mathrm{d}(\Delta\varphi)}{\mathrm{d}s}\,\mathrm{d}s = \rho_\infty V_\infty\, z\,\Delta\varphi\Big|_0^{s_{\max}} - \rho_\infty V_\infty \int_0^{s_{\max}} \Delta\varphi\,\frac{\mathrm{d}z}{\mathrm{d}s}\,\mathrm{d}s$$

$$L = \rho_\infty V_\infty \int_0^{s_{\max}} -y\,\frac{\mathrm{d}(\Delta\varphi)}{\mathrm{d}s}\,\mathrm{d}s = -\rho_\infty V_\infty\, y\,\Delta\varphi\Big|_0^{s_{\max}} + \rho_\infty V_\infty \int_0^{s_{\max}} \Delta\varphi\,\frac{\mathrm{d}y}{\mathrm{d}s}\,\mathrm{d}s$$

(integration by parts)

These terms are zero since the circulation (potential jump) falls to zero at each limit.

Far-field (control volume) analysis

$$Y = -\rho_\infty V_\infty \int_0^{s_{\max}} \Delta\varphi\frac{\mathrm{d}z}{\mathrm{d}s}\,\mathrm{d}s \equiv -\rho_\infty V_\infty \int_0^{s_{\max}} \Gamma_{\text{bound}}\frac{\mathrm{d}z}{\mathrm{d}s}\,\mathrm{d}s$$

$$L = +\rho_\infty V_\infty \int_0^{s_{\max}} \Delta\varphi\frac{\mathrm{d}y}{\mathrm{d}s}\,\mathrm{d}s \equiv +\rho_\infty V_\infty \int_0^{s_{\max}} \Gamma_{\text{bound}}\frac{\mathrm{d}y}{\mathrm{d}s}\,\mathrm{d}s$$

Change of variables [e.g. (dz/ds)ds ≡ dz] simplifies these integrals yet again:

$$Y = \rho_\infty V_\infty \int_{z_{\min}}^{z_{\max}} -\Delta\varphi\;\mathrm{d}z$$

$$L = \rho_\infty V_\infty \int_{y_{\min}}^{y_{\max}} \Delta\varphi\;\mathrm{d}y$$

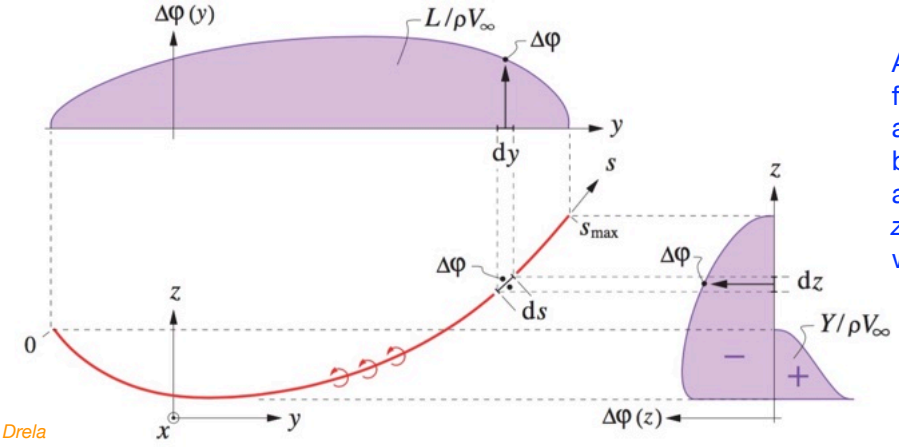

And we can see that the side force *Y* and lift *L* are evaluated as simple integrals based on the bound load per unit span $\rho_\infty V_\infty \Delta\varphi$ and its projection onto the *y* and *z* components of the trace of the wake on the Trefftz plane.

Figure 5.11: Far-field lift and sideforce are areas under projected $\Delta\varphi(y)$ and $-\Delta\varphi(z)$ distributions.

Far-field (control volume) analysis

From continuous to discrete maths.

$$D_i = -\frac{1}{2}\rho_\infty \int_0^{s_{max}} \Delta\varphi \frac{\partial\varphi}{\partial n}\, ds$$

$$Y = \rho_\infty V_\infty \int_{z_{min}}^{z_{max}} -\Delta\varphi \, dz$$

$$L = \rho_\infty V_\infty \int_{y_{min}}^{y_{max}} \Delta\varphi \, dy$$

For *Y* and *L* we can immediately approximate the integrals as

$$Y = \sum_{i=1}^{N} -\Delta\varphi_i \sin\theta_i \, \Delta s_i$$

$$L = \sum_{i=1}^{N} \Delta\varphi_i \cos\theta_i \, \Delta s_i$$

(see Drela fig 5.12) since

$$\Delta y_i = \cos\theta_i \, \Delta s_i \quad \text{and} \quad \Delta z_i = \sin\theta_i \, \Delta s_i$$

and where $\Delta\varphi_i$ is the accumulation of circulations contained in all the horseshoe vortices along chordwise strip of index *i*, carried down to the Trefftz plane, see fig. 6.6:

Finally we need to consider how the integrals we require could be approximated (on the TP) from a discrete vortex-lattice computation.

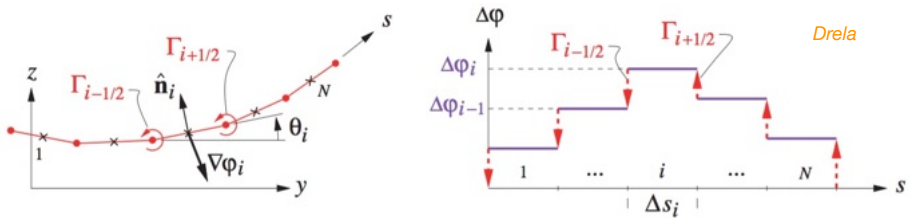

Figure 5.12: Wake paneling for evaluation of Trefftz-plane forces.

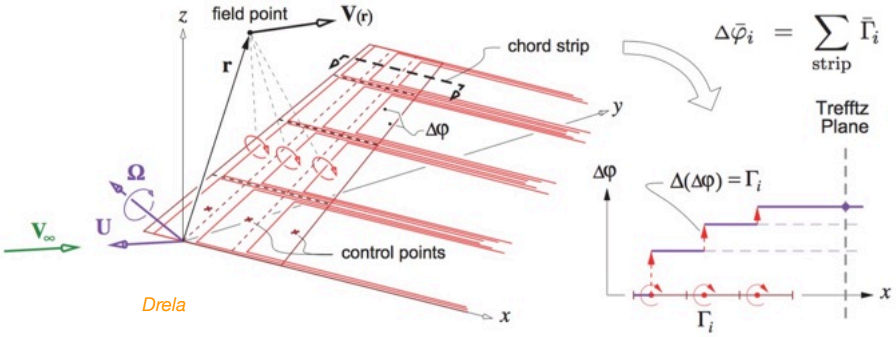

Figure 6.6: 3D lifting surface discretized by a Vortex Lattice of horseshoe vortices, which all contribute to the velocity $\mathbf{V}$ at any field point $\mathbf{r}$. Setting $\mathbf{r}$ at each control point allows imposition of flow tangency there. Each horseshoe vortex i also adds a contribution of Γ_i to the total potential jump $\Delta\varphi$ within its perimeter. Total accumulated $\Delta\varphi$ along a chord strip is the Trefftz-plane value shown in Figure 5.12.

Far-field (control volume) analysis

Drela

Now to deal with induced drag D_i.

$$D_i = -\frac{1}{2}\rho_\infty \int_0^{s_{max}} \Delta\varphi \frac{\partial\varphi}{\partial n}\, ds$$

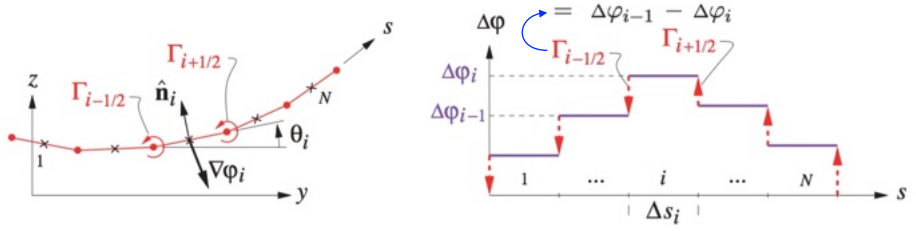

Figure 5.12: Wake paneling for evaluation of Trefftz-plane forces.

Now $\frac{\partial\varphi}{\partial n} = \nabla\varphi \cdot \hat{\boldsymbol{n}}$

where $\nabla\varphi = u\hat{\boldsymbol{x}} + v\hat{\boldsymbol{y}} + w\hat{\boldsymbol{z}} = (u, v, w)$ are velocity components induced by horseshoe vortices (lift!).

and ***n*** is a unit normal on the trace of the wake in the TP (has no *x* component).

We have the circulations for each chordwise strip upstream $\Delta\varphi_i$ from summations over vortices: $\Delta\bar{\varphi}_i = \sum_{strip} \bar{\Gamma}_i$

If we have the trailing horseshoe vortex strengths $\Gamma_{i\pm1/2}$, obtained from jumps in these net circulations (see fig 5.12) we can find the velocity components (v_i, w_i) that lie in the TP using the discrete HV model:

$$\nabla\varphi_i = \frac{1}{2\pi}\sum_{j=1}^{N+1} \Gamma_{j-1/2} \frac{\hat{\mathbf{x}} \times (\mathbf{r}_i - \mathbf{r}_{j-1/2})}{|\mathbf{r}_i - \mathbf{r}_{j-1/2}|^2} = \frac{1}{2\pi}\sum_{j=1}^{N+1} \Gamma_{j-1/2} \frac{-(z_i - z_{j-1/2})\hat{\mathbf{y}} + (y_i - y_{j-1/2})\hat{\mathbf{z}}}{(y_i - y_{j-1/2})^2 + (z_i - z_{j-1/2})^2}$$

NB: a vector quantity.

and then $\nabla\varphi_i \cdot \hat{\mathbf{n}}_i \equiv \frac{\partial\varphi}{\partial n_i} = \sum_{j=1}^{N} A_{ij}\, \Delta\varphi_j$ where ***A*** is a matrix of aerodynamic influence coefficients that depends only on wake geometry.

Finally we have all the quantities we require for a discrete approximation to the integral for D_i:

$$D_i = -\frac{1}{2}\rho_\infty \sum_{i=1}^{N} \Delta\varphi_i \frac{\partial\varphi}{\partial n_i} \Delta s_i$$

Recall that all these calculations for *Di, Y, L* are for inviscid contributions. We also need to include contributions related to BL drag, e.g

$$D_p = \rho V_\infty^2 \int_0^{s_{max}} \theta(s)\, ds$$

This can also be discretised.

Wing planform, twist, airfoil selection (subsonic)

The elliptical lift distribution

The **elliptical lift distribution** has a special significance.

$$\Gamma(y) = \Gamma_0 \sqrt{1 - \left(\frac{2y}{b}\right)^2}$$

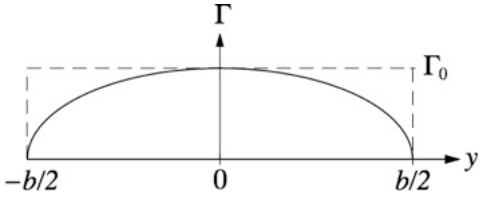

For this special case the downwash velocity is uniform across the span.

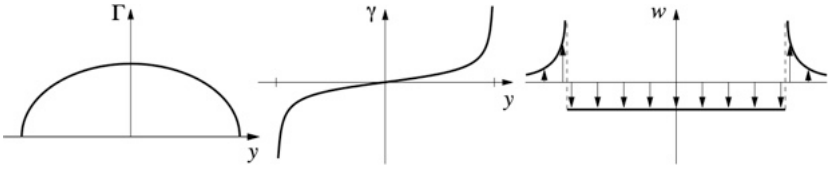

We recall the result from Aerodynamics 1 that the elliptical circulation distribution gives a spanwise-constant downwash velocity and (for a wing of fixed span) the least induced drag.

If the wing has no spanwise twist and a constant airfoil section, then this circulation distribution is provided by an elliptical chord distribution along the span. (Even better, the shape of the distribution remains elliptical, hence efficient, at all angles of attack – overall C_L – provided stall is not approached.)

However, an elliptical chord distribution is not always easy to arrange - and this shape is in any case only appropriate to straight unswept wings - so we need to consider what to do for more general wing planforms.

Load distributions on typical planforms

Shown below are three wing planforms without twist, along with their computed circulation distributions at some non-zero lift. The elliptic component of the circulation $2bV_\infty A_1 \sin\theta$ is shown as a dotted line.

Even the crude constant-chord wing is 96% efficient (at A = 10), while a double-tapered wing is clearly almost as good as a fully elliptic planform. Three-panel wings (not shown) are the practical ultimate.

NB: A = 10 in each case.

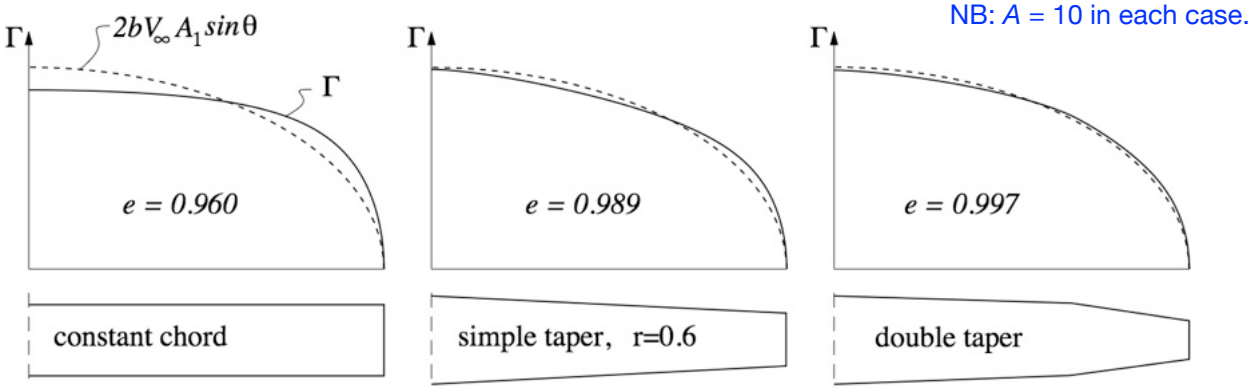

Note however that the value of e depends on the aspect ratio: surprisingly, as A increases a rectangular wing gets progressively *less* efficient than an elliptical one.

Lift vs C_l distribuitions

Another important consideration is the distribution of $C_l(y)$. Recall that $2\Gamma(y)/V_\infty = c(y)\,C_l(y)$

For an elliptic planform $C_l(y)$=const., otherwise it is variable, depending on the planform, overall C_L, and aerodynamic twist. How it varies is important for aircraft handling: tips that stall first are bad.

Lift (or load) distribution

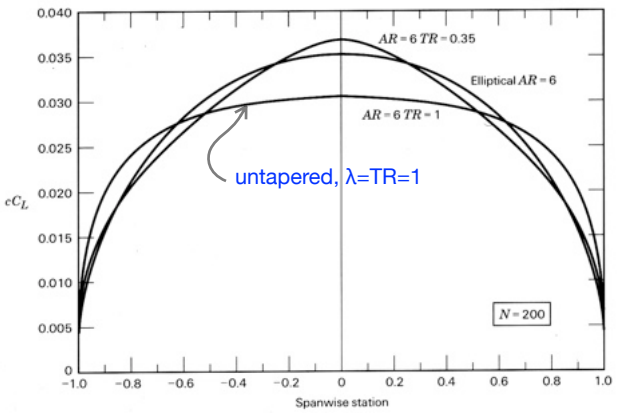

C_l distribution

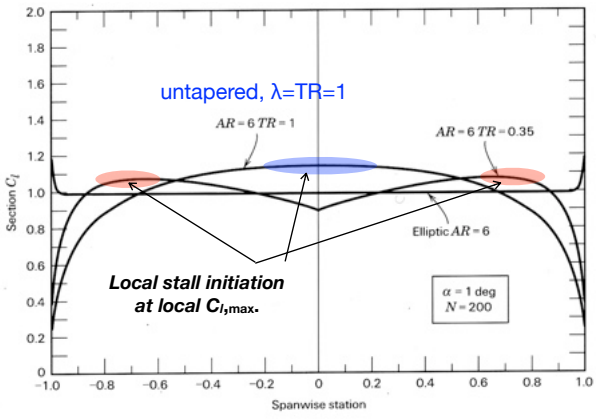

TR=λ=0.35 gives a reasonable approximation to elliptic load distribution but has elevated C_l for locations around 0.7 semispan - whereas the untapered wing has elevated C_l near the root. Thus the tapered wing will have lower induced drag but be more prone to tip-stall.

Note that for a non-elliptic planform it is only possible to achieve either an elliptic lift distribution or a chosen/constant C_l distribution using twist, not both. And this is only possible at one overall C_L.

The *basic* and *additional* lift distributions

The basic lift distribution is the spanwise distribution of $C_l(y)$ at C_L=0. It is in general non-zero owing to aerodynamic twist. Note that as speed increases and C_L reduces, this will become increasingly dominant.

The additional lift distribution is the spanwise distribution of $C_l(y)$ *for* the untwisted wing at some C_L.

These are added together with the aim of obtaining a favourable total $C_l(y)$ distribution (and also a favourable $c(y)\times C_l(y)$ distribution - e.g. elliptical) at design C_L.

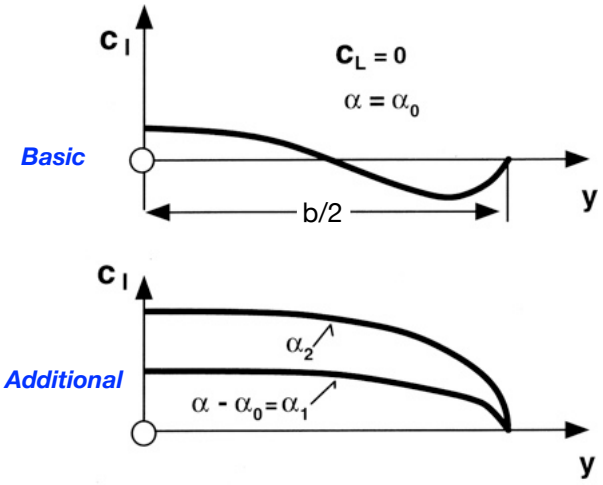

Fig. 55: Lift distribution on twisted wing.

- basic lift distribution for $\alpha = \alpha_0$
- additional lift due to angle of attack $\alpha - \alpha_0$

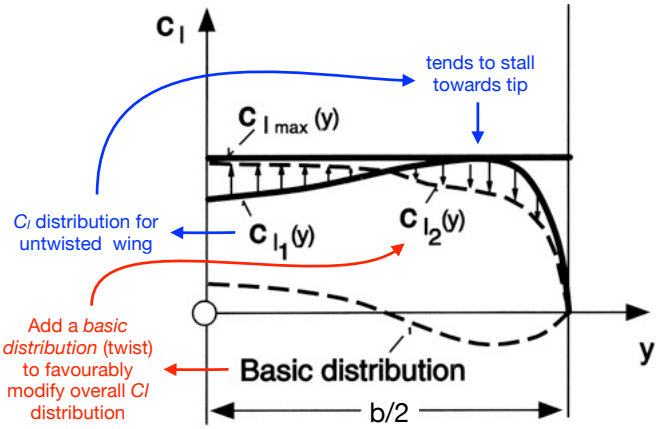

Fig. 56: Improved stall characteristics through superposition of an appropriate basic lift distribution.

But this manipulation does not guarantee good characteristics at other overall C_L values.

Localised effects owing to change of section

Deflection of a part-span flap will usually cause a significant distortion in load distribution, producing a significant increase in induced drag. The figure shows a constant-chord wing, with a central flap deflected 15°. The loading is strongly non-elliptic, and span efficiency has reduced to 0.840.

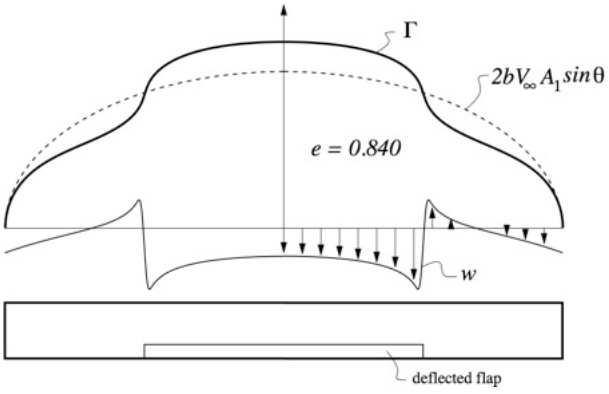

Note also the strongly non-uniform downwash distribution — there would be a strong trailing vortex at the discontinuity:

Taper and twist — 1

For trapezoidal subsonic wings, maximum span efficiency $e=1/(1+\delta)$ occurs for taper ratio $\lambda \approx 0.35$.

Note that as aspect ratio increases, plain trapezoidal wings have progressively lower span efficiency compared to an elliptical/ideal lift distribution.

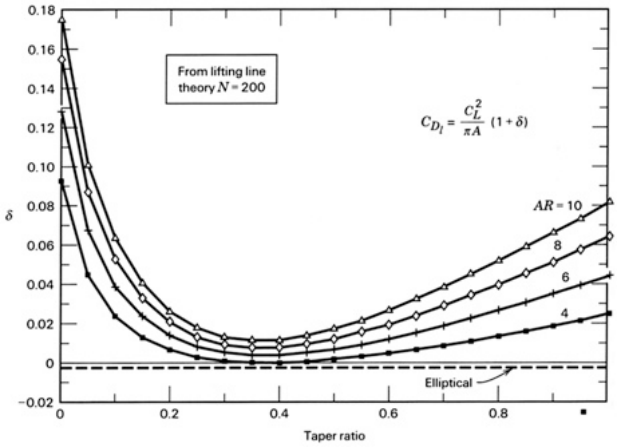

Using wing twist (geometric/aerodynamic) i.e. by altering the basic lift distribution we can perhaps do better and achieve an elliptic lift distribution at one design C_L.

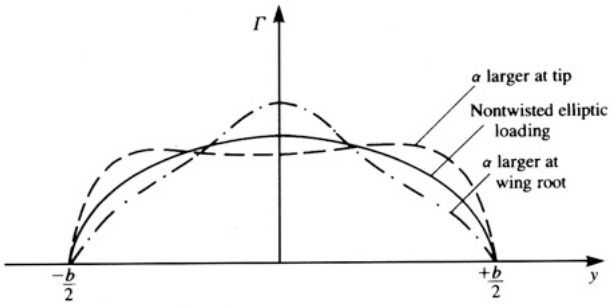

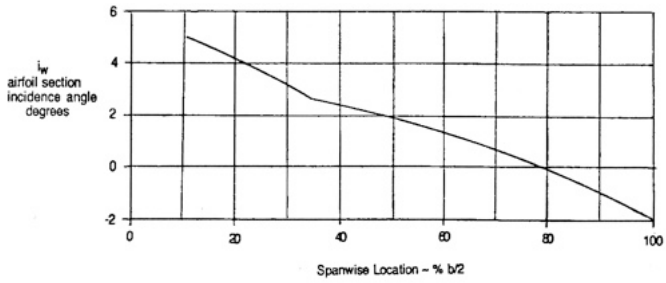

Fig. 4-11 Typical Wing Twist Distribution for a Jet Transport

Taper and twist — 2

However, highly-tapered wings also tend to have poor stall characteristics, which is revealed if we plot the ratio of local to overall lift coefficient.

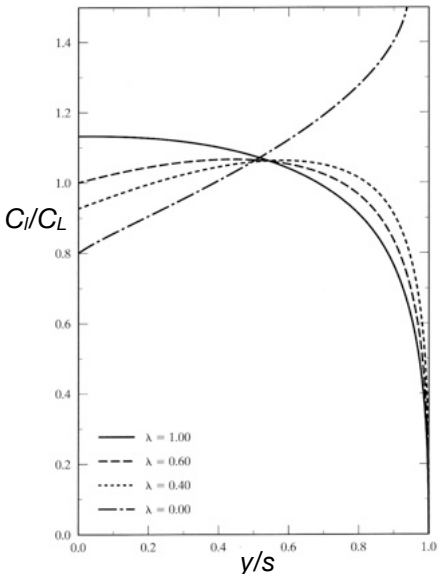

Progression of flow separation with C_L.

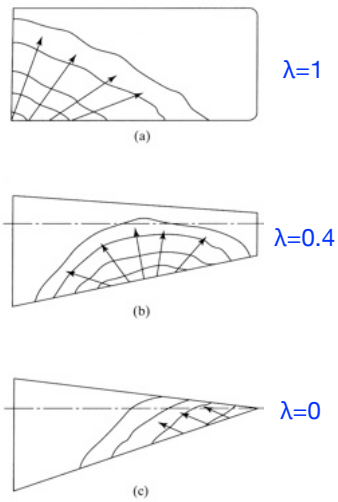

λ=1

λ=0.4

λ=0

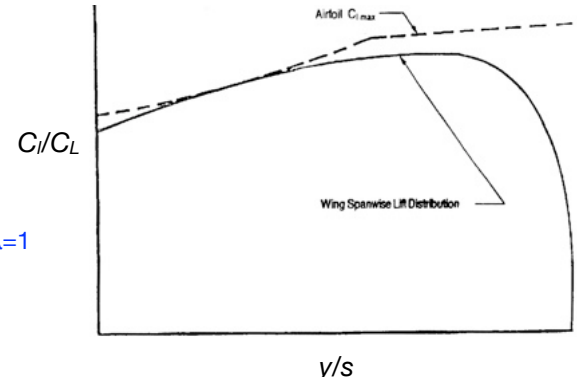

To an extent, we can compensate for this by changing airfoil selection so that earlier-stalling airfoils are used near the wing root. However, this degrades the overall maximum possible lift.

Taper and twist — 3

Some wings are so compromised by other design choices that either poor span efficiency or poor stall characteristics may have to be tolerated. Designs dominated by stealth are typical.

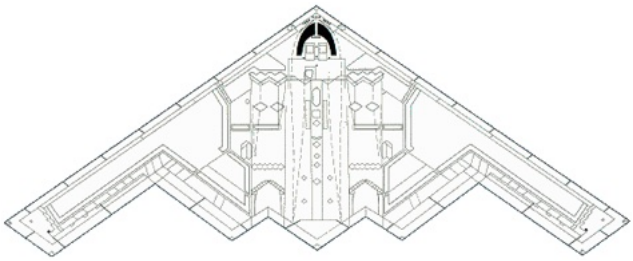

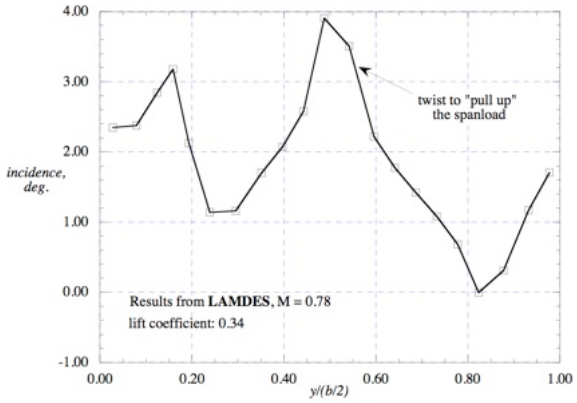

Fig. D-6. B-2 incidence distribution required for minimum induced drag.

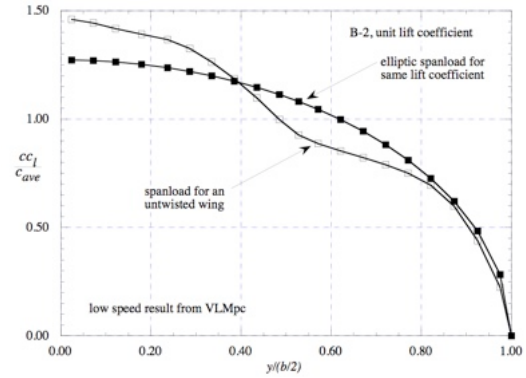

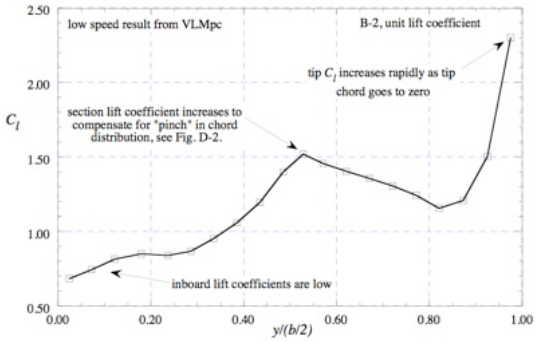

Figure D-5. Spanwise section lift coefficient distribution for the B-2

Taper and twist — 4

Flaps or other high-lift devices, non-full-span, both distort the load/C_l distribution when deployed (so decrease span efficiency) and increase local as well as overall maximum lift capability.

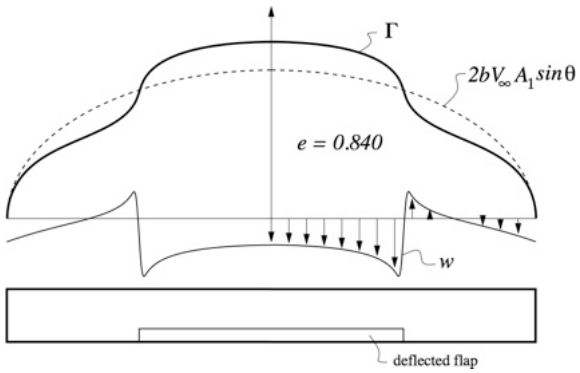

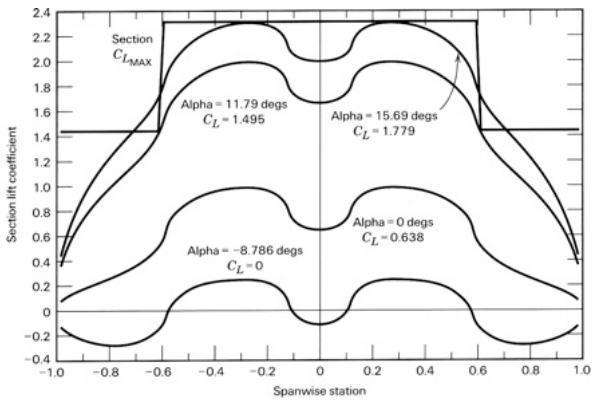

This may be helpful when we just want to maximize lift and don't care so much about span efficiency, e.g. for manouevre flaps.

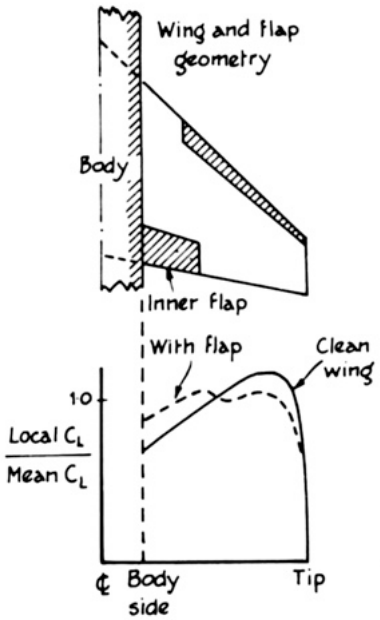

Case study of using twist and airfoil distribution to overcome tip stall for a fixed wing planform – using VSPaero VL solution

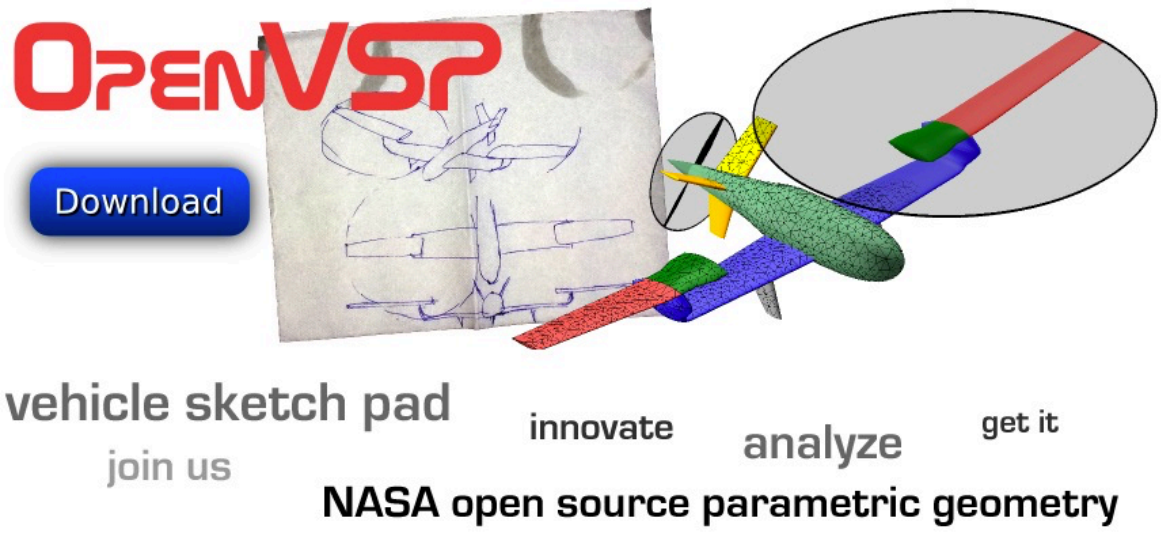

http://www.openvsp.org

http://www.openvsp.org/wiki

https://groups.google.com/forum/#!forum/openvsp

- Download executables
- Online documentation
- Where to look when problems occur

See also: Ex-youtube video files on Moodle in OpenVSP folder

OpenVSP – Vehicle Sketch Pad

A simple parametric modelling tool developed for aircraft-type geometries.

Warning: Open VSP is an open-source tool that is not completely reliable, or fully documented.

What it CAN do

1. Generate rendered/wireframe images suitable for conceptual design
2. Export .STP and files for use with other CAD packages
3. Simple/linear subsonic aerodynamic analysis using vortex lattice method - sufficient for neutral point and trim calculations, induced drag estimation. Can estimate wetted area.
4. Generate triangular surface meshes for suitable for import into CFD packages
5. Simplified/first pass Centre of Gravity estimation
6. Some limited internal layout
7. Handle propellor/rotor aerodynamics using actuator disk model

What it CAN'T do - things better done using CAD/FEA/CFD packages

1. Generate dimensioned 3-view drawings
2. Show control surfaces, windows, doors, etc. (*Can* be done but other tools may be better...)
3. Handle detailed internal layout (same comment)
4. Perform structural layout or analysis
5. Estimate maximum C_L or handle high-lift systems, transonic or supersonic aerodynamics

Example: MD90 approximation

Example starting from existing 3-view of an MD90 (as in video tutorial 5).

For initial/conceptual design only a limited amount of detail is required – about the level one would include in a first-pass wind tunnel or CFD model.

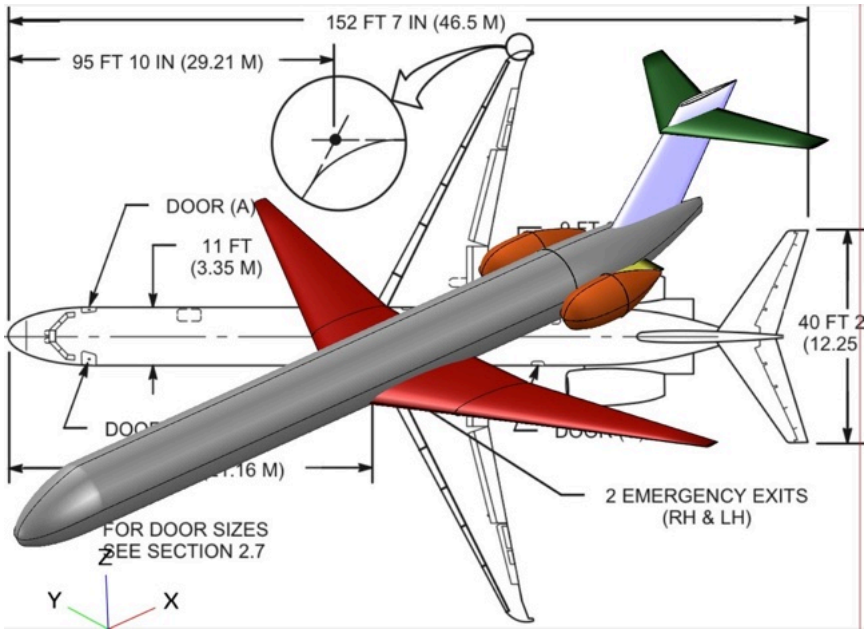

Analysis for the wing geometry for the model as built (not exact) gives:

S_{ref} = 124.0
c_{ref} = 4.71 (MAC, external calculation)
b_{ref} = 33.0.

These data are supplied as the first three lines of the XX_DegenGeom.vspaero file.

I also supplied α = AoA = 2°, also set the wing at an incidence angle of 1.5°, and used a NASA SC(2)-0714 wing airfoil.

The wing apex was at X = 0.558.

We will cover aerodynamic analysis based on OpenVSP shortly. For now, find out how to generate geometry and export .STP files for use with Solidworks/Creo/other CAD.

VSPaero

1. *vspaero* is a vortex-lattice solver that will compute linear aerodynamics.
2. It can find many useful things such as
   a. $dC_L/d\alpha$ for finite wings or whole vehicle
   b. Induced drag estimation
   c. Span loading (distribution of lift force along span)
   d. Stability derivatives and from this, location of aircraft Neutral Point and CG
3. Some of these capabilities are presently only available from running the tool via the command line and looking in files that are produced.

Online reference for *vspaero*

http://www.openvsp.org/wiki/doku.php?id=vspaerotutorial

References for vortex lattice method (all available in library)

1. Sforza, “Commercial Airplane Design Principles” Butterworth Heinemann 2015, App C
2. Kuethe and Chow, “Foundations of Aerodynamics” 5e, Wiley, 1998
3. Drela, “Flight Vehicle Aerodynamics”, MIT Press 2014, Chapters 2 and 6
4. Katz and Plotkin, “Low Speed Aerodynamics”, 2e, Cambridge University Press 2001
5. McBain, “Theory of Lift, Wiley 2012, Chapter 14

VSPaero

Before getting started with more detailed analyses with the command-line tools, it is best to check the geometry is OK by making a solution using the *vspaero* GUI in *vsp*. (You will have to make a “degenerate geometry” before running the solver.) Check the computed ΔC_p distribution and vortex wakes look reasonable. If the solver takes a few hundred iterations to converge on each iteration, rather than *O*(20), there is likely something wrong.

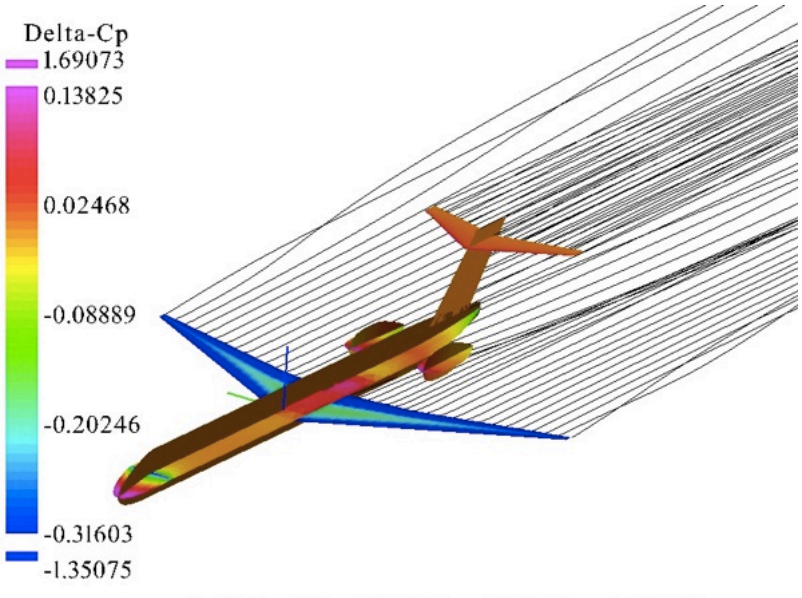

Pressure coefficient contours and vortex wake arrangement for the MD90 model shown earlier.

In order to get a reliable computation it proved necessary to delete from the model some stub pylons connecting engine pods to fuselage.

Note the “degenerate geometry” used in the analysis: round features such as fuselage and pods are represented by flat/ cruciform approximations. This is good enough for preliminary aerodynamic estimates.

Wing analysis using *vspaero*

Preliminary analysis and optimization of wing performance can be carried out with *vspaero* – enough to get the geometry into the right ballpark. It is best to deal with the wing on its own at this stage – delete other parts.

The main issues to be dealt with are balancing low-speed (stall) performance with cruise performance (induced drag minimization). A first pass at these two things can be made with the linear aero tools that *vspaero* provides.

The tradeoffs are especially demanding for swept wings – and these cannot adequately be dealt with using Prandtl's lifting line theory. A numerical tool such as *vspaero* is the only real option.

We will take the wing planform geometry as given, choose an airfoil family, and vary the wing's thickness and twist distribution to balance stall and induced drag performance.

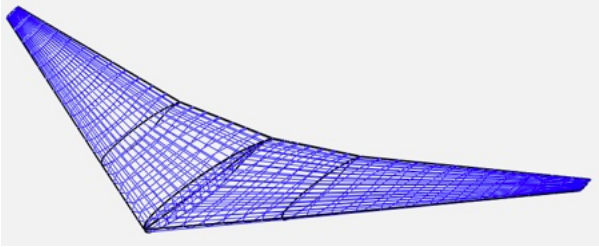

Choose an airfoil family. For swept jet transport aircraft, 'supercritical' sections are the norm. I used a NASA SC(2)-0714 which is 14% thick and has design (cruise) C_l = 0.7. (Neither the exact airfoil nor its thickness are critical at this stage, but a reasonably thick airfoil is to be preferred.)

I went to www.airfoiltools.com, put in 'supercritical' as a search term, downloaded a .dat file for the chosen airfoil. More extensive options at the UIUC airfoil database.

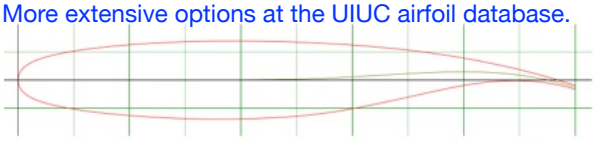

Load this airfoil into VSP under the Wing/Airfoil tab. Initially at least, all sections 0, 1, 2 (root through tip).

Spanwise lift distribution

The spanwise lift distribution $c(y)\times C_l(y)$ is proportional to the circulation distribution $\Gamma(y)$ and tells us how lift force per unit length is distributed along the span. Integral is prop. to the wing's total lift coefficient C_L.

We can also use $\Gamma(y)$ to compute the wing's shear force and bending moment diagram.

Recall that according to lifting line theory (developed for unswept wings) $\Gamma(y)$ should be as close as possible to an elliptical distribution in order to maximize span efficiency e (minimize induced drag).

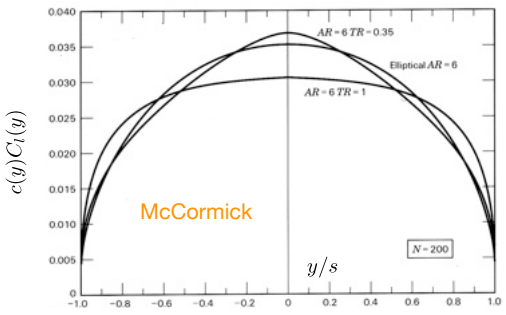

$$2\Gamma(y)/V_\infty = c(y)\,C_l(y)$$

From $\Gamma(y)$ we can work back and estimate the local C_l value (and how close it is to $C_{l,max}$).

Stall is predicted to initiate at the spanwise location where C_l first reaches $C_{l,max}$.

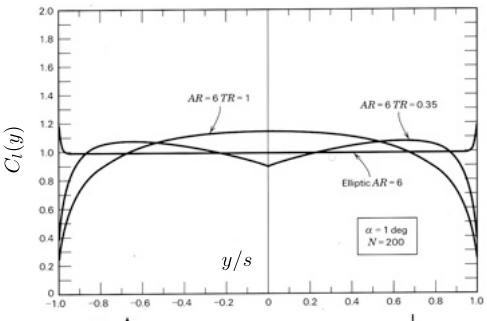

Very often, twist (typically, 'washout': airfoil twisted nose-down) is introduced in order to influence $C_l(y)$. In turn this alters $\Gamma(y)$ and hence the wing's span efficiency.

Adding twist also makes the shape of $\Gamma(y)$ a function of overall C_L (or α). The zero-C_L $\Gamma(y)$ is called the 'basic' lift distribution, and the remainder from the total $\Gamma(y)$ at any particular C_L is the 'additional' distribution.

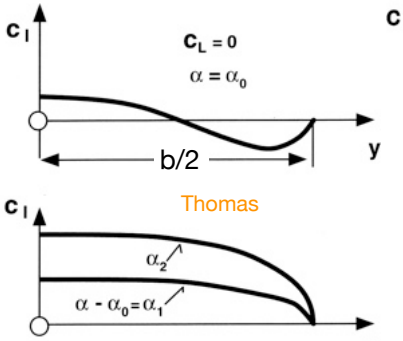

Fig. 55: Lift distribution on twisted wing.
- basic lift distribution for $\alpha = \alpha_0$
- additional lift due to angle of attack $\alpha - \alpha_0$

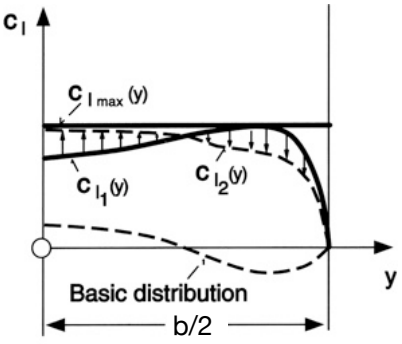

Fig. 56: Improved stall characteristics through superposition of an appropriate basic lift distribution.

Swept wing subsonic aerodynamics

The basic reason for choosing a swept wing is to delay the Mach number for onset of transonic drag rise.

However, introducing sweep has a number of undesirable aerodynamic (not to mention structural) side effects. Compared to an unswept wing of the same aspect ratio, sweep

1. Alters the spanwise circulation distribution to lower the span efficiency (increases induced drag);
2. Associated with this, relatively increases the loading on the wing tips compared to the root, promoting tip stall;
3. Decreases the lift curve slope of the wing.

To mitigate these effects, the designer chooses the least sweep that will acceptably delay transonic drag rise and alters geometry (chord, twist and airfoil distributions along the span) to achieve an acceptable compromise between the first two of these items.

Reminder: we are taking the planform (span, area, sweep and chord distribution) as fixed parameters. That leaves us with airfoil section (chiefly, its thickness, in order to change the local maximum C_l) and twist (a.k.a. washout) distributions along the span as design variables.

Problem: twisting the wing to avoid stall at the tips changes the spanwise lift distribution and typically lowers the span efficiency at all angles of attack. It may also make the tips produce negative lift at low C_L (i.e. high speed).

Problem: Making the airfoil thinner near the root (to decrease sectional C_{lmax} and hence promote root stalling first) ultimately lowers the wing's overall maximum C_L capability, reduces wing volume (fuel capacity) and strength (or for same strength, increases the weight). Conversely, increasing tip thickness, while reducing susceptibility to tip stall, lowers the drag-divergence Mach number.

The aerodynamic design engineer's task is to find an acceptable compromise between the conflicting requirements.

Swept wing subsonic aerodynamics

1

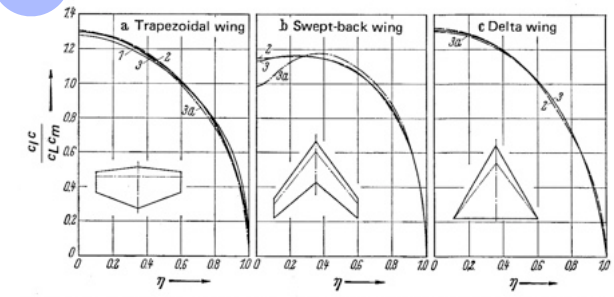

Figure 3-36 Lift distribution $c_l c/c_L c_m$ of three wings without twist of Table 3-5 and Fig. 3-33, $c'_{L\infty} = 2\pi$; $c_m = A/b$ = mean wing chord. Curve 1, simple lifting-line theory of Multhopp. Curve 2, extended lifting-line theory of Weissinger. Curve 3, lifting-surface theory of Truckenbrodt. Curve 3a, lifting-surface theory of Wagner (five-chord distributions).

2

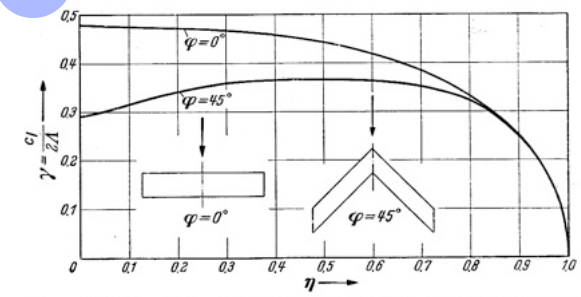

Figure 3-47 Circulation distribution and distribution of the local lift coefficients over the span for two wings of constant chord; aspect ratio $A = 5$, sweepback $\varphi = 0$ and $\varphi = 45°$; $c'_{L\infty} = 2\pi$; $\alpha = 1$; lifting-surface theory of Truckenbrodt [84].

Compared to an unswept wing of the same aspect ratio, sweep

1. Alters the spanwise circulation distribution to lower the span efficiency (increases induced drag);
2. Associated with this, relatively increases the loading on the wing tips compared to the root, promoting tip stall;
3. Decreases the lift curve slope of the wing.

3

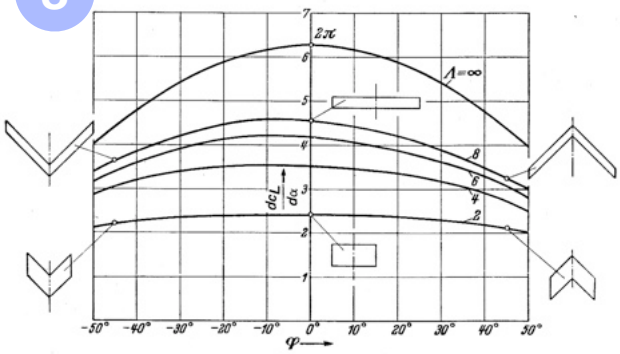

Figure 3-46 Lift slope of swept-back wings of constant chord vs. sweepback angle φ and aspect ratio A, from [103]; extended lifting-line theory. Curve for $A = \infty$: cos φ law from Eq. (3-123).

All figures here from
Aerodynamics of the Airplane
by Schlichting & Truckenbrodt.

Tip stall mitigation, clean configuration

Process (assuming sweep and basic airfoil have been chosen)

1. Estimate the tip panel airfoil $C_{l,max}$ based on the chosen basic airfoil and Fig. 11.4.
2. Estimate corresponding wing design overall $C_{L,max}$ based on Fig. 11.5 and basic wing sweep at *c/4*.
3. At an appropriate overall wing angle of attack required to achieve this value of $C_{L,max}$, choose a wing twist distribution *and* thickness distribution such that stall initiates well towards the wing root, as shown in Fig. 11.2.
4. The wing thickness distribution is not simple to change in VSPaero unless we have .dat files for a family of related airfoils*. For now we will ignore this. Reduce the wing angle of attack to place overall wing C_L at the design cruise value and compute span loading and span efficiency.
5. If span efficiency is too low, be prepared to iterate!

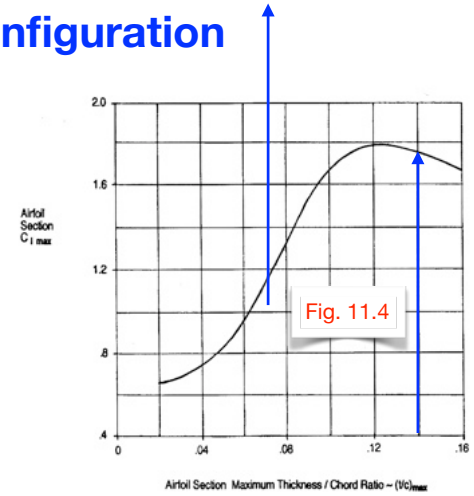

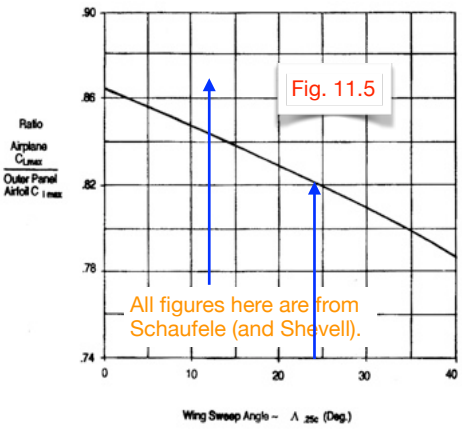

The final wing cruise angle of attack and twist distribution are inserted into the whole-aircraft .vsp3 file for computation of the neutral point and CG location.

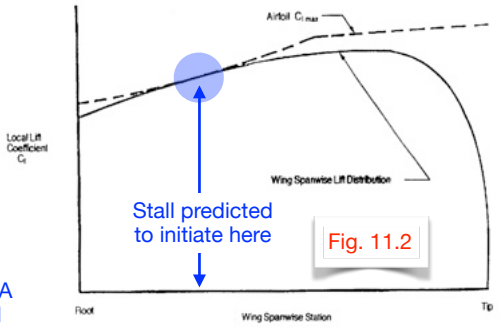

Fig.11-2 Span Loading/Airfoil $C_{L\,max}$ Relationship for Proper Stall

* Airfoil .dat files for all the NASA SC(2) supercritical foils detailed in NASA TP-2969 can be found at http://m-selig.ae.illinois.edu/ads/coord_database.html#N

Using *vspaero* for wing performance analysis

Read

http://www.openvsp.org/wiki/doku.php?id=vspaerotutorial

We have already set the wing planform and (initial) airfoil choice, and the wing is (so far) untwisted.

The process for using *vspaero* to perform wing performance analysis using the GUI is

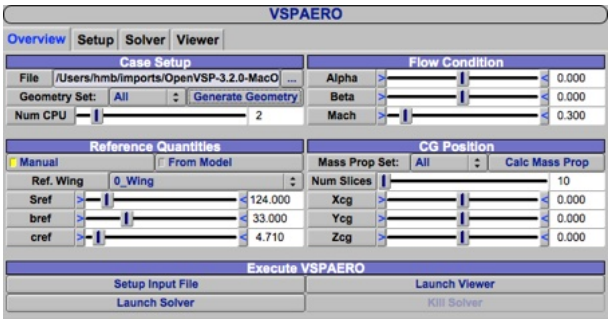

1. Create a 'degenerate geometry' using Analysis --> DegenGeom or VSPAERO --> GenerateGeometry to write out files XX_DegenGeom.csv, and .m;
2. Set Reference Quantities and Flow Condition under VSPAERO menu (note you should have the wing area *Sref*, span *bref* and MAC *cref* precomputed. Then 'Setup Input File' to write out XX_DegenGeom.vspaero;
3. Launch Solver. When it has terminated you may want to check the solution using LaunchViewer --> Aero --> Delta-Cp and Wakes;
4. Examine the XX_DegenGeom.history file to see Span Efficiency (*E*) and *CL, CDi* (you are advised not to trust the estimates of CDo and CDtot here). Examine/plot the XX_DegenGeom.lod file to see the distribution of *c* and C_l. Compute and plot the lift distribution ($c \times C_l$ vs *y*).

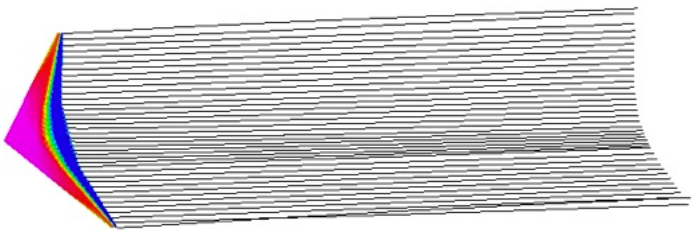

Using *vspaero* for wing performance analysis

Note the approximation by a simple trapezoid to estimate sweep angle.

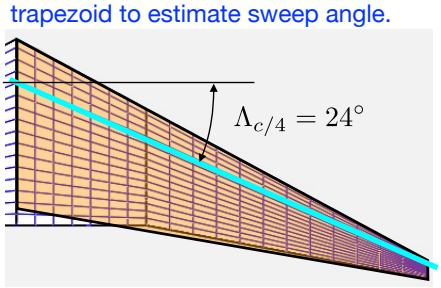

Relationship between local circulation and the product of local chord and C_l:

$$\Gamma(y) = \tfrac{1}{2} V_\infty c(y) C_l(y)$$

Now, if we plot the ratio $\dfrac{c(y)C_l(y)}{c_g C_L}$

using the geometric mean chord $c_g = S/b$

we can always compare this to the normalised elliptical (optimal) distribution

$$\frac{2\Gamma_0}{V_\infty c_g C_L}\sqrt{1-\left(\frac{y}{b/2}\right)^2} = \frac{4}{\pi}\sqrt{1-\left(\frac{y}{b/2}\right)^2}$$

which gives span efficiency e = 1.

This comparison gives us some indication of efficient ways in which to vary the twist distribution.

Using Schaufele's correlations:

Based on our assumed 14% tip airfoil thickness (probably too large), sectional maximum C_l = 1.75.

Based on $c/4$ sweep, (clean airplane $C_{L,max}$)/(tip $C_{l,max}$) = 0.82.
So the estimated clean $C_{L,max}$ = 1.75 × 0.82 = 1.43.

Back to *vspaero*:

For orientation, below we show the loading distribution for the untwisted wing at zero AoA, α = 0°, calculated using *vspaero.*

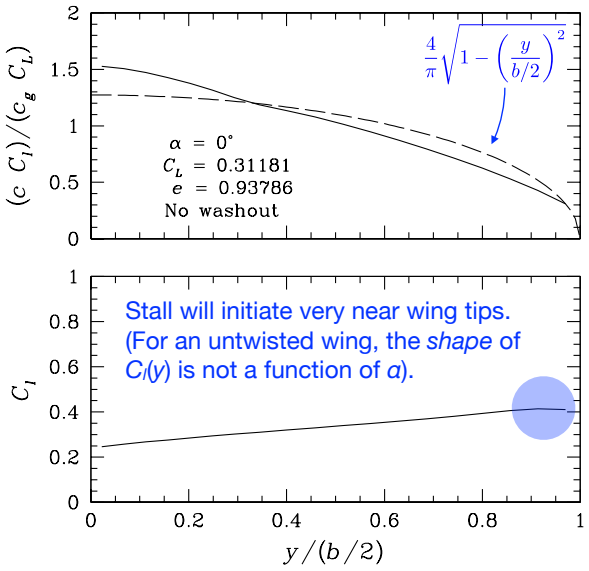

Using *vspaero* for wing performance

As a first pass, choose a linear tip washout of 10° and leave the centre panel untwisted.

After a few computations at different α, we find α = 12.5° gives C_L = 1.42.

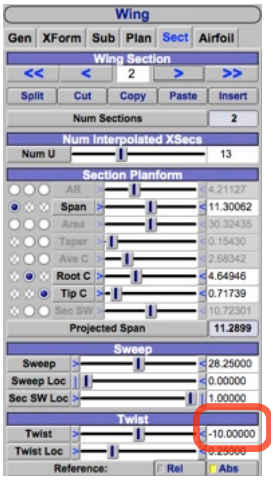

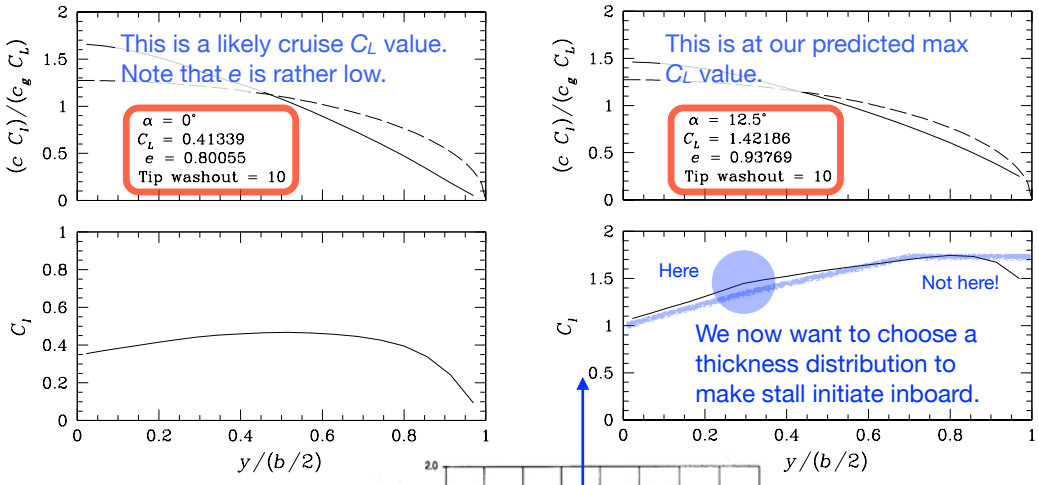

Examination of Schaufele's correlation suggests that making the airfoil 8% thick at the taper break and 6% thick (or maybe a bit less) at the wing root could be acceptable.

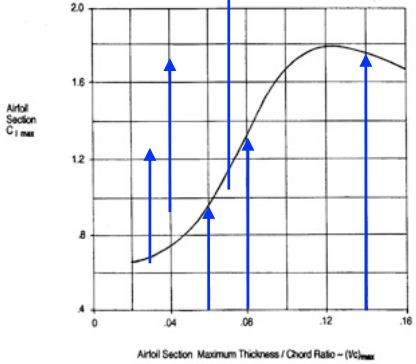

So now we can install those sections and re-run the analysis.

In fact in the NASA SC(2) family, we can only locate 4%, 6%, 10% and 14% thick foils: We will make do with 6%, 10%, 14% progression in our analysis and assume the airfoils can be designed.

We also note a concern that our cruise span efficiency may be unacceptably low.

Using *vspaero* for wing performance analysis

Here are the outcomes of analysis at α = 12.5° (assumed $C_{L,max}$) and α = 2° (assumed cruise C_L = 0.5) with the new airfoils, still with 10° washout at end of tip panels.

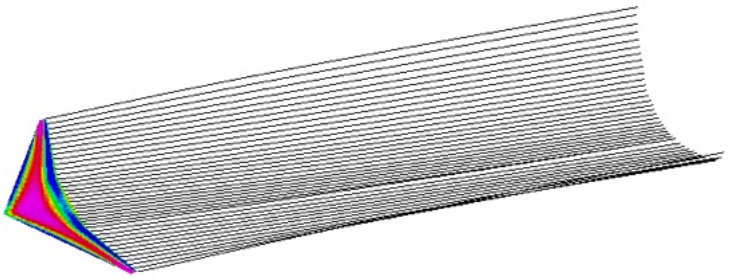

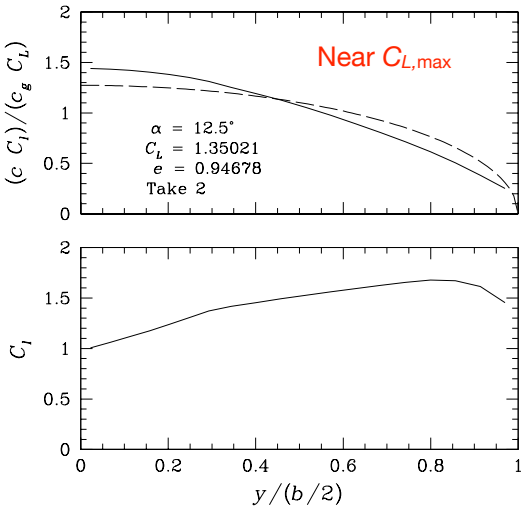

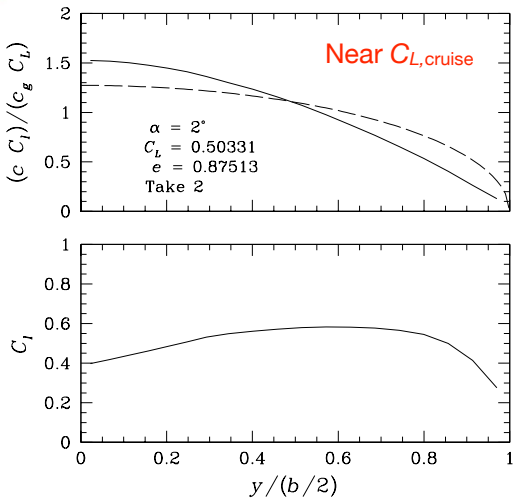

We note that the cruise value of span efficiency has now picked up to 87.5%, which is possibly acceptable.

Next we move on to stability analysis and setting the CG position for a required static stability margin.

Leading wing parameters and their selection

Approaches to wing design

1. **Direct**: find the planform and twist that minimize some combination of structural weight, drag, and $C_{l_{max}}$ constraints.
2. **Inverse**: select a desirable lift distribution and then obtain the twist, taper and thickness distributions that are required to achieve this distribution.

Notes:

1. The inverse method is used to obtain analytic solutions and insight in the design problem but it is difficult to incorporate constraints and off-design considerations.
2. The direct method, together with numerical optimization, is used in the later stages of wing design.
3. Other considerations may be important:
    a. Lift-curve slope, both for gust response and for the “tail-scrape” problem at take-off;
    b. Fuel and undercarriage storage;
    c. Transonic/spanwise flows and isobar contouring;
    d. Low wave drag if aircraft is to be supersonic.

Aerodynamic goals of wing design

While there are a wide range of wing design goals that are not strictly aerodynamic in origin, it is worthwhile listing those that are:

1. Minimum drag and especially minimum induced drag.
2. Delay or supression of flow separation, or increase maximum lift.
3. Increase drag-divergence Mach number.
4. Reduce wave drag (supersonic).

Relevant parameters:

1. Aspect ratio
2. Lift distribution. Depends on taper, twist and airfoil section distribution.
3. Sweep.
4. Thickness/chord ratio, camber, cross-section distribution (supersonic).

Design parameters — span, *b*

Span may be directly constrained by contest rules or ground facilities but otherwise, since for a given wing loading W/S the induced drag C_{Di} is inversely proportional to b^2, typically the largest span consistent with structural dynamics constraints (flutter) will be considered.

However, as the span increases the wing root bending moment and hence wing weight will also, and at some point this will overcome the induced drag benefit (because the wing loading increases, forcing a higher C_L). In practice this point is rarely reached because:

1. The optimum on the induced drag vs span curve is quite flat so a large increase in span is required to reach it;
2. Other constraints related to structural stiffness (divergence/flutter) become more pressing;
3. The cost of the wing increases with span/weight. We might spend a lot of money for small overall drag benefit;
4. The volume of the wing in which fuel can be stored is reduced — for a given wing area and t/c ratio, wing volume is inversely proportional to span;
5. It becomes more difficult to locate the main landing gear within the wing root;
6. Wing *Re* is reduced, increasing profile drag and reducing peak lift capacity.

Increased wing span (reduced induced drag) may be of benefit away from the nominal cruise design point (where e.g. $C_L^{1/2}/C_D$ is maximized) but where C_L/C_D must be maximized instead, e.g. during 'second-segment' climb, particularly in an engine-out condition.

For *supersonic* flight however, it is generally better to have small wing spans (or aspect ratios), since this reduces wave drag, mainly dependent on the overall aircraft fineness ratio.

Design parameters — area, *S*

Wing area (or loading), like span, selection is influenced by a number of considerations:

1. Cruise drag;
2. Stalling speed / field length requirements;
3. Manouevres: sustained/instantaneous turn rates;
4. Maximum speed;
5. Wing structural weight and cost;
6. Fuel volume (proportional to $S^{3/2}$)

In general, choose the smallest wing area allowed by the constraints — this also minimizes wing cost.

However wing area may need to be increased in order to reduce C_L required at cruise conditions.

Because there potentially is an interaction with cruise altitude and speed (if these are not fixed) we may need to consider the influence of these factors on engine performance.

Design parameters — sweep, Λ

Sweep is chosen to reduce transonic wave drag.

1. Higher cruise Mach number, or greater thickness/C_L at a given M_∞ without drag divergence
2. Increases tip loading and causes spanwise BL flow → increases tip stall (or reduces $C_{L\max}$).
3. Increases structural weight as for a given span it increases the effective wing length;
4. For conventional sweep: aeroelastically stabilizes wing but destabilizes aircraft (high-α pitchup);
5. Too much sweep makes it difficult to accommodate the main gear in the wing;
6. Effect is basically similar for forward/aft sweep, although there are detail differences.

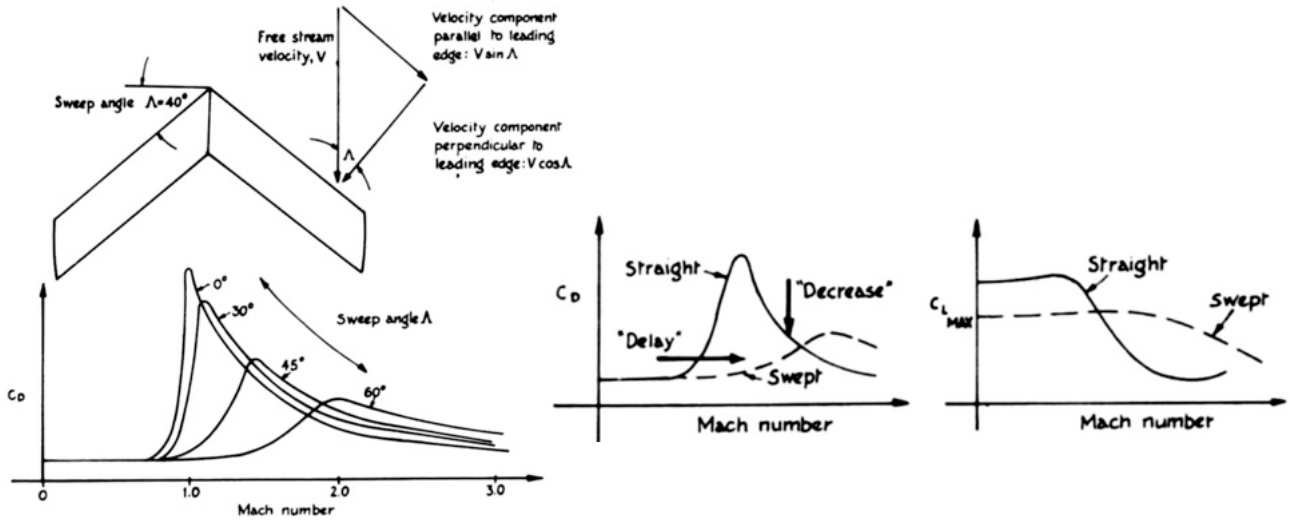

Design parameters — thickness, *t/c*

Increasing *t/c*:

1. increases bending strength, reduces wing structural weight (or increases possible span);
2. (up to a point) increases $C_{l\max}$ but gains are small above approx. 12%;
3. increases fuel volume and wing stiffness;
4. increases drag slightly, even in the absence of transition or separation produced by adverse pressure gradients;
5. reduces the drag-divergence Mach number.

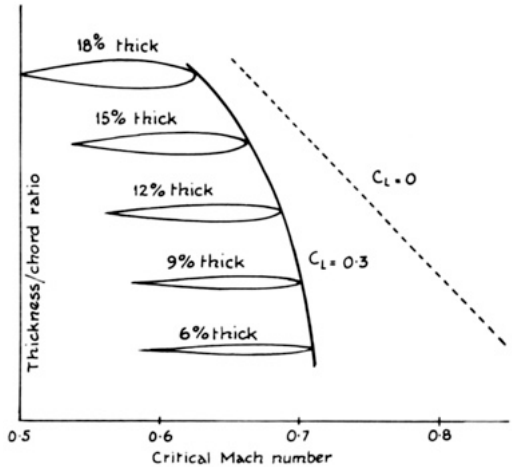

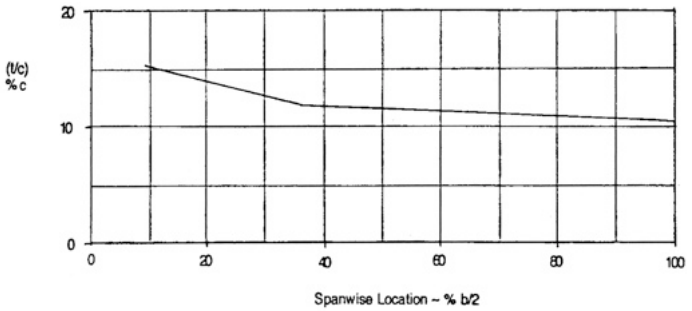

Typically, *t/c* values are greater at wing root than at tip.

Design parameters — taper, λ

1. Planform shape should not produce a lift distribution that is so far from elliptical that the twist distribution for design point/cruise drag produces large off-design induced drag penalties(elliptical is best over a wide speed range);
2. The associated C_l distribution at design point should be compatible with the required section polar performance point (e.g. $C_l^{1/2}/C_d$max);
3. The C_l distribution should not overload wing tips (i.e. promote tip stall);
4. Lower taper ratios lead to lower wing weight since they lead to thicker wing roots
5. Lower taper ratios result in increased fuel volume;
6. Lower taper ratios reduce tip Reynolds number, degrading overall performance and local $C_{l\text{max}}$;
7. Lower taper ratios/larger root chords more easily accommodate landing gear.

Generally, try to keep λ small as possible to reduce wing weight, without degrading aerodynamic performance.

Design parameters — twist

Twist distributions are used to compensate for non-ideal lift distributions (planforms) — or local stall tendencies — however complete compensation can only be achieved at one C_L or design point.

1. Twist distribution must be chosen so that the cruise (design point) induced drag is not excessive;
2. Extra washout reduces the risk of tip stall at high C_L (also increases induced drag at higher speeds);
3. Twist distribution changes the structural weight (perhaps detrimentally) because it modifies the moment distribution over the wing;
4. Washout on a swept-back wing produces an incremental positive pitching moment which has a small effect on the trimmed drag.
5. Wing flexure under load may produce extra washout on a swept wing, lowering a tendency to tip-stall in high-load manouevres.

The twist distribution is typically chosen as trade-off between cruise and other design points, then a little more washout is added to improve stall characteristics.

It is also possible to control/influence tip stall using ‘aerodynamic washout’, which is the use of airfoil sections with lower camber (and lower $|\alpha_0|$) or larger $C_{l\text{max}}$ near the wing tips.

Design parameters — dihedral

Wing dihedral provides a stabilising coupling between sideslip and roll, and the amount is determined by handling/lateral stability requirements.

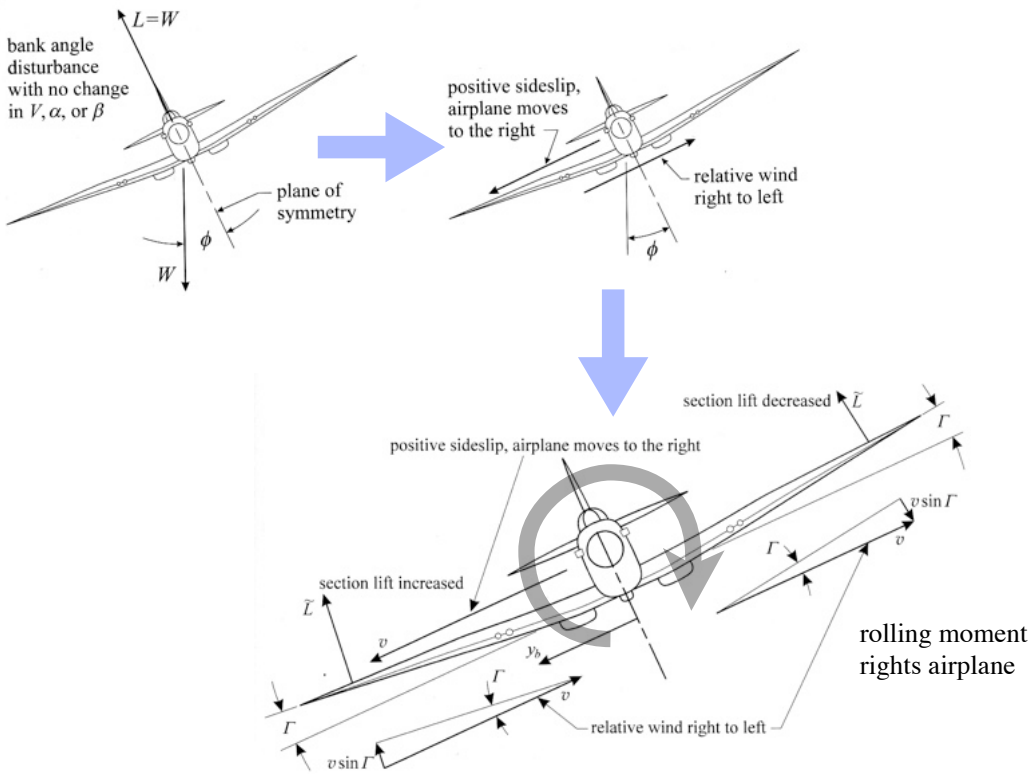

Transport aircraft parametric study — 1

J Chuprun (1980)

4-engine subsonic jet transport, same design payload and range, vary wing area and aspect ratio.

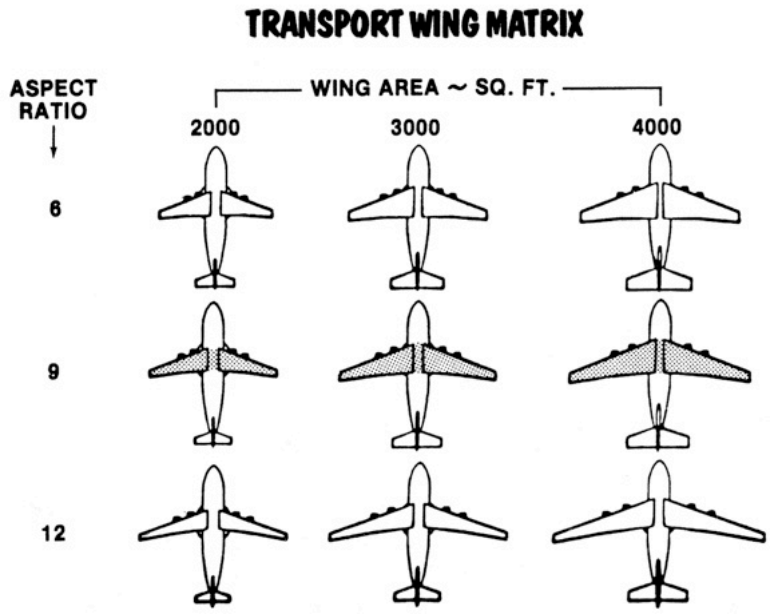

Transport aircraft parametric study — 2

WING WEIGHT

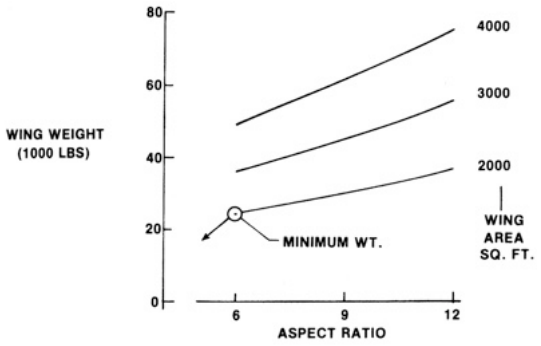

AIRPLANE LIFT TO DRAG RATIO

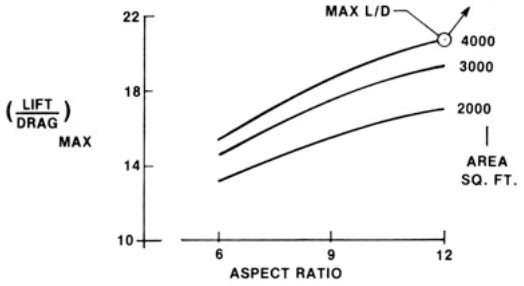

AIRPLANE GROSS WEIGHT

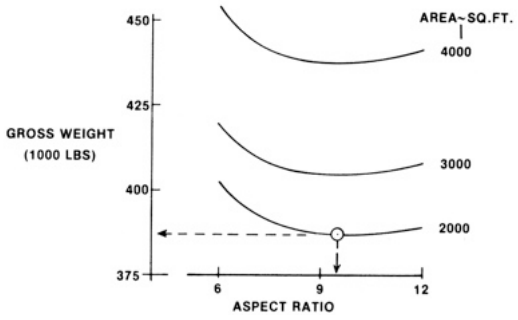

AIRPLANE EMPTY WEIGHT

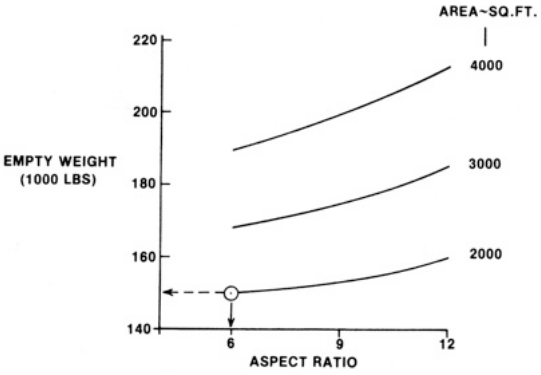

Transport aircraft parametric study — 3

FUEL REQUIRED

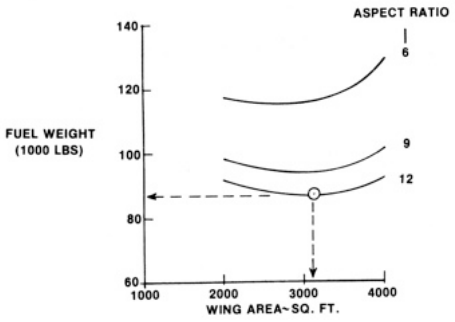

OFF-DESIGN CAPABILITIES

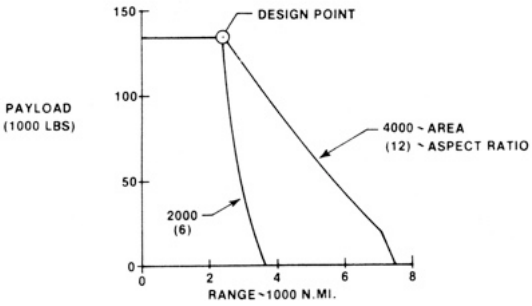

TAKE-OFF DISTANCE

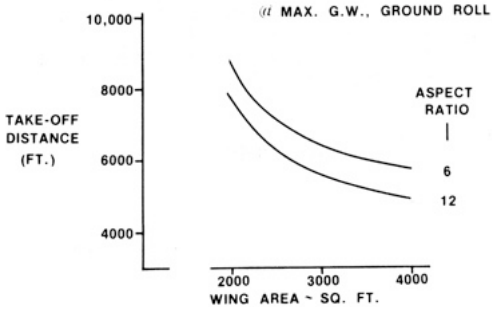

LANDING DISTANCE

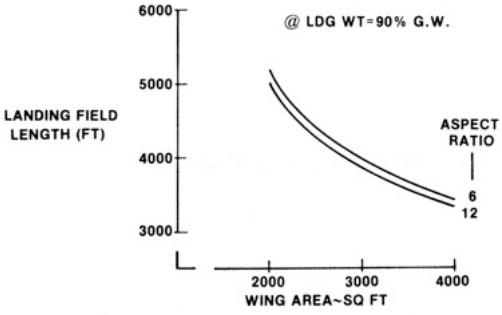

Transport aircraft parametric study — 4

The `second segment climb' problem:

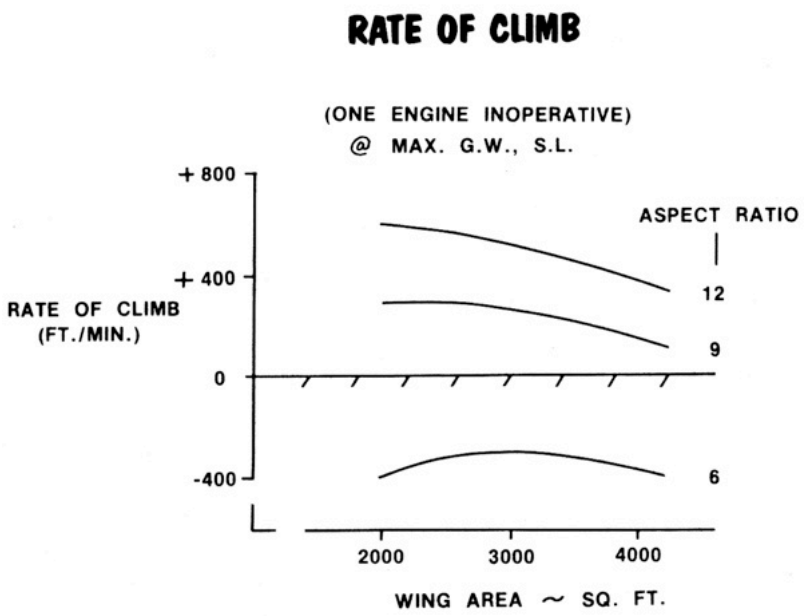

Swept wings

Note: the principal purpose of adopting wing sweep is to mitigate transonic drag rise.

Though it can do that, substantial sweep also brings with it a myriad of attendant problems for the aerodynamic designer to deal with.

If wing sweep is mild (e.g. ±5°), it has probably been employed for reasons other than transonic drag (e.g. to shift major components for CG placement).

Don't add sweep unless it is necessary.

The 2D—3D equivalence principle

Busemann (1935)
Jones (1943)

$M = M_0 \cos\varphi$ . . . . . (23)

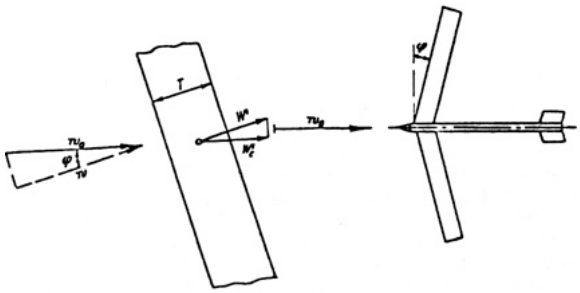

Abb. 4. Schräg aneblasner Tragflügel

Abb. 5. Pfellförmiges Tragwerk.

For inviscid flow, the pressure on an infinite swept wing depends only on the normal component of the incoming velocity.

Some theoretical consequences:

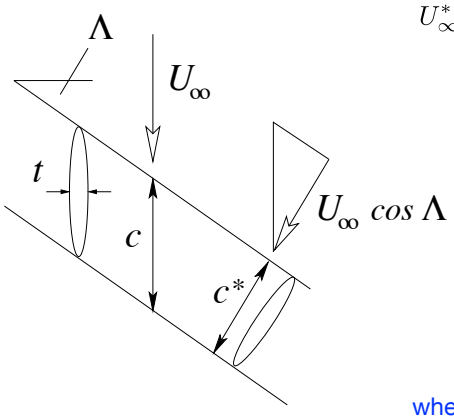

$$U_\infty^* = U_\infty \cos\Lambda \qquad M_\infty^* = M_\infty \cos\Lambda \qquad \left(\frac{t}{c}\right)^* = \left(\frac{t}{c}\right)\frac{1}{\cos\Lambda}$$

$$\begin{aligned} C_p^* &= \frac{p^* - p_\infty^*}{\frac{1}{2}\rho_\infty^* U_\infty^{*2}} \\ &= \frac{p - p_\infty}{\frac{1}{2}\rho U_\infty^2 \cos^2\Lambda} \\ &= C_p \sec^2\Lambda \\ C_l^* &= C_l \sec^2\Lambda \\ C_d^* &= C_d \sec^2\Lambda \\ \alpha^* &= \alpha/\cos\Lambda \end{aligned}$$

where * represents an equivalent 2D value

The overall C_L:

$$C_L = C_l(\alpha)\cos\Lambda$$

Hence the effective lift-curve slope of the original airfoil is reduced. So is $C_{L,\max}$.

The 2D—3D equivalence principle

A very important practical consequence is that if infinite wings are swept to lie behind the Mach cone angle μ = arcsin(1/*M*), the normal-component flows about them remain subsonic, and thus may (perhaps) not have shock waves or wave drag.

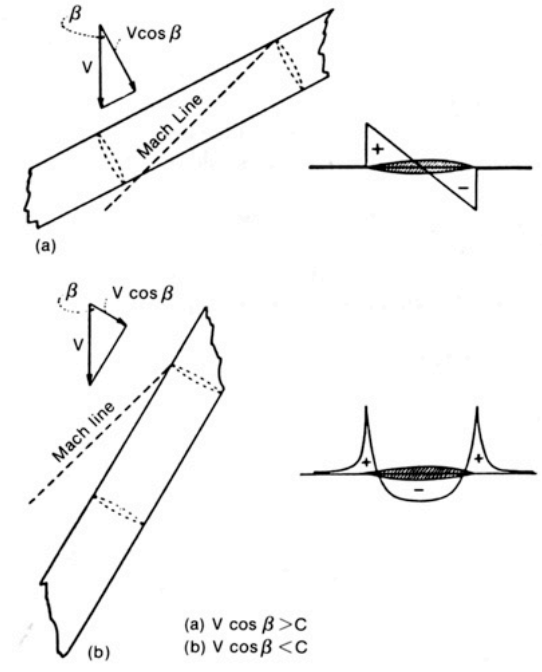

6.2. Effect of leading-edge angle on pressure distribution.

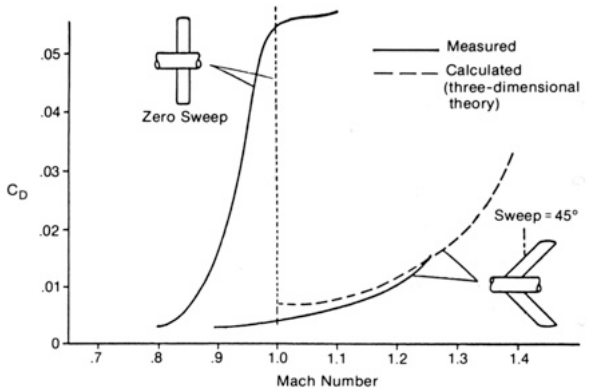

6.1. Drag coefficients of straight and swept wings, determined in free-fall experiments.

This means that airfoil sections more appropriate to subsonic flow can be employed, even if the aircraft is to be supersonic.

As a result, subsonic handling (e.g. $C_{L\max}$) can be improved and wave drag is not so important.

Using the equivalence principle: M_{cr}

Use the Prandtl-Glauert rule and the equivalence principle, i.e. relevant flow characteristics depend on normal velocity only, to obtain

$$\frac{\{C_{p,\min}\}_{M_\infty=0}^{\Lambda=0}\cos\Lambda}{\sqrt{1-M_\infty^2\cos^2\Lambda}} = \frac{2}{\gamma M_\infty^2}\left[\left(\frac{1+\frac{\gamma-1}{2}M_\infty^2\cos^2\Lambda}{1+\frac{\gamma-1}{2}}\right)^{\gamma/(\gamma-1)} - 1\right]$$

(Effective dynamic pressure is reduced by $\cos^2\Lambda$, but the thickness ratio perpendicular to sweep line increases by $1/\cos\Lambda$. Overall, the dynamic pressure (hence, C_p) reduces by a factor of $\cos\Lambda$. The relevant Mach number in the Prandtl-Glauert correction is reduced by factor $\cos^2\Lambda$.)

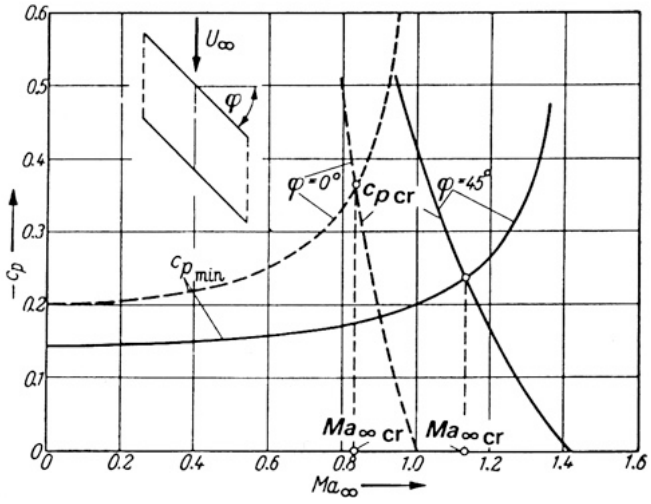

Using the equivalence principle: $\partial C_L/\partial\alpha$

For unswept elliptic wing, aspect ratio *A*,

$$\frac{\partial C_L}{\partial\alpha} = \frac{a\pi A}{a+\sqrt{(\pi A)^2+a^2}}$$

where *a* is the airfoil lift-curve slope.

Using the equivalence principle we can write

$$a = \frac{a_0\cos\Lambda}{\sqrt{1-M_\infty^2\cos^2\Lambda}}$$

where a_0 is the incompressible-flow airfoil lift-curve slope.

Then

$$\frac{\partial C_L}{\partial\alpha} = \frac{a_0\pi A}{a_0+\sqrt{\left(\frac{\pi A}{\cos\Lambda}\right)^2+a_0^2-(\pi A M_\infty)^2}}$$

Note that adding sweep further reduces the lift curve slope over what occurs for finite *A*.

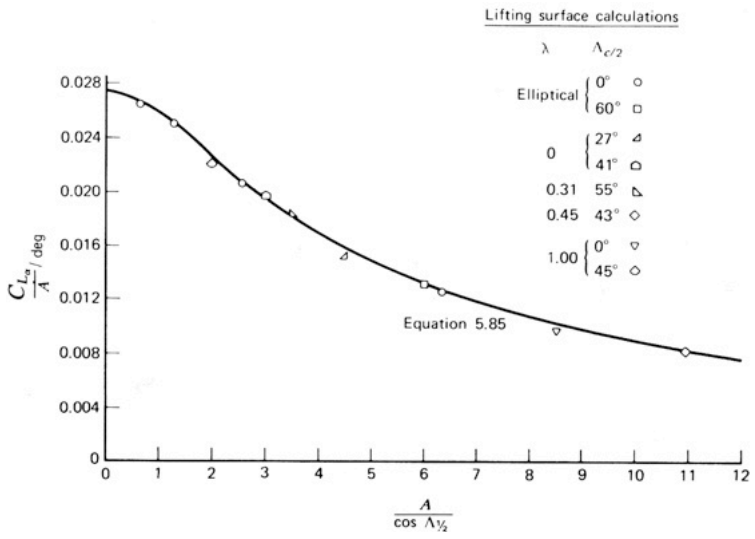

Experiments by Jacobs & Ward (1936) show that the formula is independent of taper ratio λ if Λ is taken to be the mid-chord sweep angle.

Delayed onset of drag divergence — 1

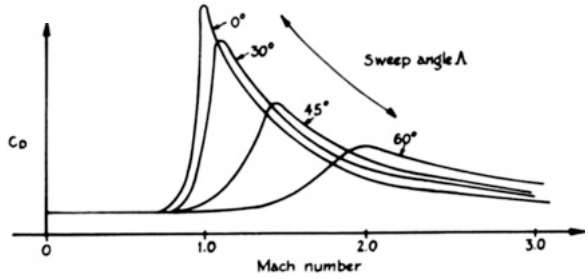

Wing sweep delays the onset of transonic drag rise (increases M_{CR} & M_{DD}) and is almost invariably used on subsonic jet transport aircraft, since the range parameter *ML/D* is increased.

$$M_{CR} \approx \frac{M_{CR,\Lambda=0}}{\cos^m \Lambda}$$ where m<1 is a function of C_L.

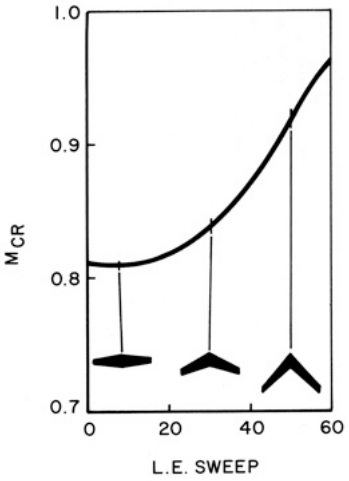

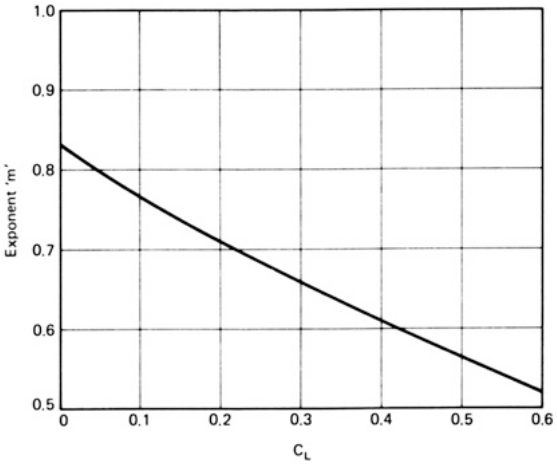

Delayed onset of drag divergence — 2

A preliminary (correlation) estimate of M_{DD} for ΔC_D=0.002 can be obtained from

$$M_{DD} \approx M_{DD,L=0} \times LF_{DD} - 0.05 \times C_{L,\text{design}}$$

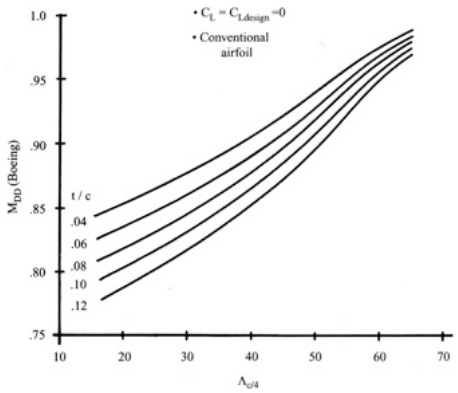

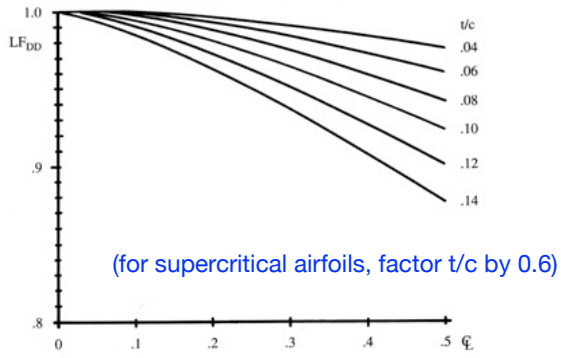

(for supercritical airfoils, factor t/c by 0.6)

The effect of compressibility drag can also be estimated from data correlations:

$$C_D = C_{Dp} + \frac{C_L^2}{\pi e A} + \Delta C_{Dc}$$

parasite induced compressibility

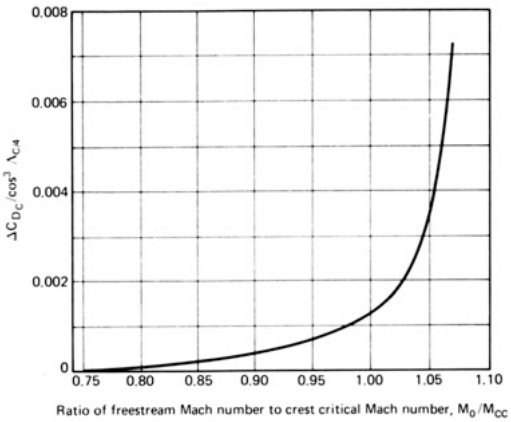

Wing-root effect

In reality, even for an inviscid flow, 3D effects near the wing root will produce significant wave drag even if the whole wing is swept behind the wing-apex Mach cone when $M_\infty > 1$.

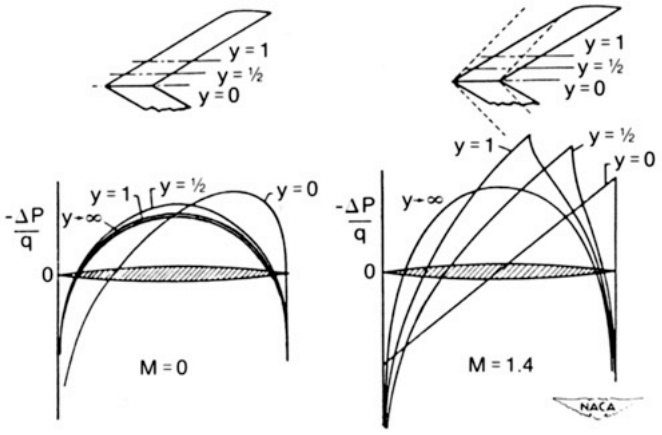

6.10. Pressure distributions at several sections of a swept wing at zero lift.

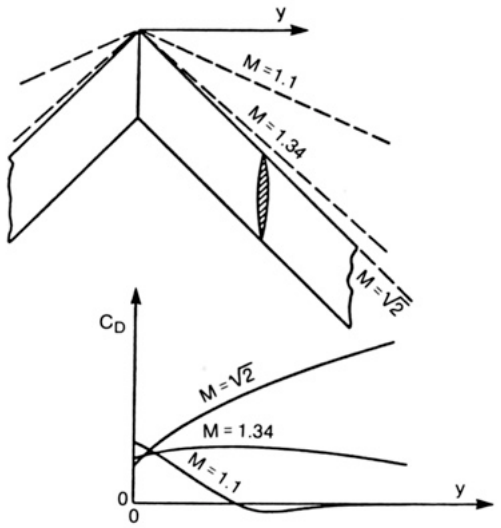

6.11. Spanwise distribution of drag at different Mach numbers.

This implies that, just as for an isolated airfoil, obtaining small wing wave drag — largely produced by having low t/c — is still important for supersonic aircraft, even if the wing has a nominally subsonic LE.

If the aircraft has a supersonic LE, then a sharp airfoil and small t/c are definite requirements.

Sub/supersonic leading and trailing edges — 1

Since wings are typically tapered, note that it is possible to have leading and trailing edge that differ as to whether the flow is super- or subsonic.

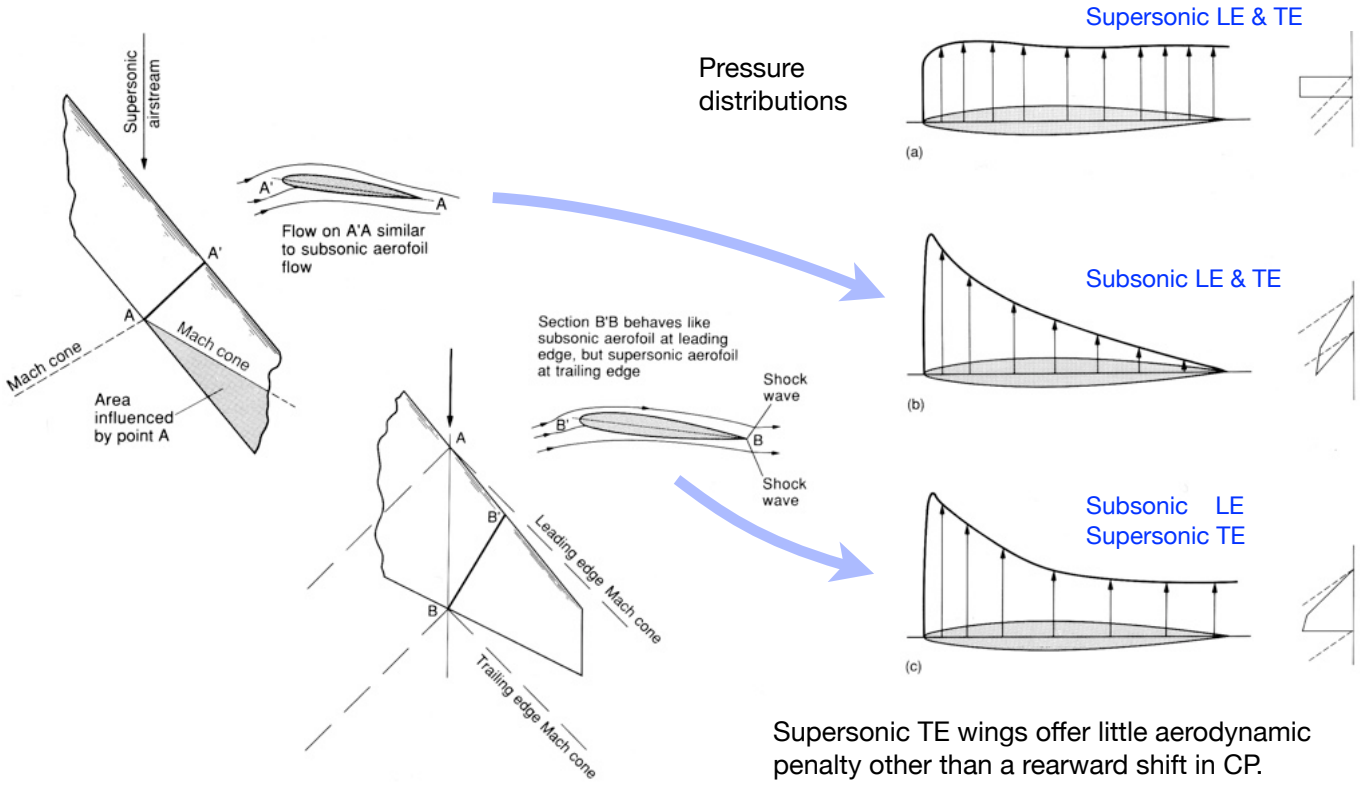

Supersonic TE wings offer little aerodynamic penalty other than a rearward shift in CP. They are quite common.

Sub/supersonic leading and trailing edges — 2

Supersonic LE wings are common for high Mach numbers because otherwise they would be very highly swept/flexible, also because less-swept wings become more efficient at large *M*.

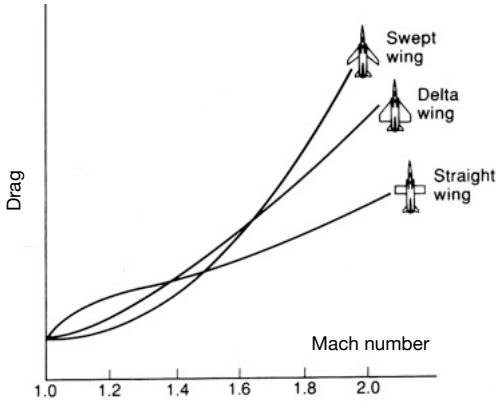

Airplane	Sweep	Mach No.	Mach No. Normal to Leading Edge	Wing Type
British Aerospace Hawk	26.00	0.88	0.79	Swept
Boeing E-6a	36.00	0.79	0.64	Swept
Boeing 747	41.00	0.90	0.68	Swept
Boeing 757	30.00	0.80	0.69	Swept
Boeing 777	35.00	0.83	0.68	Swept
Cessna 750 Citation X	38.00	0.90	0.71	Swept
Airbus A300	31.00	0.82	0.70	Swept
McDonnell-Douglas F-15	45.00	2.50	1.77	Swept
McDonnell-Douglas F-18	26.00	1.80 +	1.62	Swept
Dassault Mirage F1	50.00	2.20	1.41	Swept
GD F-16	40.00	2.00	1.53	Swept
MiG-23	72.00	2.35	0.73	Variable Sweep
Tupolev TU-160	66.00	1.88	0.76	Variable Sweep
Panavia Tornado	68.00	2.20	0.82	Variable Sweep
Grumman F-14A	68.00	2.34	0.88	Variable Sweep
Dassault Mirage 2000N	60.00	2.20	1.10	Delta
Dassault Rafale C	47.00	2.00 E	1.36	Delta-canard
Eurofighter EFA	52.00	1.80 +	1.11	Delta-canard

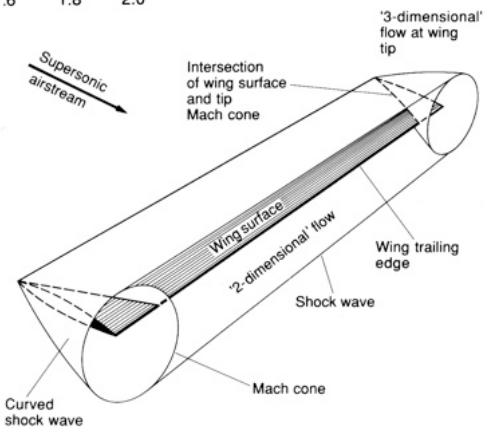

If the LE is supersonic, then tip effects are unable to propagate outside their Mach cones, and so downwash and induced drag effects become minimal.

Hence, if wing flow is everywhere supersonic aspect ratio effects are far less important, and relatively efficient wings may be of low aspect ratio.

Aerodynamic effects of sweep — 1

Following remarks assume that the swept wing has a subsonic LE.

1. Sweep strongly affects spanwise circulation distribution, owing to the fact that trailing vortices from inner panels can now induce *upwash* on outer panels.

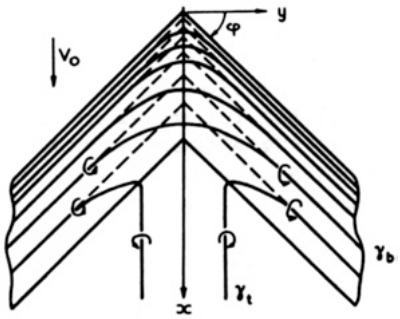

This effect occurs because vortex lines resist kinking.

2. Resulting effect on circulation distribution:

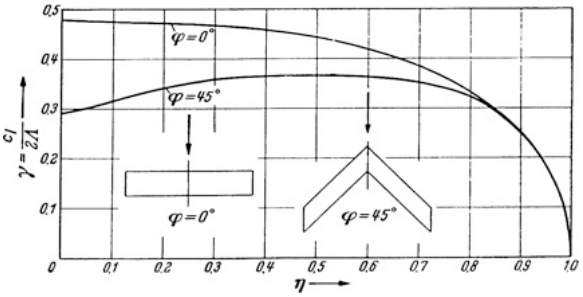

Tips get more highly loaded and tend to stall first, compared to an equivalent unswept wing.

and C_l distribution:

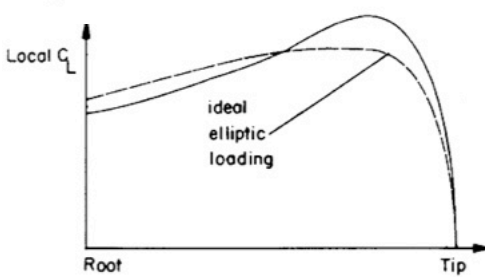

Swept wings almost invariably have substantial tip washout and lower maximum lift capacity.

Aerodynamic effects of sweep — 2

3. As a result of sweep, the chord distribution for constant C_l, i.e. elliptical loading, no longer provides minimum induced drag. Nor does an elliptical chord distribution provide elliptical loading for an untwisted wing.

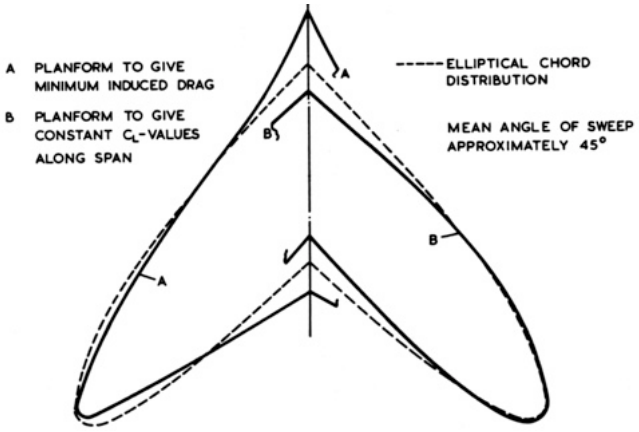

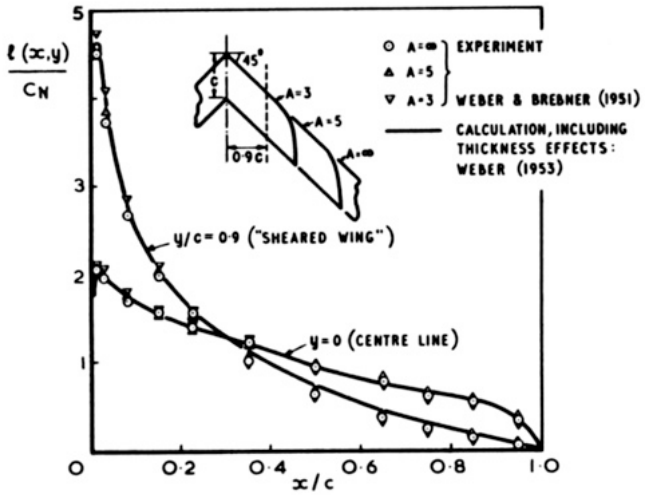

4. However, the effects of the root discontinuity are rather localised and essentially independent of aspect ratio. This plot shows that at y/c=0.9, the chordwise load distribution is effectively independent of aspect ratio for A>3.

Aerodynamic effects of sweep — 3

5. The effect of sweep on load distribution is reflected in the chordwise pressure distribution. Large adverse streamwise pressure gradients occur near the tips, tending to promote flow separation and early stall. The effect is exacerbated by spanwise increases in BL thickness created by spanwise flow.

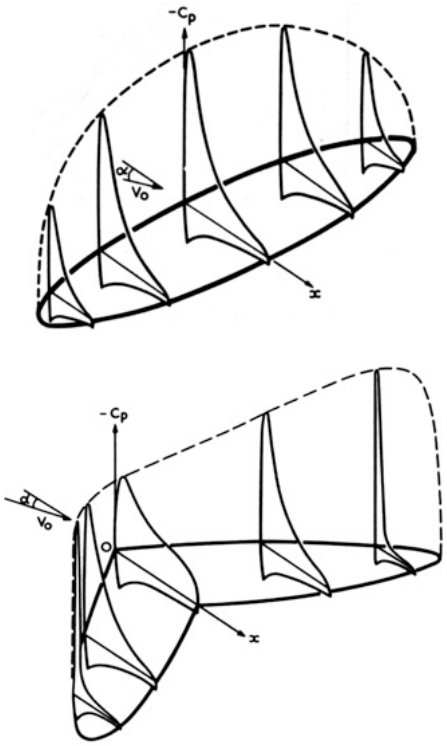

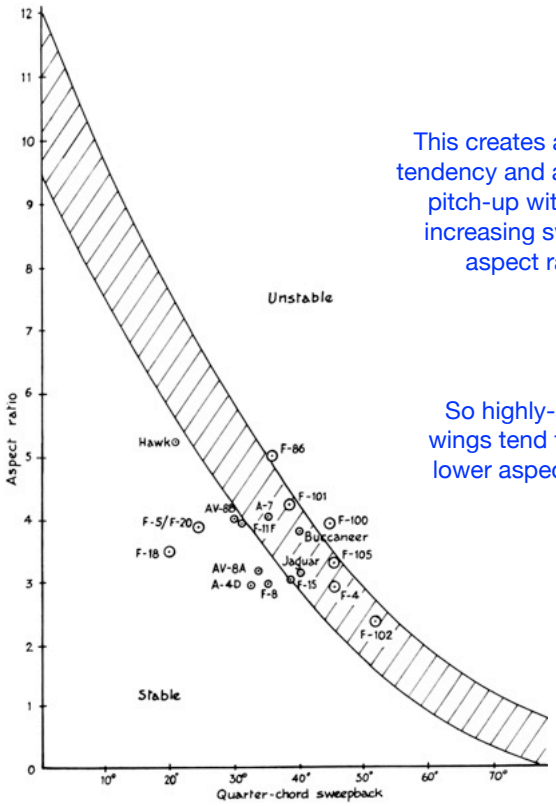

This creates a tip-stall tendency and associated pitch-up with either increasing sweep *or* aspect ratio.

So highly-swept wings tend to be of lower aspect ratio.

LE thrust/suction — 1

1. Recall that for inviscid attached flow a lifting airfoil (even a flat plate) has no drag. This apparent paradox is resolved by the presence of leading edge suction, which may be quite intense.

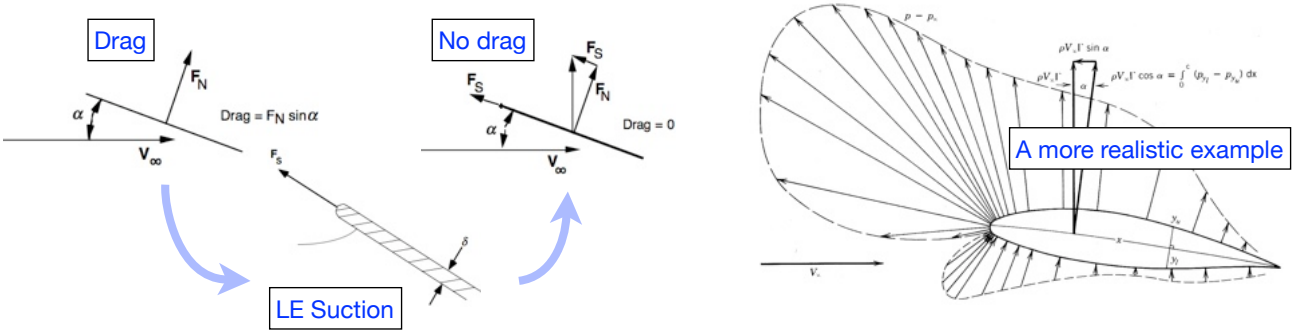

2. Highly-swept and thin wings tend to suffer LE separation at moderate-to-high C_L when flow is subsonic relative to LE. This separation leads to a loss of LE suction and an extra (profile) drag penalty which is seen as a change in the drag polar. However, substantial lift is still available.

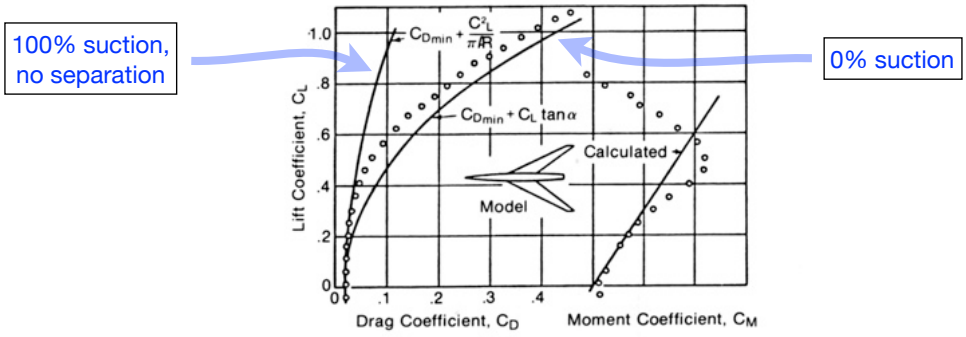

6.7. Force measurements indicating flow separation on model with large angle of sweep.

LE thrust/suction — 2

3. A possible remedy is to add LE camber/droop to reduce separation and recover some thrust even if separation does occur. It's a balancing act because the camber adds some extra drag once the flow goes sonic relative to the LE. The solution tends to be seen on aircraft designed for supersonic flight.

The idea.

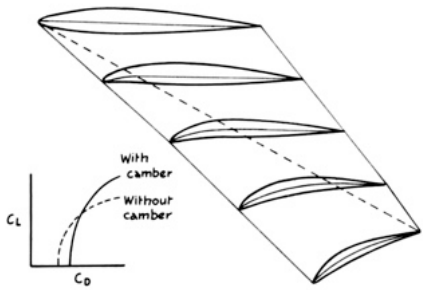

Effect is subtle on F15 wing.

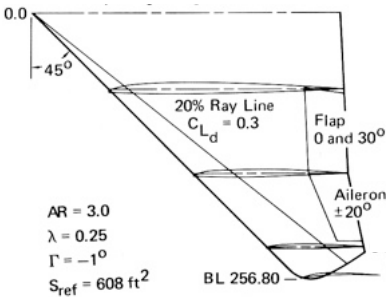

In practice.

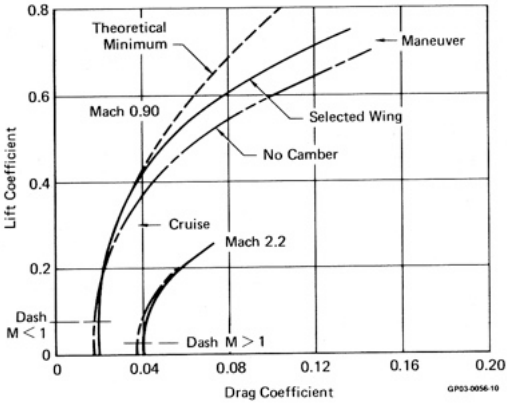

May be seen on subsonic aircraft.

Isobar straightening — 1

The ideal wing sweep effect is difficult to achieve for a finite wing owing to wing root and tip effects, which tend to straighten vortex lines and isobars so they become normal to direction of flight.

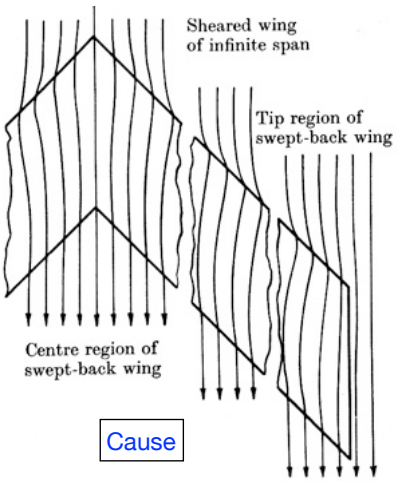

Cause

Result without adequate remediation

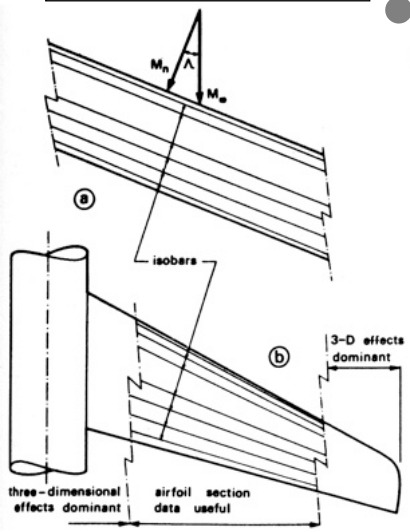

What can be achieved

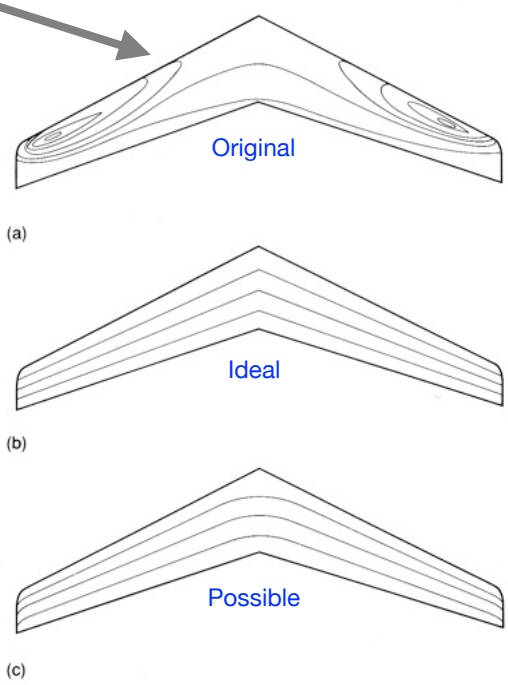

Isobar straightening — 2

Remedies

1. Shaping fuselage/wing near junction
2. Changing wing section/thickness near root
3. Altering tip shape
4. Contouring tip stores
5. Wing shape optimisation + CFD

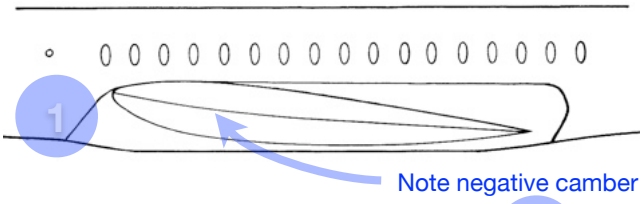

Note negative camber

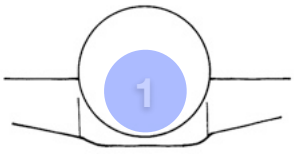

2

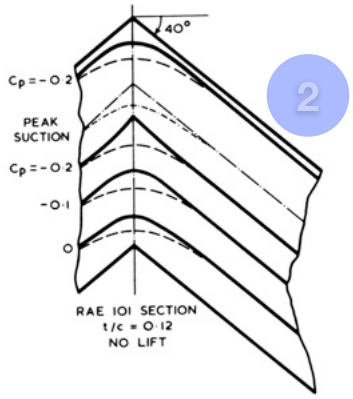

2

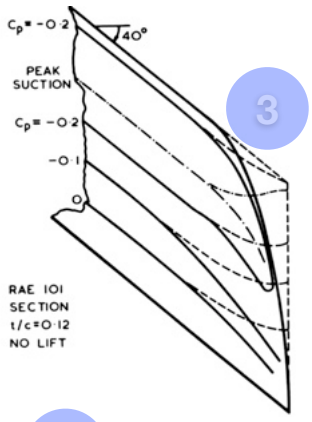

3

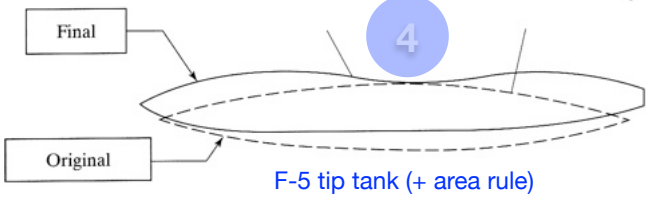

4

F-5 tip tank (+ area rule)

5

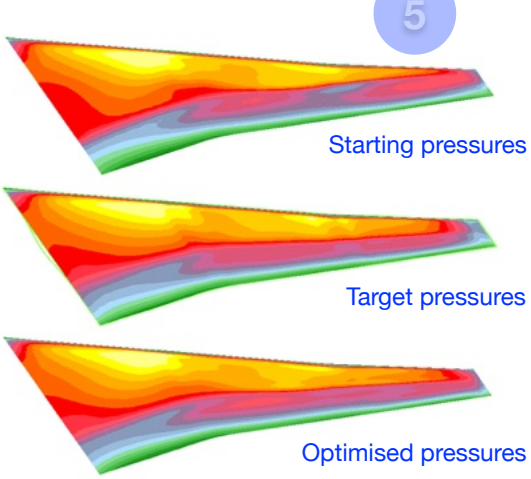

Transonic flow effects — 1

1. Owing to the overall pressure distribution for swept wings, shock waves tend to form at the tips first. Also these tend to be less swept and hence stronger, may lead to local separation, increased drag.

(a) Typical shock pattern for high-aspect ratio

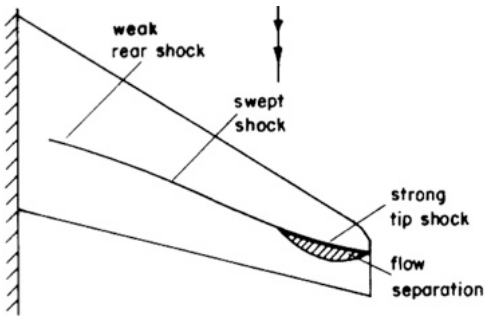

(b) Typical for lower aspect ratio/more sweep

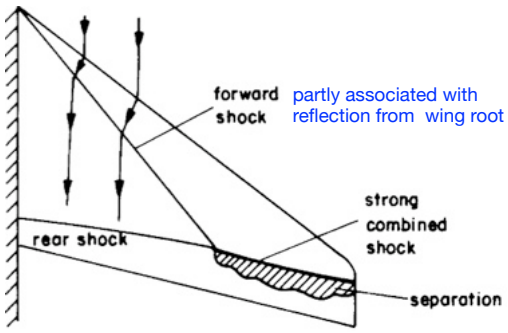

(c) Progression with Mach number

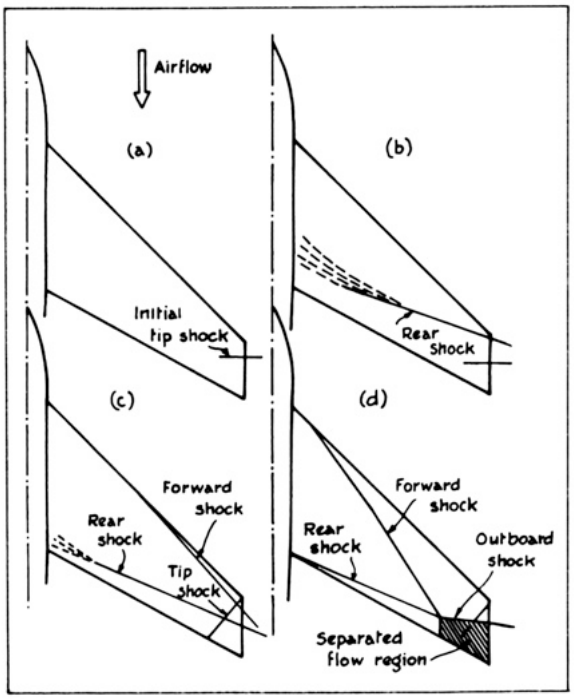

Transonic flow effects — 2

2. One of the main goals of transonic aerodynamic design of swept wings is to push the intersection point of the forward and aft shocks as far outboard as possible, weakening the combined shock and straightening isobars.

3. At increasing C_L, separated flow vortices tend to appear and interact with the shock wave system. These flows can still provide substantial lift (and high drag).

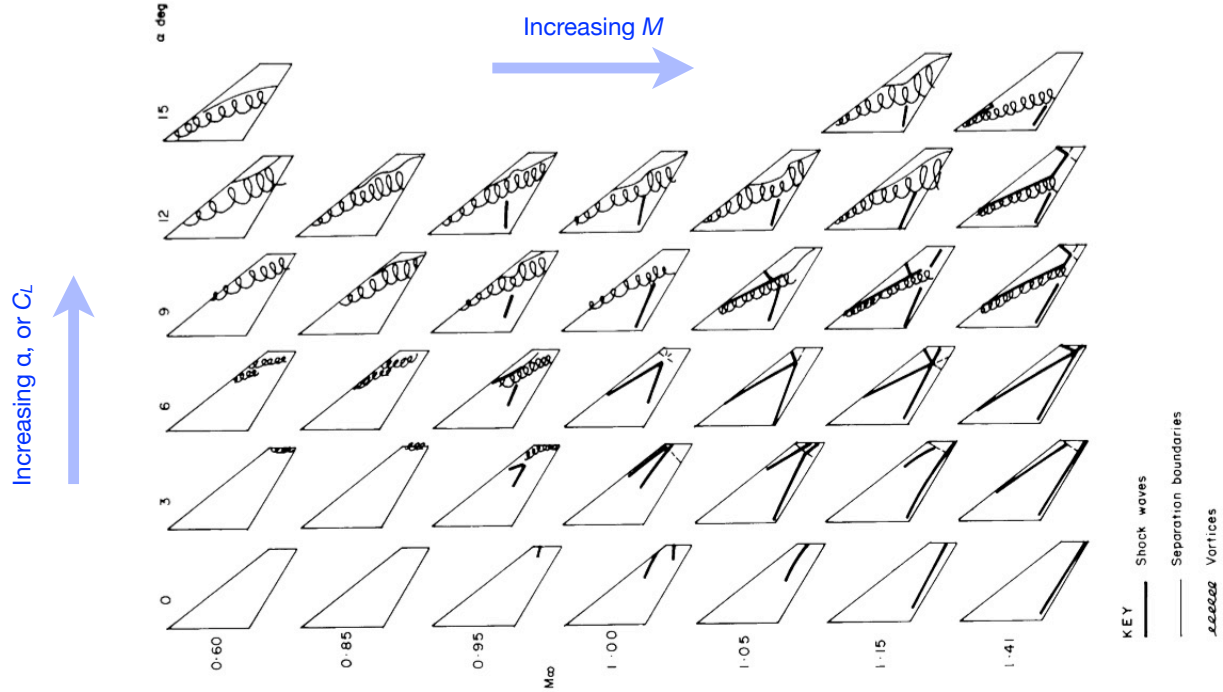

Boundary-layer behaviour on swept wings — 1

1. Owing to sweep, there is always an external flow component directed along the wing.
2. Also there is a spanwise pressure gradient created by the sweep of the chordwise pressure distributions.
3. For conventional i.e. back-swept wings, both effects lead to boundary layers becoming increasing thick and prone to separation towards the wing tips.

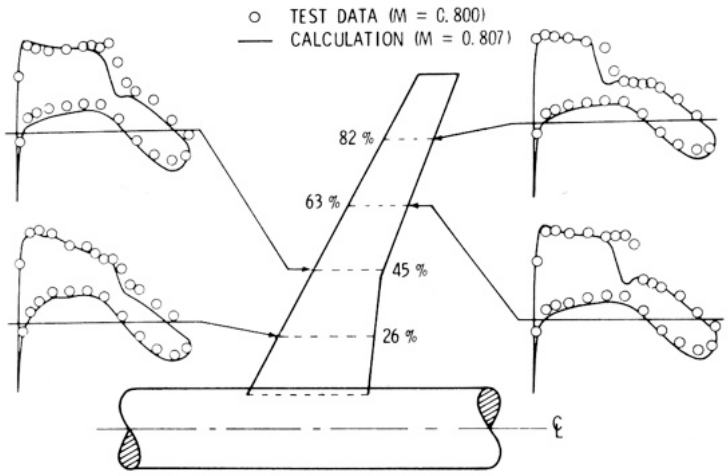

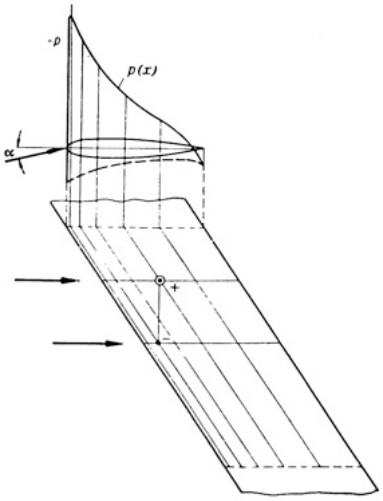

Boundary-layer behaviour on swept wings — 2

4. The combined effect of normal and streamwise flows gives rise to special cross-flow boundary layers with curvature effects which affect their stability and separation properties.

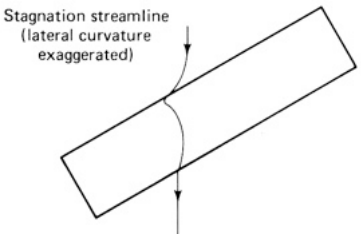

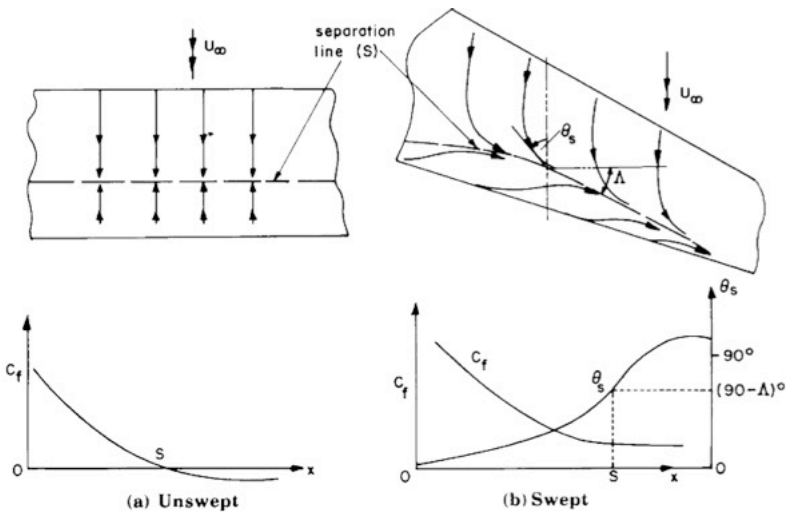

Note that on a swept wing, skin friction may not change sign at a flow separation.

Boundary-layer behaviour on swept wings — 3

5. The fuselage may need shaping near the wing root in order to accommodate wing BL flows and avoid flow separation on the fuselage as well as the wing itself. These BL considerations may interact with designing to reduce wave drag effects in transonic flows.

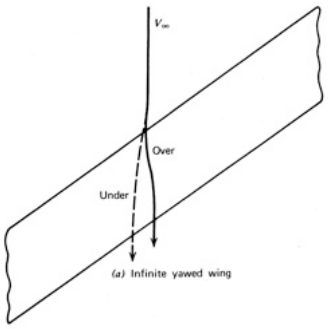

BL contouring

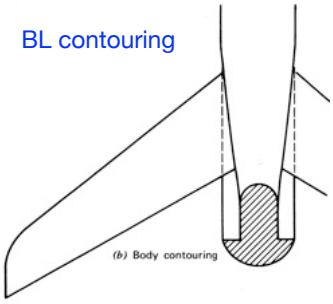

Shock-wave contouring

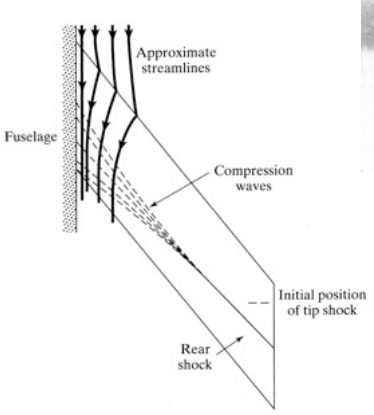

The resulting shapes may be effective but expensive to manufacture.

Forward- vs Backward-swept wings — 1

Ju-287

X-29

1. Wing sweep increases the drag-divergence Mach number and produces weaker shock waves in transonic flow for both FSWs and BSWs.
2. The main difficulty with FSWs is static aeroelastic divergence associated with tip washin arising with loading — for BSWs the tips tend to washout, thus reducing the loading. This causes both structural and control problems. These can be countered:
   a. Aeroelastic tailoring using composite wing structures
   b. Augmented dynamic stability using canard and/or FBW

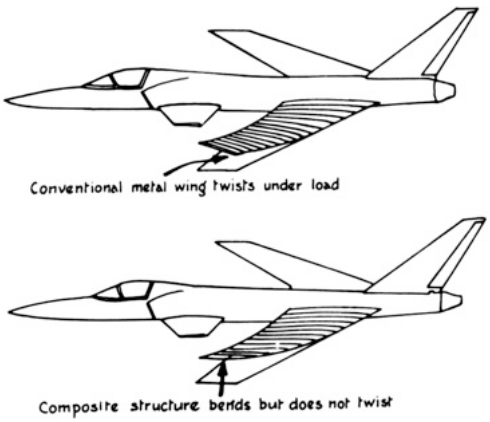

Forward- vs Backward-swept wings — 2

Advantages of FSW

1. Wing root tends to stall first as a result of both spanwise loading and BL effects — OTOH this is not necessarily desirable and might be countered by a sweep reduction at wing root, twist, or fences.
2. For the same LE sweep the shock inclination in FSW is larger than in BSW — this reduces wave drag.
3. Alternatively, for the same wave drag the FSW could use a smaller LE sweep, giving smaller lift-slope reduction.
4. For the same area, span and shock sweep, FSW has a shorter structural wing span and an aerodynamic centre closer to the wing root.
5. Fuselage volume may be increased near the centre of gravity, allowing larger stores capacity.

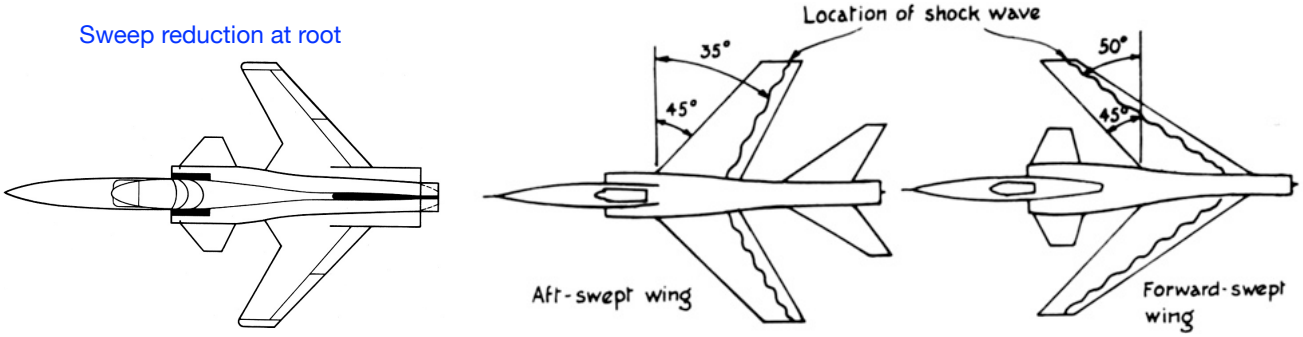

Variable sweep — 1

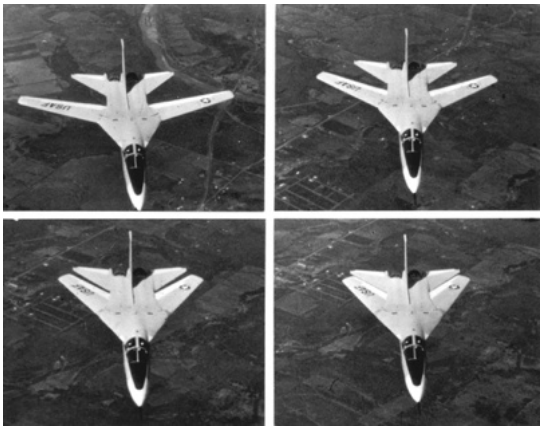

The idea of using variable geometry in the form of wing sweep to achieve optimal aerodynamic characteristics over a wide speed range was apparently conceived by Messerschmitt designers during WW2, although their aircraft was only designed for ground-variable sweep.

Since then a wide range of supersonic-capable aircraft have employed VS. Invariably they are designed to have subsonic wing LEs at maximum speed.

Advantages of VS

1. At low speeds/high C_L, wing has high aspect ratio for low induced drag and good *L/D.* Since the wing LE will always be subsonic, wing sections suitable for low speeds can be used.
2. Good use can be also made of high-lift devices, further reducing landing speeds.
3. At transonic/cruise speeds, sweep increases drag divergence Mach number.
4. High lift can be obtained for combat manouevring at subsonic speeds
5. At supersonic speeds/low C_L, wing is fully swept and low effective *t/c* reduces wave drag.
6. Reduced span at high speeds reduces wing-root bending moments in manoeuvres.

Variable sweep — 2

Range benefit

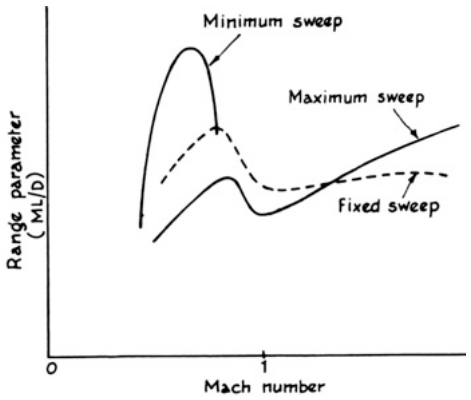

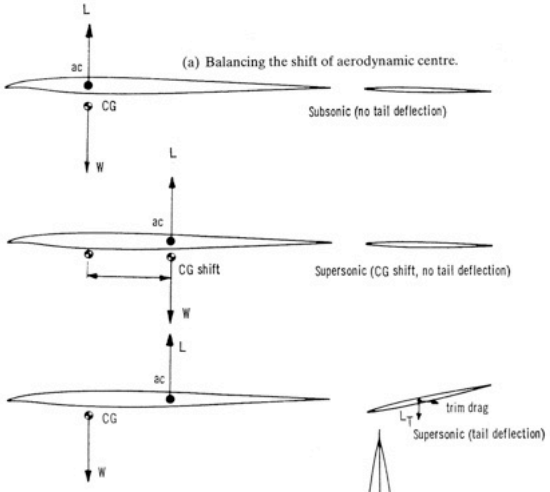

Disadvantages of VS

1. VS is costly, adds weight, is complex to maintain.
2. Aerodynamic centre moves aft both with wing sweep and change to supersonic flow, which can substantially increase static margin and hence trim drag unless remedial action is taken:
   a. move CG (fuel) to reduce static margin
   b. move wings (i.e. AC) forward as they are swept, or move pivot points outboard (same effect)
   c. use canard/extendable wing gloves to move AC forward as wings are swept back

Static margin issue

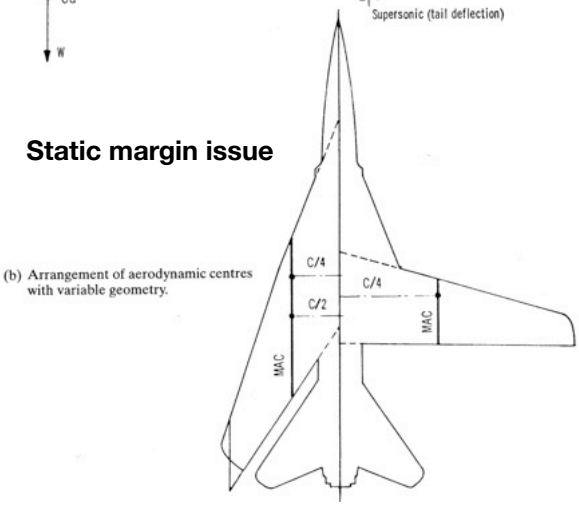

Variable sweep — 3

F-14 (1972-present*)

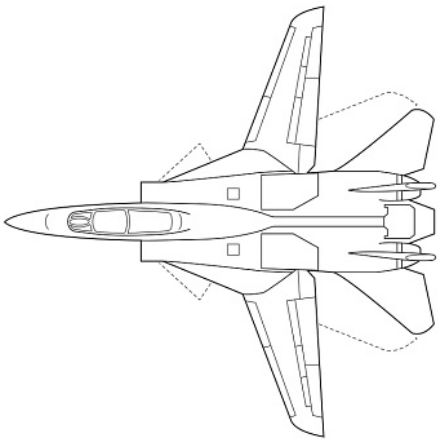

Islamic Republic of Iran

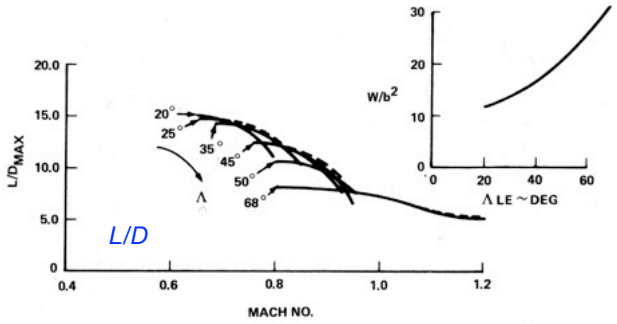

span loading
i.e.
1/aspect ratio

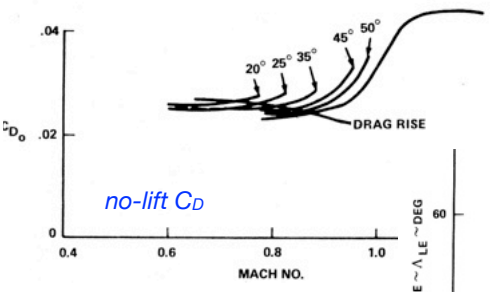

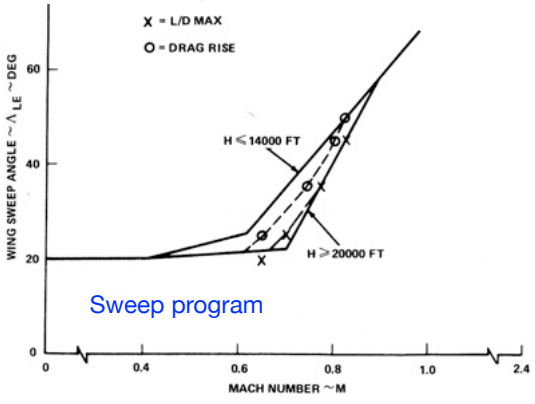

Sweep program

Variable sweep — 4

Original reason for sweep was strength

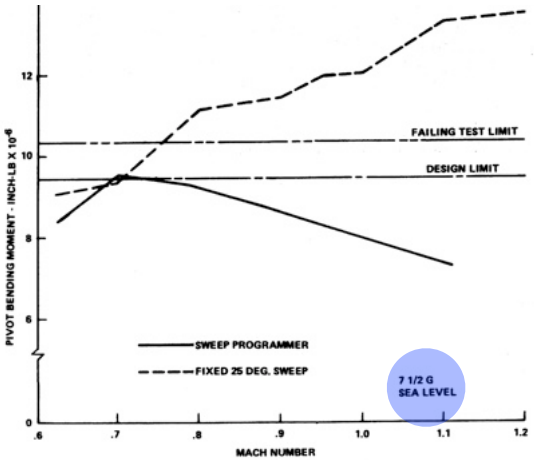

Other variable-geometry devices on F-14.

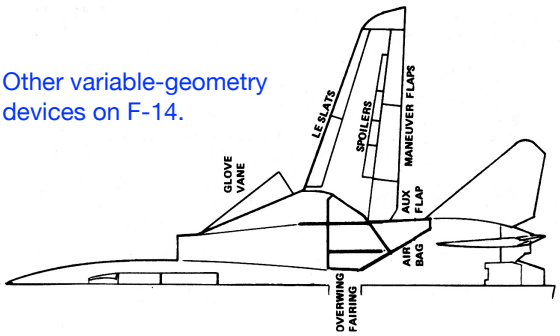

Favourable *t/c* across flight regimes

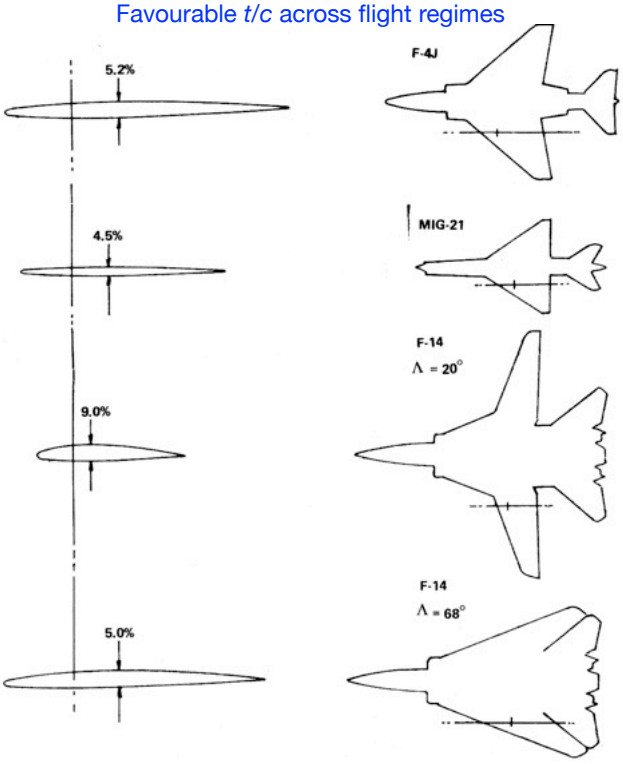

Variable sweep — 5

F-14 vs F-111

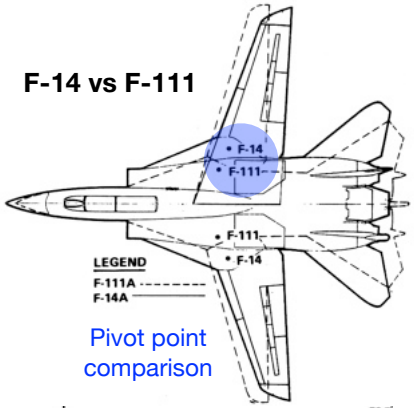

Pivot point comparison

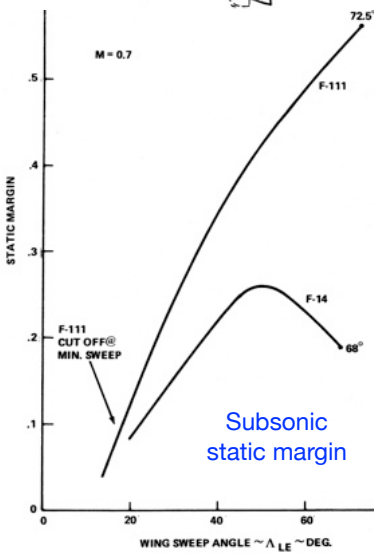

Subsonic static margin

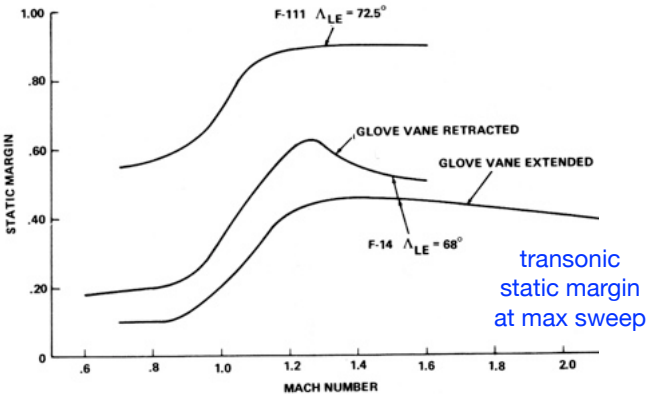

transonic static margin at max sweep

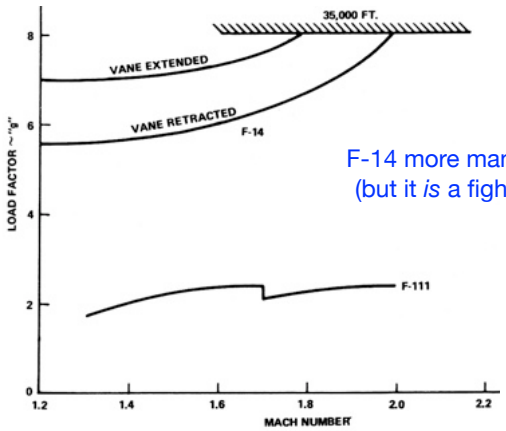

F-14 more manouevreable (but it *is* a fighter aircraft)

Wave drag and the Area Rule — 1

YF-102: *M*<1, level flight

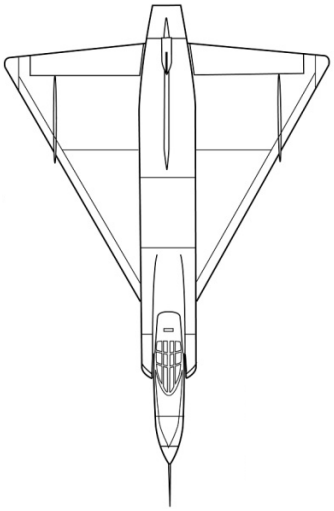

F-102A: *M*=1.5

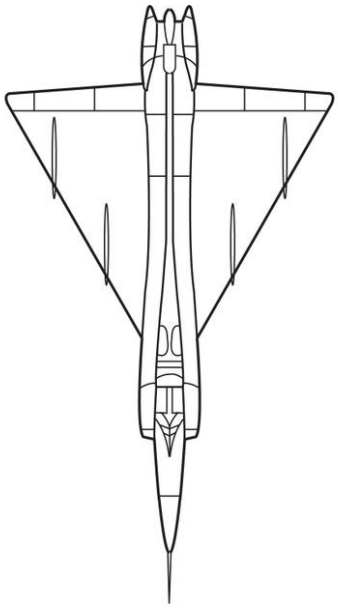

F-106A: *M*=2.3

The *Area Rule* is another idea that was first invented by a German engineer (Otto Frenzl) late in WW2. It was later 're-invented' in the USA, first by Wallace Hayes (Caltech, 1947) and then Richard Whitcomb (NACA, 1952), who usually gets the credit. Dieter Kuchemann developed similar ideas.

While related to the total aircraft axial volume distribution, it has important implications in wing design for upper-transonic/supersonic aircraft. Not so important for typical transonic jet transport aircraft.

Wave drag and the Area Rule — 2

The Sears-Haack slender symmetric body of revolution gives minimum wave drag for a specified length and volume in inviscid supersonic flow. Its radius is given by

$$\frac{r}{l} = \frac{1}{2F}\left(1 - \frac{4x}{l} + \frac{4x^2}{l^2}\right)^{3/4}$$

where *F* is the *fineness ratio* l/d_{max}. The wave drag coefficient based on projected frontal area is

$$C_{Dw} = \frac{9.87}{F^2}$$

Note the inverse dependence on F^2 (similar to the dependence on $(t/c)^2$ for an airfoil). Supersonic aircraft bodies have large *F*. In very preliminary design a factor of 1.5 on this estimate may be used to estimate supersonic wave drag.

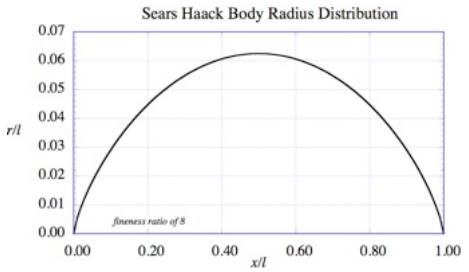

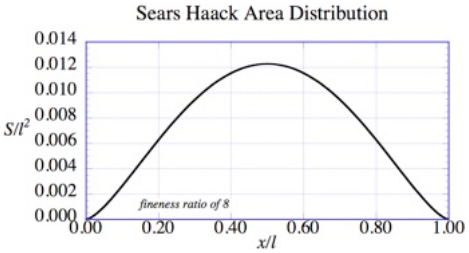

Area Rule: For low wave drag, the overall axial cross-sectional area distribution of the *whole aircraft* should approximate the Sears-Haack shape. The distribution should also be smooth.

So when the wing is thick and extends spanwise significantly, the fuselage section should be reduced. This gives a characteristic waisted or 'coke-bottle' fuselage shape as seen on the F-102A, F-106A.

It may be advisable to *add* extra volume-filling shapes that do little but help approximate a Sears-Haack distribution.

Wave drag and the Area Rule — 3

Equivalent body concept

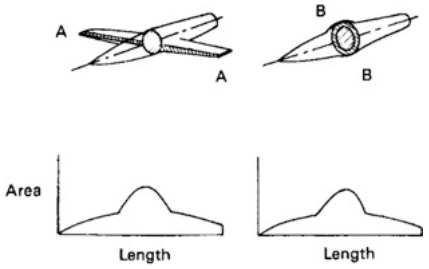

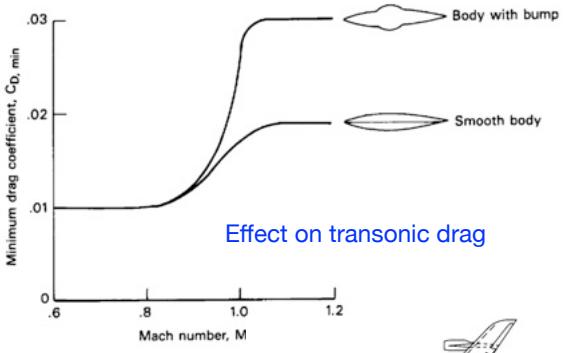

Effect on transonic drag

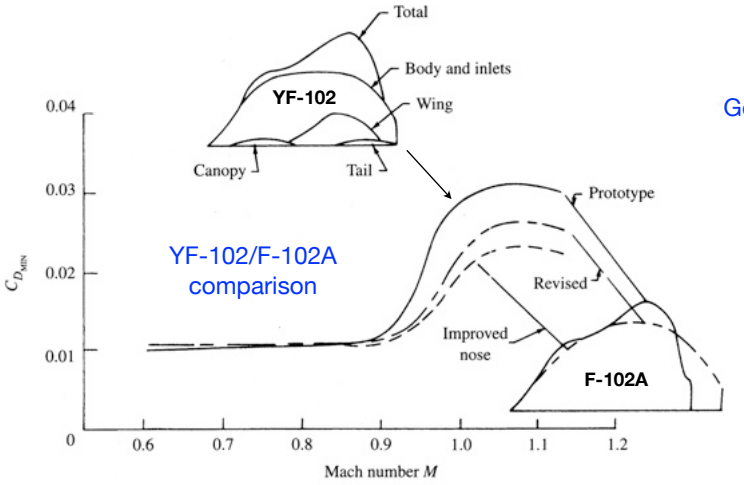

YF-102/F-102A comparison

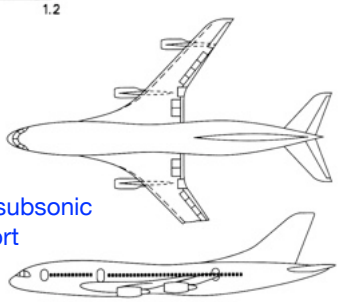

Generic high-subsonic transport

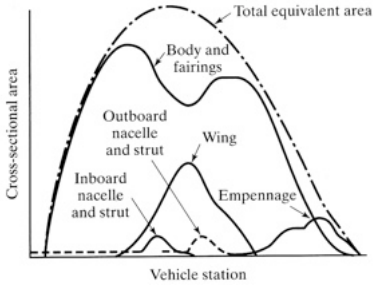

Wave drag and the Area Rule — 4

Effect on C_{D0}

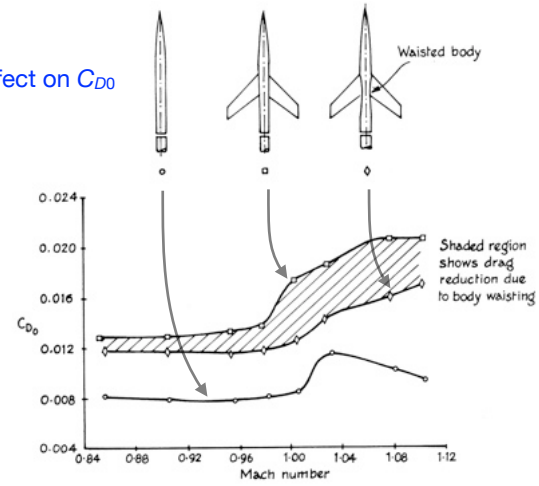

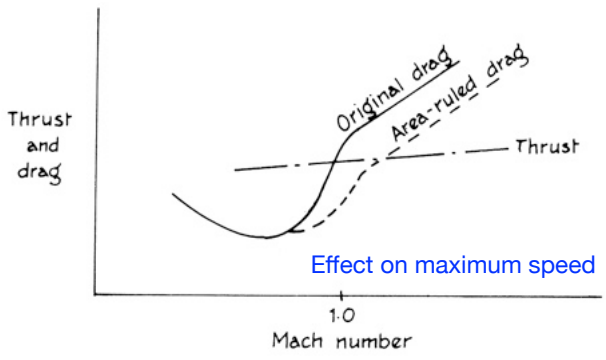

Effect on maximum speed

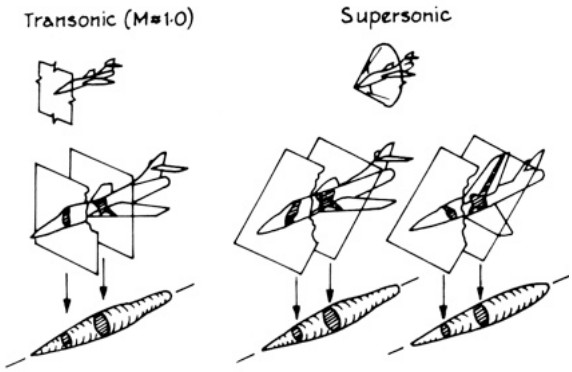

Area ruling for $M>1$.

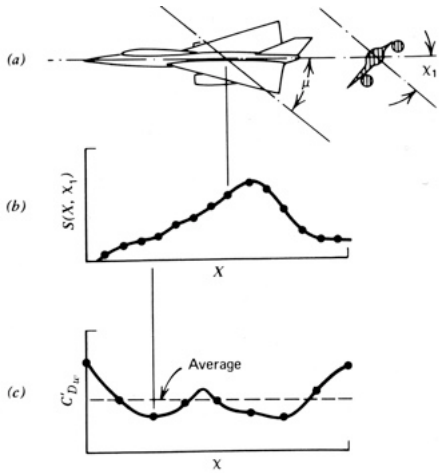

Wave drag and the Area Rule — 5

Even “minor” variations may elevate M_{DD} beneficially.

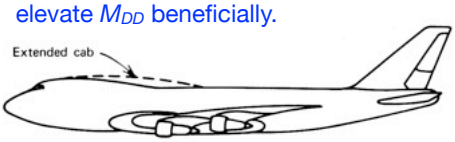

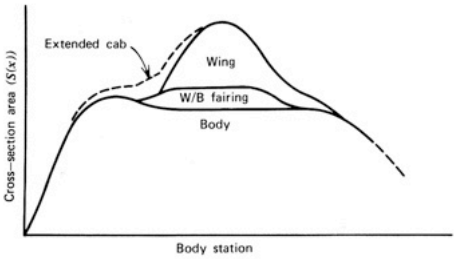

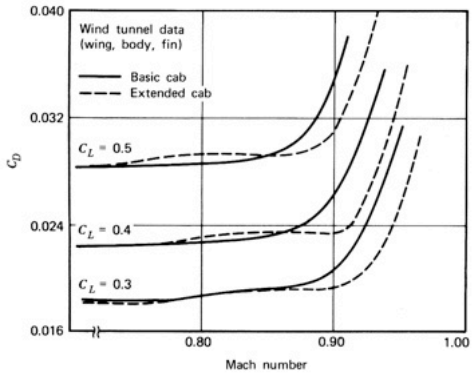

Devices deployed on wings can smooth the axial area distribution, too.